Henrik Forsback

Reliability of Thermal Interface Materials for Power Semiconductor Devices

Aalto University

School of Electrical Engineering

This study is a thesis submitted in partial fulfillment of the requirements for the degree of Master of Science in Technology.

Espoo 23.1.2017
Supervisor: Professor Jorma Kyyrä
Instructor: Kari Huotari, M. Sc. (Tech.)

AALTO UNIVERSITY
SCHOOL OF ELECTRICAL ENGINEERING

ABSTRACT OF THE
MASTER'S THESIS

Author: Henrik Forsback

Title: Reliability of Thermal Interface Materials for Power Semiconductor Devices

Date: 23.1.2017 Language: English Number of pages: 10 + 73

Department: Department of Electrical Engineering and Automation

Professorship: Power Electronics Code: S-81

Supervisor: Prof. Jorma Kyyrä

Instructor: M. Sc (Tech.) Kari Huotari

The purpose of this thesis is to study the reliability and the life time of preselected thermal interface materials and to develop an accelerated life time test system for this task. Thermal interface materials are used between power semiconductor devices and thermal solution to enhance the heat transfer between the two objects. Being one of the critical components in the path of heat flow, any weakening can cause severe damage to the component itself or to the whole application. The theoretical background in this study presents the basics of power semiconductor devices, thermal management and reliability related issues. In addition, as secondary objectives, different thermal interface materials are compared and heat transfer between two solid surfaces is examined.

The aim of this thesis is to develop a test system that can be used to analyze the life time behaviour of different thermal interface materials. To achieve this, a mechanical test frame, a control circuit and a printed circuit board will be designed and implemented. The aging of different materials is done by switching power transistors on and off causing heat gradients in the thermal path. Two thermal interface materials, an elastomer film and a phase change material, are tested and a regression analysis will be done to predict the thermal performance further. Furthermore, a general degradation model is established based on the measurement data. In addition, the thermal performance with different interface pressures is compared and the uncertainty of measurements is discussed.

Finally, the developed empirical model for thermal interface materials is presented. To fully benefit from the degradation models, additional research must be done. Based solely on the thermal performance analysis, the phase change material should be used instead of elastomer film on similar applications. Futhermore, based on the uncertainty analysis, without the calibration of the temperature measurement device, the results of this study could have been useless.

Keywords: power electronics, power semiconductor device, reliability, thermal interface material, life time

AALTO-YLIOPISTON DIPLOMITYÖN
SÄHKÖTEKNIIKAN KORKEAKOULU TIIVISTELMÄ

Tekijä: Henrik Forsback

Työn nimi: Tehopuolijohteiden lämmönhallintamateriaalien luotettavuus

Päivämäärä: 23.1.2017 Kieli: englanti Sivumäärä: 10 + 73

Laitos: Sähkötekniikan ja automaation laitos
Professuuri: Tehoelektroniikka Koodi: S-81

Työn valvoja: Prof. Jorma Kyyrä
Työn ohjaaja: DI Kari Huotari

Tämän työn tarkoituksena on tutkia ennalta määriteltyjen lämmönhallintamateriaalien elinikää ja luotettavuutta ja kehittää tätä tarkoitusta varten testausjärjestelmä. Lämmönhallintamateriaaleja käytetään tehopuolijohteiden ja jäähdytyselementin välissä parantamaan lämmönsiirtymistä. Koska lämmönhallintamateriaali sijaitsee jäähdyttämisen kannalta kriittisessä paikassa, voi sen heikkeneminen aiheuttaa komponentin tai koko laitteen tuhoutumisen. Tutkimuksen teoreettinen tausta esittelee tehopuolijohteita sekä lämmönhallintaan ja luotettavuuteen liittyviä aiheita. Lisäksi työssä verrataan eri lämmönhallintamateriaaleja ja tutkitaan kahden kiinteän pinnan välistä lämmönsiirtoa.

Työn tavoitteena oli kehittää testausjärjestelmä, jolla voidaan analysoida eri lämmönhallintamateriaalien käyttäytymistä niiden eliniän aikana. Tätä varten työssä suunnitellaan testirunko, ohjauspiiri transistoreille sekä piirikortti. Eri materiaalien vanhentaminen toteutetaan tehosyklauksen avulla. Työssä on tarkoitus tutkia kahta erilaista lämmönhallintamateriaalia, elastomeeria sekä faasimuunnosmateriaalia. Elinikää arvioidaan mittaustuloksiin perustuen regressioanalyysin avulla pidemmälle. Lisäksi mittausdatan avulla materiaaleille kehitetään yleiset hajoamismallit, joita voidaan käyttää apuna suunnittelussa. Tämän lisäksi työssä mitataan lämmönsiirtymistä eri liitospaineilla sekä arvioidaan mittausten luotettavuutta.

Työn tuloksena esitellään materiaaleille kehitetyt hajoamismallit. Lisäksi esitellään tarvittava lisätutkimustyö, joka vaaditaan eliniän estimoimiseen. Perustuen pelkästään lämmönsiirto-ominaisuuksiin, faasimuunnosmateriaalia pitäisi käyttää elastomeerin sijasta samanlaisissa käyttökohteissa. Mittausten luotettavuusanalyysin perusteella ilman lämpöantureiden kalibrointeja, mittaustulokset olisivat voineet olla käyttökelvottomia.

Avainsanat: tehoelektroniikka, tehopuolijohde, luotettavuus, lämmönhallintamateriaali, elinikä

Preface

This thesis was carried out in Kone Failure analysis department at Hyvinkää and I want to express my gratitude towards the whole organization for providing this opportunity.

I would like to thank all the people from Kone who has helped me during this project. Special thanks for my instructor Kari Huotari for guidance and support through the process. I also want to address my gratitude to my colleagues Matti Björklund and Pekka Leppäaho for the time and effort they put in this thesis.

I also wish to thank my supervisor Jorma Kyyrä for all the professional suggestions and corrections he has made.

Finally, I want to thank my family for the support they have given me during the time of my studies.

Espoo
23.1.2017

Henrik Forsback

Contents

Abbreviations and Symbols

ALT	Accelerated life test
BJT	Bipolar junction transistor
BLT	Bond line thickness
CTE	Coefficient of thermal expansion
DBC	Direct bond copper
EUT	Equipment under test
GTO	Gate turn off thyristor
HALT	Highly accelerated life test
IGBT	Insulated gate bipolar transistor
LMA	Low melting alloy
MTTF	Mean time to failure
MTBF	Mean time between failure
MOSFET	Metal oxide semiconductor fiel effect transistor
ORT	Ongoing reliability test
PCM	Phase change material
PC	Power cycling
PCB	Printed circuit board
PDF	Probability density function
PWM	Pulse-width modulation
RBO	Rescue brake opening
SMPS	Switching mode power supply
TC	Temperature cycling
TIM	Thermal interface material
TIM1	Thermal interface material between silicon die and heat spreader
TIM2	Thermal interface material between heat spreader and heat sink
VAC	Alternating voltage
VSD	Variable speed drive

AF	Acceleration factor
A	Coefficient
A	Cross-sectional surface area
$A_{nominal}$	Nominal contact surface
A_{real}	Actual contact surface
a	Test setup parameter
a_i	Upper and lower limits
B	Coefficient

C	Coefficient
C_{th}	Thermal capacity
C_{el}	Electric capacitance
c	Speed of light
c_0	Speed of light in vacuum
c_{th}	Specific thermal capacity
D	Coefficient
dt/dx	Temperature gradient
E_a	Activation energy
E_{cond}	Conduction energy losses
E_{off}	Off-state energy losses
E_{max}	Total switching losses
E_{sw}	Switching losses
E_{tot}	Total energy losses
$F(x)$	Cumulative density function
$f(x)$	Probability density function
f	Frequency
f	Function
f_{sw}	Switching frequency
H	Micro-hardness
h	Convection heat transfer coefficient
h_c	Thermal interface conductance
h_g	Thermal gap conductance
h_s	Thermal solid conductance
$h(x)$	Hazard rate function
I_D	Average current
$I_{D_{RMS}}$	RMS current
I_Q	Average current
$I_{Q_{RMS}}$	RMS current
$i(t)$	Current
K	Estimated life
k	Boltzmann's constant
k	Thermal conductivity
k_{TIM}	Thermal conductivity of thermal interface material
k_g	Thermal gap conductivity
k_s	Harmonic mean thermal conductivity
$k_{substrate}$	Thermal conductivity of substrate
k_1	Thermal conductivity
k_2	Thermal conductivity
L	Lenght
L_{meas}	Mean life of tested units
L_{test}	Time after product fails in accelerated test

L_{use}	Expected lifetime of a product
M	Gass parameter
m	Mass of object
m	Effective absolute surface slope
N	Test sample size
n	Cycle number
n	Refractive index of the medium
P	Pressure
$P_{failure}$	Probabilities to failure
P_{th}	Heat current
P_{pd}	Power dissipation
$P_{D(cond)}$	Diode conduction losses
$P_{Q(cond)}$	Conduction losses in transistor
P_{sw}	Switching losses
ΔQ_{th}	The amount of heat stored with each temperature cycle
q	Rate of heat transfer
R_c	Total contact resistance
R_k	Thermal resistance
R_s	Solid contact resistance
R_{shunt}	Resistance
R_{th}	Thermal resistance
$R_{th,forced}$	Thermal resistance in forced air cooling
$R_{th,convection}$	Thermal resistance in natural air cooling
R_{c1}	Contact resistance above TIM
R_{c2}	Contact resistance below TIM
$R_{TIM\ ideal}$	Thermal resistance with ideal TIM
$R_{th}(T,t)$	Degradaded TIM resistance
$R_{th}(T,0)$	Thermal resistance at the beginning
$R(x)$	Reliability of a product
r	Correction factor
r_D	Conduction resistance
r_Q	Conduction resistance
S	Thermo-mechanical stress
T_a	Ambient temperature
T_c	Case temperature of power semiconductor device
T_{hs}	Temperature of heat sink
T_{si}	Surface temperature of emission material
T_j	Junction temperature of power semiconductor device
T_m	Medium temperature for the power cycling
T_{max}	Maximun temperature of the junction
T_{min}	Minumum temperature in power cycling
T_{TIM}	Temperature of thermal interface material

T_1	Temperature
T_2	Temperature
ΔT	Temperature difference
ΔT_j	Temperature differences in junction temperature
t	Time
t_{on}	On – time in power cycling
t_{off}	Off – time in power cycling
t_q	Thyristor recovery time
t_{sw}	Switching time
U_D	Constant voltage drop
U_{DC}	DC – voltage
U_Q	Constant voltage drop
U_{shunt}	Voltage over shunt resistor
$u(t)$	Voltage
$u(\bar{x})$	Standard deviation of the mean
$u(x)$	Type B standard uncertainty
$u_c(y)$	Total uncertainty
v	Speed of electromagnetic waves
$\bar{x}$	Arithmetic mean
x_i	Measurement
Y	Effective gap thickness
Z_{th}	Thermal impedance
β	Shape parameter
β	Constant
ϵ	Surface emissivity
γ	Location parameter / failure free period
η	Scale parameter
λ	Wavelenght
δ	Test setup parameter
σ	Stefan-Boltzmann constant
σ	Effective root mean square surface roughness
σ	Population standard deviation
σ_1	Surface roughness
σ_2	Surface roughness
τ_k	Thermal time constant
τ_{th}	Thermal time constant
x	Interval

1 Introduction

Power semiconductor devices are used in electrical devices designed for power conversion. They appear in almost every field of technology, including consumer goods, industrial applications and transportation. Various benefits are achieved by using power semiconductor devices. These power components enable, for example, variable speed drives (VSD), uninterruptible power supplies (UPS) and higher efficiency of certain power supplies.

However, like with any other electronic component, heat is generated during operation. This heat must be removed efficiently from the power semiconductor package in order to ensure safe operation and higher power densities of electric devices. To overcome this challenge, power semiconductor devices are attached to thermal solutions which are further cooled by liquid or air. Difficulties in thermal management are further provoked by the fact that the sizes of electric devices are decreasing while their performance requirements are increasing. Heat causes several failure mechanisms that can lead to degradation of components. Manufacturers are obsessed to know how reliably electric devices function over designed life time in determined operation conditions.

To improve heat transfer from the power semiconductor device to the heat sink, thermal interface material (TIM) is inserted between the two elements. However, as we will see later in this study, the TIM layer represents the highest thermal resistance in the whole thermal path from the power semiconductor device to the heat sink. Therefore, degradation in TIM layer can cause severe damage to components or to the whole application. Several reliability studies can be found in open literature which are related to thermal interface materials. Different materials have been tested by different researchers using different stresses and stress levels. However, the reliability testing of TIM lacks uniform testing guidelines and the interpretation of results is dependent on researcher's competence.

Power cycling is a well-known reliability test method for power semiconductors. In power cycling, the power component is turned on and off causing heat gradients across elements in the heat transfer path. These heat gradients cause failure mechanisms which occur from mismatches in the coefficient of thermal expansion (CTE) between layers. This is critical for TIM while it is inserted between two layers with different CTE.

There are three main objectives related to this study:

A. Develop and implement an accelerated test method for thermal interface materials and to analyze reliability and life time of certain TIMs
B. To analyze the effect of the interface pressure to the heat transfer from the power semiconductor device to the heat sink
C. To study the heat transfer mechanisms between two solids

For the aging of different TIMs, a mechanical test frame, control circuit and a printed circuit board will be designed and implemented in this thesis. In total of two different thermal interface materials, an elastomer film and a phase change material (PCM), are tested. Moreover, a regression analysis will be done to estimate the thermal performance further. Furthermore, general degradation model is established based on the measurement data.

Chapter 2 introduces power semiconductor devices and applications where components are used. In addition, Chapter 2 discusses losses and thermal models of power semiconductor devices. Chapter 3 presents the actual object of this study: thermal interface material. Heat transfer mechanisms between two solids are also studied in this Chapter. In Chapter 4, the aim is to analyze the reliability aspect and accelerated test methods are introduced. Finally, in Chapter 5, the developed test method is introduced and measurement results are discussed. Futhermore, uncertainty of the measurement results is discussed and conclusions are made.

2 Power semiconductor devices

The motives for this study come from the urge to operate electric devices, such as frequency converter, more reliably. Power semiconductor devices form the main circuit in such application. Therefore, it is natural to begin this study by introducing basic power semiconductor devices and their role in electric products. First, a brief overview of the components that are available is made. Second, applications where power semiconductor devices are used in Kone Oyj, are introduced. Third, losses of power semiconductor devices are discussed. Moreover, cooling of electric components is reviewed. Finally, thermal models and thermal principles are discussed. This Chapter focuses on giving a general overview of power semiconductors devices and topics related to them, thus Chapter does not deeply explain, for example, semiconductor physics.

2.1 Components

Power semiconductor devices are used in variable speed drives (VSD) to alter the frequency and amplitude of the voltage which is fed to an electric motor. Recently, VSDs appear in almost every field of technology, for example in industry (pumps), in consumer goods (washing machines) and in transportation (electric vehicles). Power semiconductor devices can be divided into three main categories which are diodes, thyristors and power transistors. Power transistors can be further divided into bipolar transistors, power MOSFETs (Metal Oxide Semiconductor Field Effect Transistor), GTOs (Gate Turn-Off Thyristor) and IGBTs (Insulated Gate Bipolar Transistor). Depending on application and operating field, different power components are used. Figure 1 presents different power components and the area where they are typically operated.

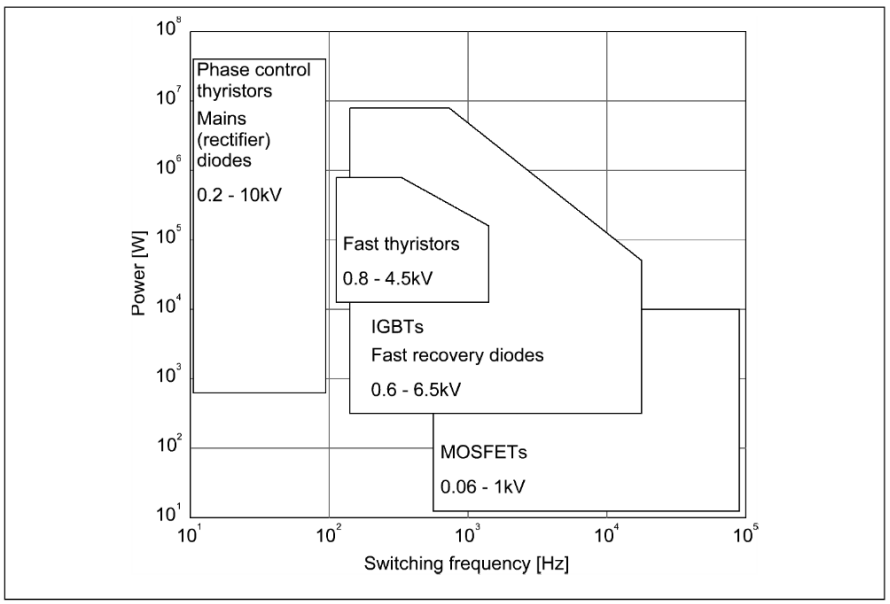

Figure 1: Comparison of different power semiconductor devices. (Volke & Hornkamp, 2012)

2.1.1 Diodes

Diode is a component which works as a valve in electrical circuits. If a positive anode-cathode voltage is applied, it is forward biased and begins to conduct. Usually the required forward voltage is around 1V. With negative voltage, the diode is reverse biased and acts as an open

circuit. In reverse biased state, a negligible leakage current flows through the diode until the reverse breakdown voltage is achieved (Mohan, et al., 2003). In ideal case, the diode turns rapidly after the voltage across the diode changes. Operation characteristics of a diode can be seen in Figure 2.

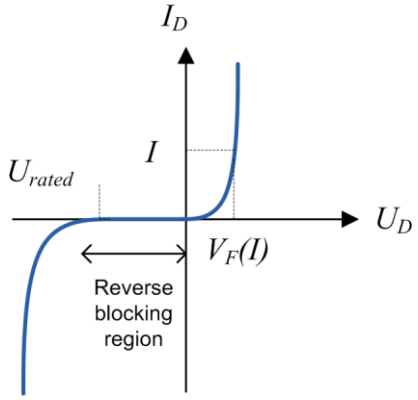

Figure 2: *I-U* characteristics of diode.

2.1.2 Thyristors

Thyristors operate in almost the same way as diodes except, along with positive anode-cathode voltage, a pulse of positive gate current must be applied to the control terminal (gate). The control current can be removed after the thyristor has started to conduct and the conduction occurs until anode current tries to go negative. During conduction, the thyristor can not be turned off.

An important parameter regarding the thyristors is recovery time t_q. This is the time in which a thyristor can not be turned on after the anode current has reached zero. If anode-cathode voltage turns positive before the time t_q has passed, the device may prematurely turn on and damage itself or other components. The operation characteristics of thyristors is shown in Figure 3.

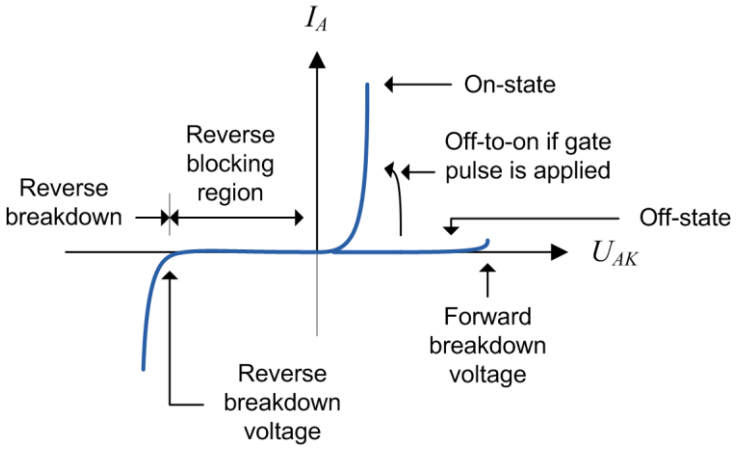

Figure 3: Thyristor characteristics.

2.1.3 Power transistors

As mentioned, several power transistors are used to alter the frequency and amplitude of voltage. These include bipolar transistors, MOSFETs, IGBTs and GTOs. A common factor is that a power transistor can be switched on and off anytime by control terminal.

Ideal power transistors do not have leakage current and the current flows only in the direction of the arrow when switched on. Obviously, real power transistors do not function as ideal switches and dissipation of heat occurs. This must be taken into consideration in order to avoid over heating of devices. Fortunately, the dissipation of power semiconductors is fairly generic which means that the dissipation analysis is rather similar for all components (Mohan, et al., 2003). The switching characteristics of power transistors and dissipation of heat are further discussed in Section 2.3.

Power semiconductor devices consist of various layers. Figure 4 presents the different layers in a typical IGBT module which is attached to a heat sink. A silicon die is soldered to the direct bond copper (DBC) layer, which is further soldered to a copper baseplate. A thermal interface material layer is installed between aluminum heat sink and copper baseplate. Heat sinks are discussed more in Section 2.4.1 and thermal interface materials in Section 3.3.2.

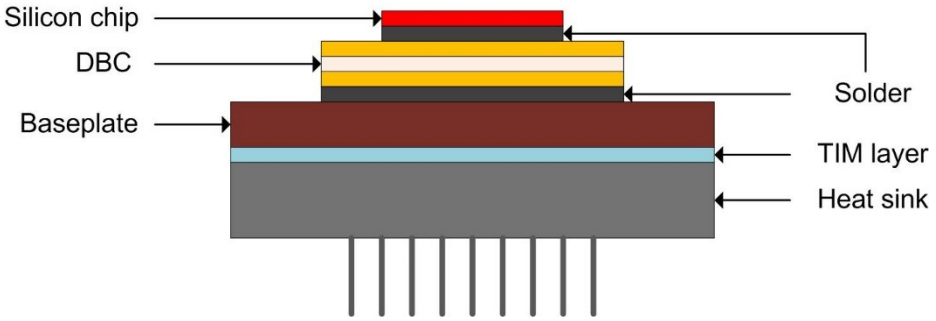

Figure 4: Different layers in the power semiconductor devices along with a heat sink.

2.2 Power semiconductor devices in Kone products

Kone Oyj is one of the world's leading elevator and escalator manufacturing companies. Elevators are almost always operated with electric motors. In order to achieve stepless speed control and a good dynamic control response, electric motors are controlled by frequency converters. A good dynamic response to speed variations from electric motor is especially important in elevator drives while a person is experiencing these variations.

Several safety functions exist for elevator drives. In case of power failure, emergency brakes are activated. The brakes can not be mechanically switched off and rescue brake opening (RBO) unit is required. The control of the brakes is done with power transistors in RBO unit. Elevator drive and frequency converter is discussed in more detail below.

2.2.1 Elevator drive and frequency converter

Electric drive converts electrical energy into mechanical energy. Electric drives consist of voltage source, frequency converter, electric motor and control electronics. In elevator applications, the voltage source is usually constant grid voltage which can be three-phase or one-phase power system. In addition, batteries and supercapacitors can be used as voltage source, for example, in electric vehicles. In such a case, frequency converter is replaced by

an inverter. A block-diagram of an electrical drive which controls elevator can be seen in Figure 5.

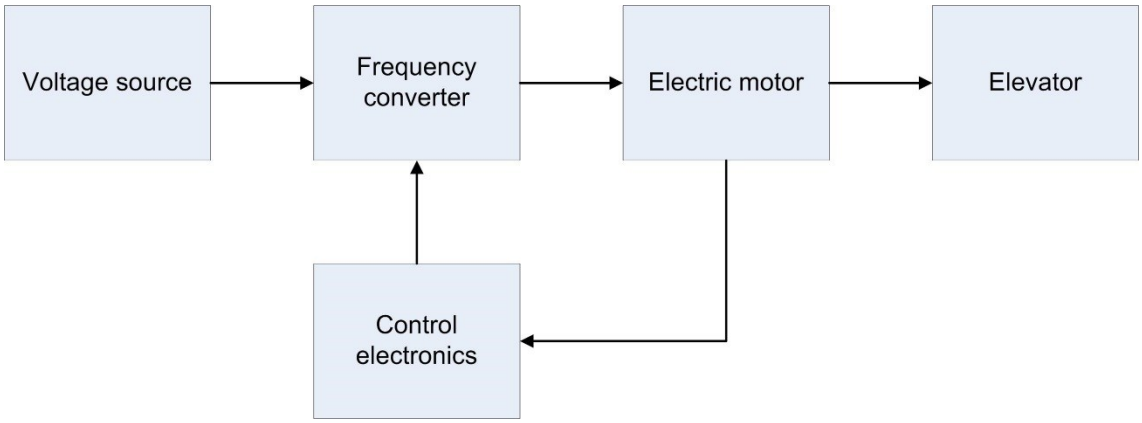

Figure 5: A block diagram of electric drive and elevator.

A frequency converter is used to modify the frequency and magnitude of a constant grid voltage. The device consists of rectifier circuit, DC circuit, and inverter circuit along with filters and control electronics. The rectifier unit converts the three-phase or one-phase voltage to DC voltage. The simplest rectifier circuit is made of a diode bridge. However, self-commutating bridges (power transistor bridges) can also be used in order to achieve reactive power control, regenerative operation and higher DC voltage. The DC circuit consist of capacitors which act as energy storages for the inverter unit. The inverter unit converts DC voltage into desired three – phase alternating voltage. Inverter circuits are made of power transistors in parallel with diodes for the reactive current. In low voltage high power applications, IGBTs are the most common power semiconductors to be used in an inverter unit. (Mohan, et al., 2003)

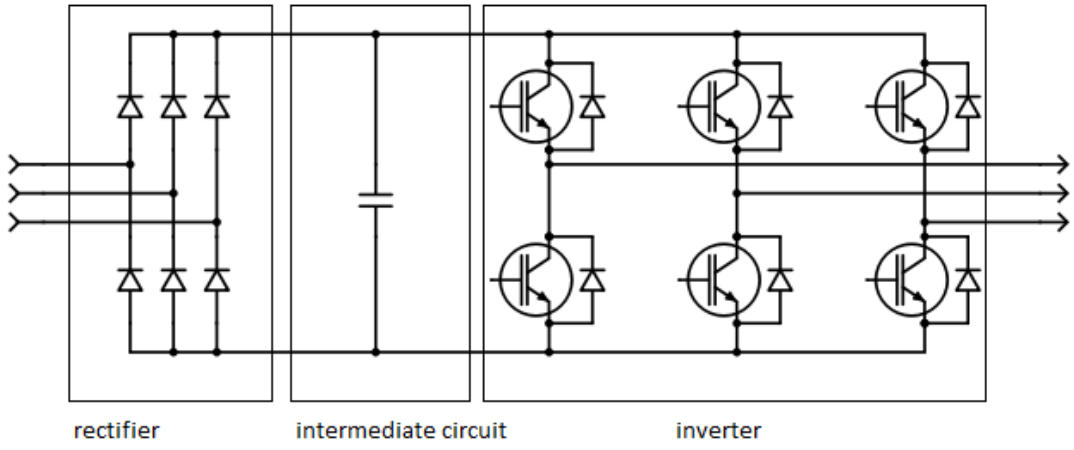

Figure 6: Voltage source frequency converter. On the left is a rectifier unit, in the middle is the intermediate circuit and on the right is an inverter unit.

The variable AC output voltage in a voltage source converter is achieved typically with Pulse-Width Modulation (PWM). In the PWM the power semiconductor switches are turned off and on to achieve alternating voltage for the output of the frequency converter. Frequency

and magnitude can be altered by changing the polarity and width of the output pulses. The number of the pulses used in half period has an effect on the RMS value of the harmonic voltages, which decreases with increased pulse numbers (Kyyrä, 2013). The PWM is illustrated in Figure 7. In the upper figure, density and thickness of pulses is lower resulting in lower frequency and magnitude of output voltage. In the lower figure, density and thickness of pulses is higher resulting in high frequency and higher magnitude of output voltage.

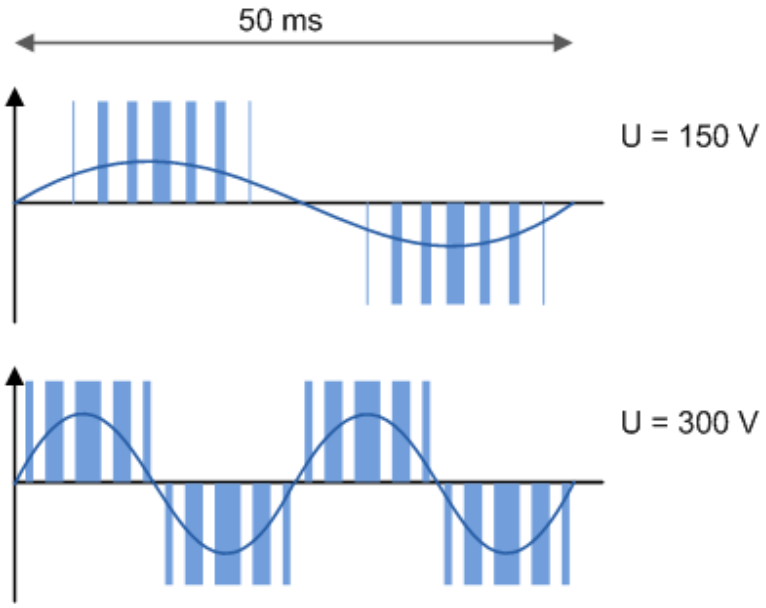

Figure 7: Pulse-Width Modulation.

2.3 Losses in power semiconductor devices

With ideal power semiconductor devices, the dissipation of heat would not occur. However, real components generate heat during operation. The dissipation of heat is generally called losses in electronic components. This Section explains why and how the losses are generated.

Losses in power semiconductor devices can be divided into turn-on, turn-off, off-state and on-state losses. Turn-on and turn-off losses are usually called simply switching losses. On-state energy losses are also called conduction losses. In general losses occur always when there is a voltage drop over and current flow through the power semiconductor device simultaneously. Furthermore, losses appear due to the non-idealities of power semiconductor devices. Off-state losses, for example, occur due to the leakage current of power semiconductors and on-state losses due to the on-state voltage drop. With ideal components the leakage current and on-state voltage drop is considered zero. The total energy losses of power semiconductors is: (Niiranen, 2007)

$$E_{tot} = E_{off} + E_{cond} + E_{sw} \quad (1)$$

where, E_{tot} is total losses, E_{off} is off-state energy losses, E_{cond} is conduction losses and E_{sw} is switching losses. According to Niiranen (2007), the leakage current is usually relatively small and can be assumed zero. Therefore off-state energy losses are considered zero ($E_{off} = 0$).

Conduction losses can be calculated with device's dc electrical characteristics. Equations (2) and (3) are derived by Berringer et al. (1995). The power dissipation in a device can be calculated from the average current and from corresponding constant voltage drop over the device. Futhermore, the power dissipation in resistive element is calculated with device's RMS current. Total losses is the sum of previous elemets. For conduction losses in transistors:

$$P_{Q(cond)} = I_Q U_Q + I_{Q_{RMS}}^2 r_Q \tag{2}$$

where I_Q is the average current, U_Q the constant voltage drop and r_Q is the conduction resistance in transistor. The equations for the average current and the RMS current are functions of duty cycle. For a paraller diode, conduction losses can be written similarly:

$$P_{D(cond)} = I_D U_D + I_{D_{RMS}}^2 r_D \tag{3}$$

Furthermore, the total conduction losses in inverter are:

$$6 * (P_{Q(cond)} + P_{D(cond)}) \tag{4}$$

Swithing energy losses can be calculated from typical swithing characteristics of power semiconductor device. The swithing energy varies over the sine wave period since it is a function of drain current. According to Berringer et al. (1995) switching losses for power semiconductor device is:

$$P_{sw} = \frac{f_{sw} E_{max}}{\pi} \tag{5}$$

where f_c is switching frequency, E_{max} is the total switching losses which is calculated at the peak current of the sine wave. From Equation (5) it can be seen that switching losses are directly proportional to the switching frequency of a power semiconductor device.

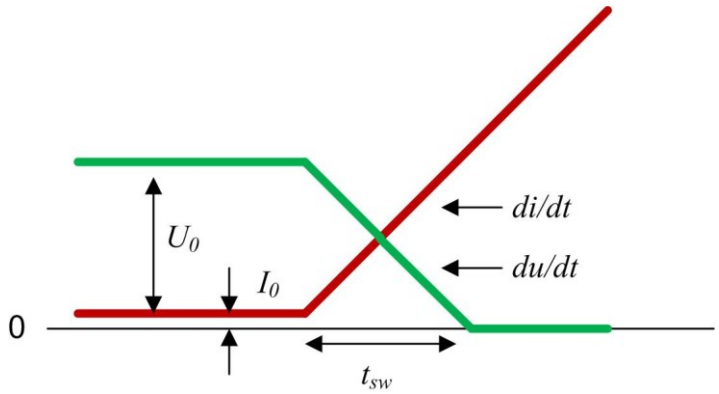

Figure 8: Turn-on of the power semiconductor device.

2.4 Cooling of power semiconductor devices

Heat losses are removed from a power semiconductor device to ensure a safe operation of electric devices. Moreover, efficient cooling provides higher power densities of components. Cooling is usually made so that the components are attached first to heat sinks which are

further cooled with a cooling medium. The cooling medium can be air or liquid such as water. Air cooling can be further divided into forced air cooling and into natural air cooling.

2.4.1 Heat sink

Heat sinks are highly thermally conductive elements which are attached to the bottom of a power semiconductor device. Aluminum is typically used as material. The purpose of a heat sink is to transfer thermal energy from a power semiconductor device to a cooling medium as efficiently as possible. In addition, a heat sink may function as a mechanical element, as a part of, for example, an inverter (Volke & Hornkamp, 2012).

2.4.2 Air cooling

Air cooling may be done either by natural or by forced cooling. Heat energy is transferred from the heat sink by radiation and convection. The advantage in air cooling is that the cooling is relatively easy to arrange and even easier if natural air cooling is used. Natural air cooling is based on the fact that warm air rises upwards and is replaced by cold air. If the natural cooling is not efficient enough, a forced air cooling must be used. Ventilator can be placed below or above of the heat sink and the cool air is blown or pulled through the fins of the heat sink. In natural and forced cooling, the cool air is usually obtained from surrounding air. Therefore, it is important to keep the ambient air near the cooling process at an acceptable level. Additional difficulties in air cooling are impurities in the cool air such as dust, moisture and chlorine. These conditions can be reduced by filtering the cool air or by keeping the cool air in the device with higher pressure relative to the ambient air. (Niiranen, 2007)

In forced air cooling, the thermal resistance between surrounding air and heat sink can be influenced greatly. The thermal resistance can be expressed as a function of cool air speed. Thermal resistance decreases as cool air speed increases. This holds true to a certain point where thermal resistance does not decrease further and evens to a certain value. The superiority of forced cooling can be studied from equation given by (Volke & Hornkamp, 2012):

$$R_{th,forced} = rR_{th,convection} \tag{6}$$

where r is a correction factor which varies between 0 and 1 and is dependent on cool air speed. $R_{th,forced}$ is thermal resistance in forced air cooling and $R_{th,convection}$ is thermal resistance in natural air cooling.

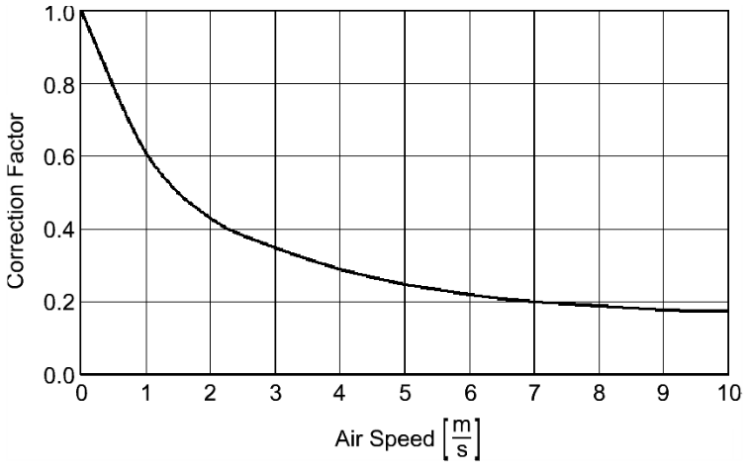

Figure 9: Example of R_{th} between heat sink and ambient as function of air speed. (Volke & Hornkamp, 2012)

2.4.3 Liquid cooling

In liquid cooling the heat sink is cooled by fluid which flows through it. Water is often used as a cooling medium because of its great cooling abilities and a relatively low cost. Compared to air cooling, liquid cooling has better efficiency towards a power density unit. Heat energy is transferred more easily into water than it is transferred into air. However, being efficient in heat transfer, liquid cooling has several disadvantages in a cooling process. First, an external heat exchanger and other cooling equipment (e.g a cooling circuit, pumps, valves) must be used, which can prove to be expensive. Second, water may cause corrosion in a cooling circuit which can reduce the efficiency of liquid cooling. Corrosion may even cause the entire system to fail. Moreover, in cold places glycol must be used in order to prevent the cooling medium from freezing. In this case, it must be borne in mind that glycol water mixture lacks greatly in cooling abilities compared to pure water. Mixtures should be avoided if they are not required. Finally, even with liquid cooling, an additional air cooling circuit may be required to ensure that all components are cooled sufficiently. (Niiranen, 2007)

Corrosion in liquid cooling circuits can be prevented in several ways. Few suggestions are given by Volke & Hornkamp (2012): cooling medium has to be ensured to flow continously, deionised and demineralised water and corrosion inhibitors can be used, chloride content can be reduced in water and closed cooling circuits can be used. In addition, Niiranen (2007) notes that using similar materials in cooling circuits helps to prevent the corrosion.

A few parameters should be kept in mind when considering liquid cooling: Flow velocity of cooling medium and drop pressure in the total cooling circuit. Those influence the cooling efficiency of a liquid cooling circuit. The flow rate follows the pressure drop with exponential function as it is shown in Figure 10. (Volke & Hornkamp, 2012)

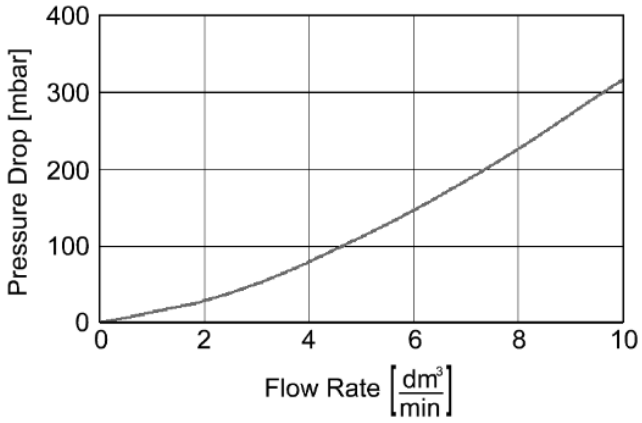

Figure 10: Pressure drop over cooling circuit vs flow rate of cooling medium. (Volke & Hornkamp, 2012)

2.5 Thermal models

It is useful to know the dynamic thermal behaviour of power semiconductor devices when designing cooling of the system. Power semiconductor devices along with the heat sink consist of several different layers which all have thermal resistance and thermal capacity in between. Different layers were shown in Chapter 2: Figure 4. With the thermal resistance and thermal capacity, thermal models for power semiconductors can be established. The thermal model is needed to determine the thermal behaviour during changes in power dissipation. The thermal response of a component is also described with a curve of thermal resistance change (Niiranen, 2007). Furthermore, according to Volke & Hornkamp (2012), thermal models help the design engineers to dimension the required heat sink, and dynamic temperature variations can be calculated efficiently with modern computers. This Section begins by introducing thermal principles which are needed for establishing thermal models and are useful for the analysis of the other subjects of this study. Afterward, two different thermal models are introduced.

2.5.1 Fundamentals of heat transfer

Heat transfer

Heat transfer is the movement of heat flow which results from temperature difference. Temperature difference indicates the amount of thermal energy which is stored in material. Heat flow is thermal energy movement between the two objects. At the atomic level, the thermal energy is related to the kinetic energy of molecules. The higher the temperature of material, the more kinetic energy these molecules posesses. Kinetic energy appears as the linear and vibrational movement of molecules. Regions containing greater molecular kinetic energy pass this energy to regions with less kinetic energy. (Tong, 2011)

Heat transfer mechanisms are usually divided into conduction, convection and radiation. Conduction occurs when a temperature gradient exists within continous, non-moving medium, solid or stationary fluid. Convection occurs when a surface is in contact with moving fluid, liquid or gas, with a different temperature and the heat is transferred between the surface and fluid. In radiation, heat energy is transferred by electromagnetic energy emitted by the surfaces. (Tong, 2011)

Conduction

The conduction of heat is direct transfer from one object to another, whereas convection and radiation do not need a direct contact between two objects. And to further emphasize, the conduction of heat requires an actual contact of two surfaces and the heat is transffered by conduction only in the parts where two surfaces actually mate. Thermal conduction is a dominant mechanism for heat transfer within solids. In addition, liquids and gases conduct thermal energy but to a significantly lesser extent. This is due to the fact that when material changes its phase from solid to liquid and from liquid to gas, the number of intermolecular bonds decrease, and there is more freedom for thermal motion of the molecules. This makes the thermal conductivity lower in liquids and gasses. (Tong, 2011)

Based on Fourie's law of heat conduction, for a one dimensional, steady state heat flow, the rate at which heat is conducted through a material is given in Equation (7). (Bejan & Kraus, 2003)

$$q = -kA\frac{dT}{dx} \tag{7}$$

where q is the rate of heat transfer, k is the thermal conductivity of the material, A is the cross-sectional area for heat flow, dT is the temperature difference across two solids, and dx is the path length. dT/dx is also called the temperature gradient, which is negative thus the equation needs a minus sign to ensure that the heat flow is positive. In Equation (7), we defined thermal conductivity as k. Thermal conductivity is the ability of material to transfer thermal energy. The higher the thermal conductivity of the material, the lower the temperature gradient of material is. Conductivity is independent of material size, shape or orientation (Tong, 2011).

Convection

Heat transfer from one location to another location by movement of fluids is called convection. Convection occurs between two surfaces due to a relative velocity between them. If temperature rises, the volume of fluids increases. Therefore, the density of fluids decreases. This density difference gives a rise to fluids with greater temperature. This phenomenon can be seen from the fact that warm air rises upwards. Another example is a heating of water in a pot which makes the hot water rise from the bottom of the pot to its surface. This is called natural convection. (Bejan & Kraus, 2003)

In Forced convection, fluids are forced from one location to another by fans or pumps. The difference between natural and forced convection is that in forced convection the externally imposed flow is known while in natural convection it results from the interaction of density differences. This makes the analysis of natural convection more difficult. (Bejan & Kraus, 2003) The most practical application for convection is a solid surface and a fluid circulating it. The heat exchange between solid surface and circulating fluid is expressed by Newton's law: (Tong, 2011)

$$q = hA\Delta T \tag{8}$$

where, h is convection heat transfer coefficient.

Radiation

In thermal radiation, heat energy is transferred by electromagnetic waves. Electromagnetic waves are formed when materials change their internal energy on a molecular level, thus emitting and/or absorbing photons. All materials constantly emit and absorb electromagnetic waves and the strength of emission is dependent on the temperature of the material as well as wavelength λ and frequency f. Electromagnetic radiation can be characterized by the basic equation of wave motion: (Bejan & Kraus, 2003)

$$v = \lambda f \tag{9}$$

where, v is the speed of electromagnetic waves, λ is wavelength and f is frequency. For electromagnetic waves,

$$v = c = \frac{c_0}{n} \tag{10}$$

where n is a refractive index of the medium, c is speed of light and c_0 is speed of light in vacuum. Thermal radiation does not require a medium to transfer heat energy, unlike thermal conduction and convection. Due to this fact, the thermal radiation becomes a dominant heat transfer method in low pressures and outer space applications (vacuums). Another feature, which separates thermal radiation from conduction and convection, is temperature dependency. Intensity of thermal radiation is proportional to the fourth power of temperature while intensity of conduction and convection is somewhat linearly dependent on temperature. For this reason, thermal radiation tends to become significant in high temperature applications such as solar emission and fires. The transfer of energy by electromagnetic waves, for infinite parallel plates, can be expressed by Stefan-Boltmann's Law (Tong, 2011):

$$q = \epsilon\sigma A(T_{s1}^4 - T_{s2}^4) \tag{11}$$

where, ϵ is surface emissivity, σ is Stefan-Boltzmann constant and T_{si} is the surface temperature of emission material.

Resistance

Thermal resistance resists the heat flow between two temperatures in a similar way that resistance resists current flow in electrical circuits. Therefore, the analysis of heat flow is fairly identical to the analysis of current flow in electrical circuits. Thermal resitance is given in Equation (12). (Bejan & Kraus, 2003)

$$R_{th} = \frac{T_1 - T_2}{P_{th}} = \frac{L}{kA} \tag{12}$$

where, T_1 and T_2 are temperatures, P_{th} is heat flow, k is thermal conductivity of the medium, L is path length and A is cross-sectional area. The equation above assumes that k and A are constant. The analogy to electrical circuits is obvious while $T_1 - T_2 = \Delta T$ is the potential difference and P_{th} is the electrical current in electrical circuits.

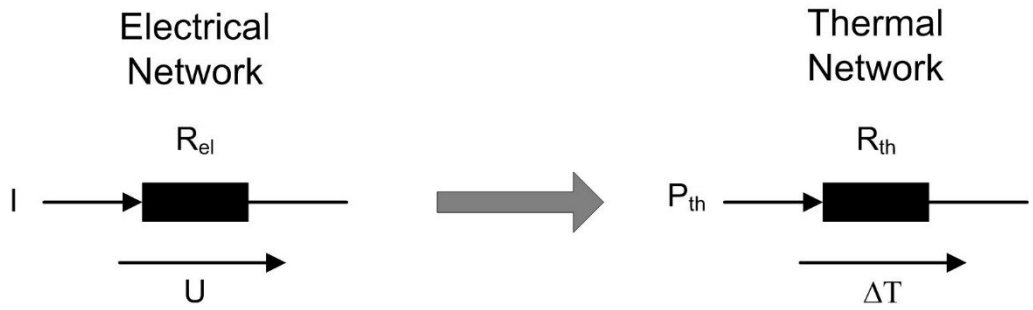

Figure 11: Electrical network vs Thermal network.

Capacity

Thermal resistance is fairly similar to its electrical variant, an so is thermal capacity (also known as heat capacity). Just like electrical capacitance, thermal capacity functions as energy storage. Thermal capacity describes the ability of a medium to store heat energy when temperature changes. The ability to store heat energy depends on the material properties and is described with specific thermal capacity c_{th}. Thermal capacity can be written as follows:

$$C_{th} = \frac{\Delta Q_{th}}{\Delta T} \tag{13}$$

where ΔQ_{th} is the amount of heat stored with each temperature cycle ΔT. For the amount of heat ΔQ_{th} stored, we may write:

$$\Delta Q_{th} = c_{th} m \Delta T \tag{14}$$

where c_{th} is specific thermal capacity and m is mass of object. Therefore, the thermal capacity can be shorted into:

$$C_{th} = c_{th} m \tag{15}$$

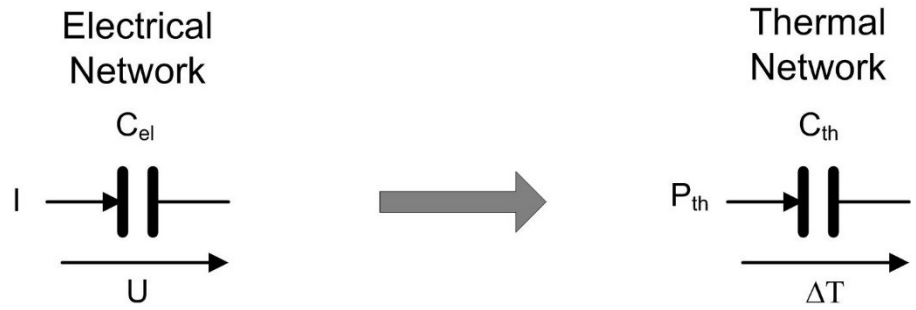

Figure 12: Electrical network vs Thermal network.

Impedance

Thermal impedance is formed of thermal resistance R_{th} and of thermal capacity C_{th}. Because of the ability of material to store and release heat energy the thermal impedance must be presented in time domain. Consider, for example, a steel hotplate which has thermal resistance and thermal capacity. It takes a while to heat the hotplate to its maximum

temperature because its ability to store heat energy since the hotplate has thermal capacity. After the heat storage is full, the hotplate is heated to its maximum temperature value. If heating is turned off, the heat storage dissipates heat energy from the heat storage with time constant that is dependent on material properties. For thermal impedance we may write: (Volke & Hornkamp, 2012)

$$Z_{th} = \frac{\Delta T(t)}{P_{th}} = R_{th}(1 - e^{-\frac{t}{\tau_{th}}}) \tag{16}$$

where τ_{th} is thermal time constant,

$$\tau_{th} = R_{th}C_{th} \tag{17}$$

Now we have established basic thermal concepts which should help to understand thermal behaviour of different materials. Also, with previous concepts the thermal models for power semiconductor devices can be established. This is done in the following Section.

2.5.2 Foster and Cauer model

Two thermal models for power semiconductor devices are used which are called the Cauer model (continued fraction model) and the Foster model (partial fraction model). These models are shown in Figure 13. The difference between the Cauer model and the Foster model is further explained by Volke & Hornkamp (2012) and Niiranen (2007): The Cauer model is based on actual physical layers and materials of the power electronics module and requires parameters from mechanical dimensions and properties. However, this is not the case with the Foster model, which does not require precise material dimensioning and has no relation to the actual physical layers and materials. Nonetheless, the Foster model provides sufficient information about the dynamic thermal response. Cauer model is also difficult to use without simulations, and if such tools are not available, the Foster model is preferred. The number of RC-circuits enhances the accuracy in the Cauer model while in the Foster model the number of RC – circuits depends on measuring points and is usually set between 3 and 6. Furthermore, it is noted by Niiranen (2007) that power semiconductor manufacturers inform parameters such as R_{th} and time constant $\tau_{th} = R_{th}C_{th}$ for Foster model.

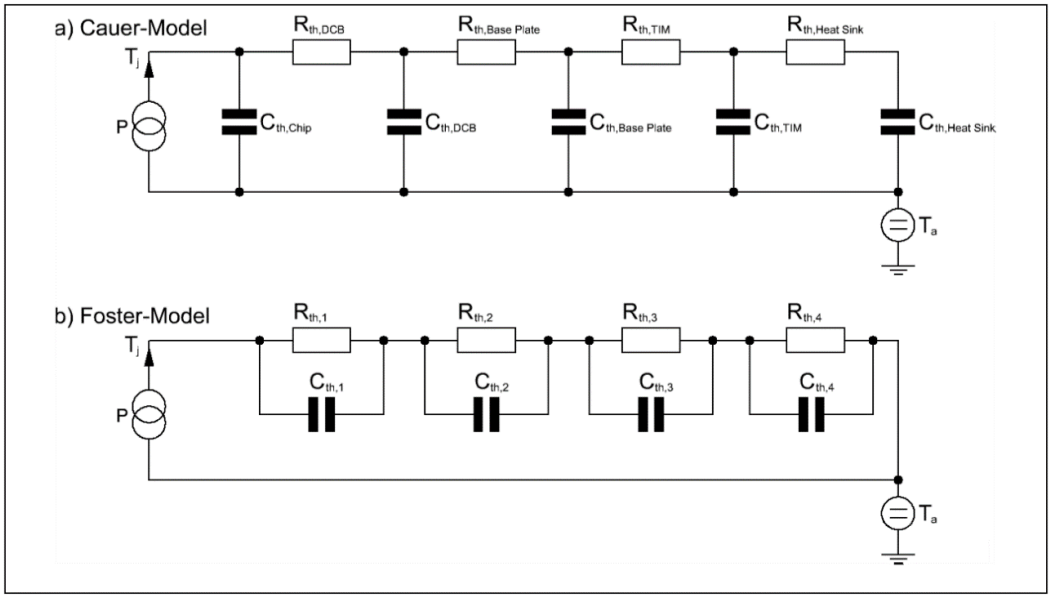

Figure 13: Thermal models for power semiconductor devices. a) Cauer model and b) Foster model. (Volke & Hornkamp, 2012)

The thermal impedance of the whole model can be measured or calculated analytically. If parameters for Foster model are given, the thermal impedance Z_{th} can be calculated according to Equation (18) (Niiranen, 2007):

$$Z_{th} = \sum_{k=1}^{n} \mathrm{R_k}(1 - e^{-\frac{t}{\tau_k}}) \tag{18}$$

After obtaining the thermal impedance of the device, the junction temperature T_j can be determined by measuring case temperature T_c and using the following equation:

$$T_j = P_{th}\, Z_{th} + T_c \tag{19}$$

However, it is possible that manufacturers do not provide resistances and time constants. In this case, the thermal impedance can be determined by measuring heating of power semiconductor T_j and T_c. In general this is done by using stepwise voltage dissipation P_{th} for power semiconductor at time $t = 0$. After measuring temperatures, the thermal impedance of the design can be obtained (Niiranen, 2007):

$$Z_{th} = \frac{T_j - T_c}{P_{th}} \tag{20}$$

With thermal models, users can simulate the thermal behaviour of power semiconductor systems. The following simulation example is given by Volke & Hornkamp (2012). IGBT module has been simulated with Simplorer. Simulation has taken the layer design and material parameters into account. Virtual power dissipation is exposed and a thermal response can be seen. From this example it can be seen how much heat is captured in each layer between power semiconductor and its heat sink.

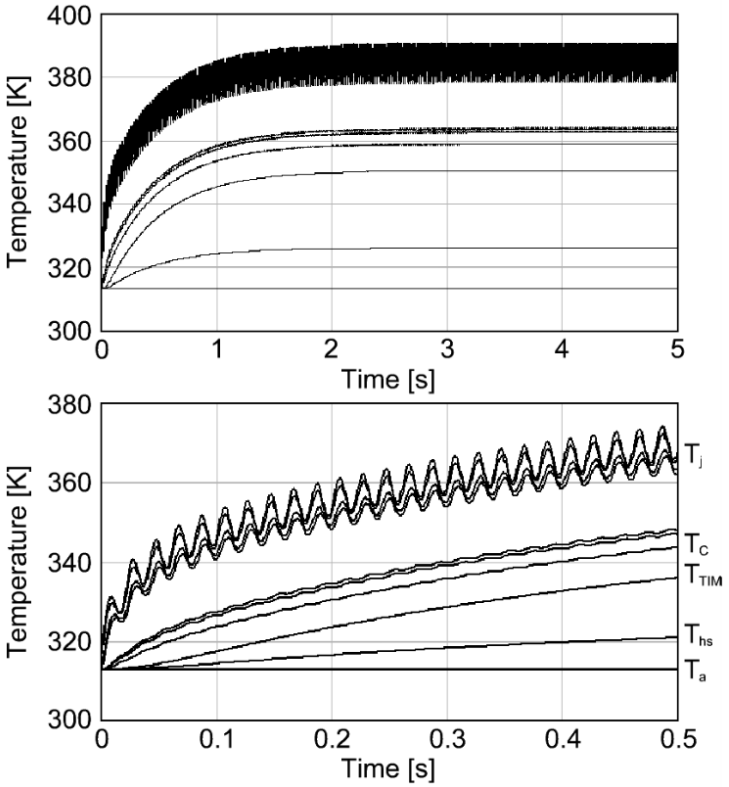

Figure 14: Thermal model simulation for an IGBT module. (Volke & Hornkamp, 2012)

On the upper graph of Figure 14, the time scale is from 0 s to 5 s and on the lower graph of Figure 14 the time scale is from 0 s to 0.5 s. Furthermore, T_j is junction temperature, T_c is case temperature, T_{TIM} is thermal interface material temperature, T_{hs} is temperature of heat sink and T_a is ambient temperature. From Figure 14 it can be seen that the temperature difference is the highest between T_c and T_{hs}. This interval is studied in this thesis and is discussed more in the following Chapter.

3 Thermal Interface Material

Thermal interface materials are used to thermally connect various components to each other. While the power densities of electronic components are increasing, there is an increased demand for reliable and efficient thermal energy transfer materials. Thermal interface materials serve two purposes in an electronic device. The first TIM (TIM 1) is used between the die package and a heat spreader while second TIM (TIM 2) is used between the heat spreader and a heat sink. Some TIMs are produced to be used only in TIM 1 or TIM 2 while others can be used for either application. (Tong, 2011)

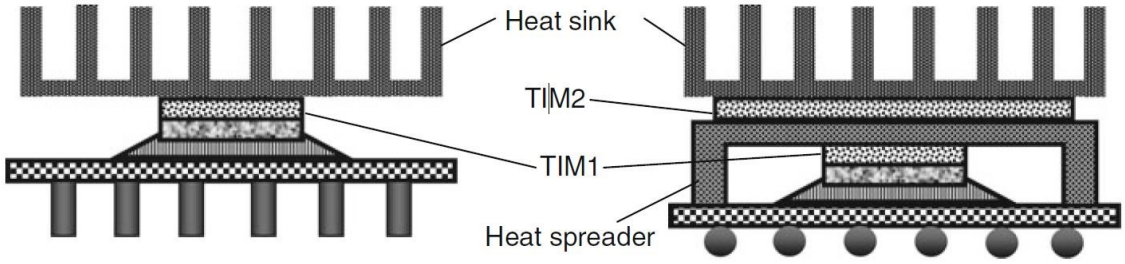

Figure 15: TIM 1 is used between silicon die and heat spreader while TIM 2 is used between heat spreader and heat sink. (Tong, 2011)

The previous Chapter introduced power semiconductor devices and their role in electric products. Losses and thermal subjects were also discussed. However, to fully understand heat transfer between two solids, one should know how surface features effects heat transfer between two solid layers. Therefore, this Chapter analyses the interface between the heat sink and the power semiconductor device in more detail. As a second part of this Chapter, a review of important characteristics of TIMs are made and comparison of different thermal interface materials is done.

3.1 Surface chemistry

It is commonly known that when two surfaces are joined, imperfect interfaces are formed. Real surfaces are not perfectly smooth and flat causing the actual contact area to decrease. The actual interface consists of numerous discrete micro-contacts. The size of the contact area is dependent on various parameters including surface roughness, the physical properties of the contacting asperities and the contact pressure. Furthermore, the distribution of contact spots is controlled by the flatness of solids, elastic and plastic properties and mechanical load. In this type of joint, micro and macro gaps are formed which are occupied by substances, for example air. Problems exist since the thermal conductivity of substances is typically much lower than thermal conductivity in contacting solids. (Bejan & Kraus, 2003) This phenomenon can be seen in Figure 16.

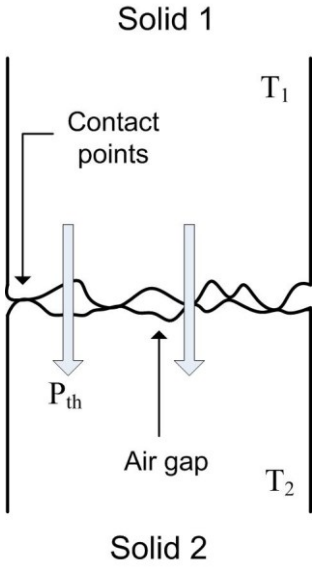

Figure 16: Heat flow through two solid surfaces.

The principal heat transfer method (conduction, convection, radiation) through a solid-solid interface is dependent on interface type. Several types of interfaces exist. These are mainly divided into nonconforming smooth solids (Figure 17 a), conforming rough solids (Figure 17 b) and nonconforming rough solids (Figure 17 c). In case of conforming rough surfaces, for example, heat is transferred mainly by conduction. The main purpose of thermal management is to ensure a long term lifetime and functioning of electronic components. Knowledge of the thermal behaviour of the interface aids this objective. The following Section derives thermal joint conductance and joint resistance between a heat sink and a power semiconductor device.

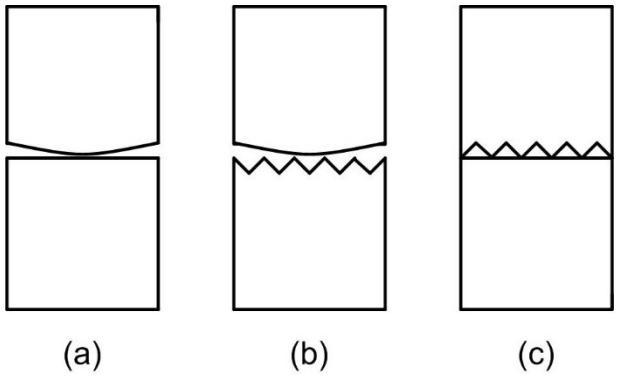

Figure 17: Three types of joints. a) nonconforming smooth solid, b) nonconforming rough solid, c) conforming rough solid.

3.1.1 Interface conductance and resistance

According to Bejan & Kraus (2003), if two solid surfaces are joined together, the actual contact area between these surfaces can be reduced even to 1-2 % of the apparent area, for lightly loaded interfaces. The heat transfer across such interface is thus performed through solid to solid area as well as through a non contact area. The total heat flow across this interface occurs by conduction through the actual area, conduction through the substance in the gap and by radiation across the gap. Radiation comes into consideration if surface temperatures are high, otherwise it can be ignored. This restriction, which heat flow must

cross, is referred to as thermal contact resistance R_c. If temperatures across the joint and heat flow through the joint are known, Equation (12) can be used to calculate thermal contact resistance. However, by analyzing surface features in more detail, one can see how the contact resistance can be influenced.

For a power electronic device, a conforming rough surface model can be assumed (Section 3.1, Figure 17 b). The formed air gaps are so small that thermal energy is mainly transferred by conduction and not by convection. Radiation can be ignored while it is negligible or nonexistent. Following derivation, Equations (21) – (29), for thermal interface conductance is done by Yovanovich (1997).

The thermal interface conductance h_c is the sum of solid contact conductance and gap conductance,

$$h_c = h_s + h_g = 1.25 k_s \frac{m}{\sigma} \left(\frac{P}{H}\right)^{0.95} + \frac{k_g}{Y + \sigma M} \tag{21}$$

where, h_s is solid contact conductance, h_g is the gap conductance, k_s is the harmonic mean thermal conductivity for solid 1 and solid 2,

$$k_s = \frac{2 k_1 k_2}{k_1 + k_2} \tag{22}$$

where, $k_1$and k_2 are thermal conductivities of surfaces, σ is the effective root mean square (rms) surface roughness,

$$\sigma = (\sigma_1^2 + \sigma_2^2)^{0.5} \tag{23}$$

m is the effective absolute surface slope,

$$m = (m_1^2 + m_2^2)^{0.5} \tag{24}$$

For an aluminum heat sink and ceramic packages, m can be approximated as:

$$m = 0.125\ (\sigma \times 10^6)^{0.402} \tag{25}$$

which was developed for the surface roughness range:

$$0.216\ \mu m \leq \sigma < 9.6\ \mu m \tag{26}$$

Furthermore, H is the surface microhardness of the softer material and, P is the contact pressure. According to Yovanovich (1997) the microhardness is hard to define while it is dependent on several physical and geometric parameters. M stands for gas parameter and is, for example, dependent on gas pressure, the temperature, thermal accommodation coefficients and Prandtl number. k_g is the conductivity in the gaps between two surfaces. Y is the effective gap thickness and can be calculated by power-law correlation equation:

$$Y = 1.53 \sigma \left(\frac{P}{H}\right)^{-0.097} \tag{27}$$

The thermal resistance is inverse of thermal conductance. Thus, the solid contact resistance R_s can be calculated according to Equation (28).

$$R_s = \frac{1}{h_s} = \frac{0.8\sigma}{mk_s}\left(\frac{H}{P}\right)^{0.95} \quad (28)$$

3.1.2 TIM contact resistance

To reduce the total thermal contact resistance R_c, gaps and voids are filled with TIMs. With TIMs, the thermal resistance of interface is considerably lower though it still represents the highest resistance in the whole heat transfer path as discussed in Chapter 2.5 and was shown in Figure 14. Several different TIMs can be used varying from thermal greases to highly conductive thermal films and thermal pads. Different materials and material properties are studied in Section 3.3.

Ideal case analysis

In ideal case analysis, the formed voids and gaps are filled completely and the bulk resistance (R_{bulk}), which exist due to the thickness and finite thermal conductivity of TIMs, is ignored. Furthermore, if perfect wetting of thermal greases is assumed, gas parameter M is considered zero. (Tong, 2011) Hence, the ideal thermal resistance of TIM $R_{TIM\ ideal}$, can be calculated according to Equation (29): (Prasher, 2006)

$$R_{TIM\ ideal} = \frac{1.53\sigma}{k_{TIM}}\left(\frac{H}{P}\right)^{0.097} \quad (29)$$

Equation (29) assumes plastic deformation and two nominally flat surfaces. Now in the junction of two metals, solid contact resistance R_s and $R_{TIM\ ideal}$ are in parallel and total contact resistance can be written as:

$$R_c = \frac{R_{TIM\ ideal}R_s}{R_{TIM\ ideal} + R_s} \quad (30)$$

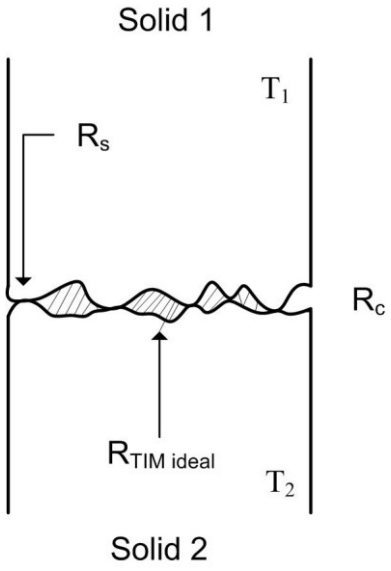

Figure 18: In ideal case the voids and gaps are completely filled and R_{bulk} is ignored.

Since the recent model is developed for bare surfaces, for most of TIMs it can not be applied. According to Prasher (2006), ideal TIMs are not possible to achieve in reality. As mentioned, Equation (29) assumes an ideal wetting of TIMs, which means that the voids and gaps are completely filled. Moreover, TIMs also consist of bulk resistance. This results in that Equation (29) can be used only to estimate the thermal performance of TIMs. For thermal greases ideal wetting can be assumed in some cases. However, with thermal compounds, elastomers and tapes, the joint conductance problem becomes more complicated and the previous model can not be used. The thermal performance of those TIMs might fall short from given Equations.

Actual case analysis

In literature (R & S, 2001), (Rohsenow, et al., 1998), (Grujicic, et al., 2005) there are several mentions of the work done to model the actual contact resistance between thermal interface material and metal surfaces. Both analytical and experimental research has been done by several researchers. Basically, the resistance which the heat flow must cross, is divided into contact resistances R_{c1}, R_{c2} and bulk resistance of TIMs. Bulk resistance is dependent on bond line thickness (BLT) and thermal conductivity k_{TIM}. The thermal resistance with non-ideal TIMs is given in Equation (31). (Prasher, 2006):

$$R_c = \frac{BLT}{k_{TIM}} + R_{c1} + R_{c2} \tag{31}$$

Various authors have modelled the contact resistance $R_{c1} + R_{c2}$ (Prasher, 2006). For fluidic TIMs a surface chemistry model is presented: (Prasher, 2001)

$$R_{c1} + R_{c2} = \frac{\sigma_1 + \sigma_2}{2k_{TIM}} \left(\frac{A_{nominal}}{A_{real}} \right) \tag{32}$$

Equation (32) assumes $k_{TIM} \ll k_{substrate}$. A_{real} can be calculated from penetration length of the TIM. Hence, with non-ideal TIMs the total contact resistance can be calculated according to Equation (33).

$$R_c = \frac{BLT}{k_{TIM}} + \frac{\sigma_1 + \sigma_2}{2k_{TIM}} \left(\frac{A_{nominal}}{A_{real}} \right) \tag{33}$$

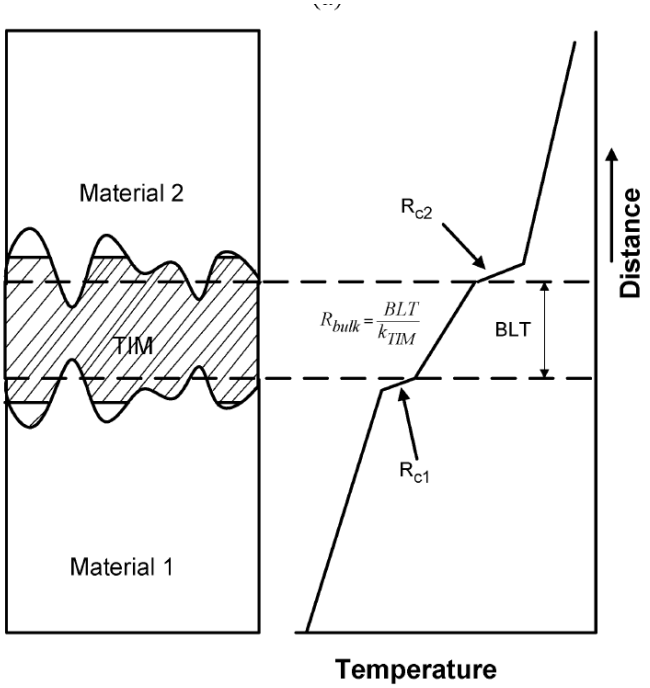

Figure 19: Real TIMs have finite BLT and they do not completely fill the formed voids and gaps. (Prasher, 2006)

By examining the Equations for ideal TIMs and non-ideal TIMs, some conclusions can be made about how the thermal contact resistance can be reduced. This is important since, by minimizing R_c, the heat dissipation across the interface can be improved. First the bond line thickness can be reduced. This can be achieved, for example, by increasing the pressure or by choosing a thinner TIM. However, the initial thickness of TIM should be high enough since thicker TIMs fill the air gaps more efficiently. In adition, increase in pressure minimises air gaps. However, it should be noted that pressure can not be increased indefinitely without breaking the component. Moreover, high pressures might lower the insulation resistance of TIMs. Other methods for improving the heat dissipation are to reduce surface roughness and to employ a TIM with highest possible thermal conductivity. Futhermore, according to Tong (2011), increase in the capillary force can reduce the thermal contact resistance.

3.2 Important charasteristics of TIM

According to Tong (2011) there are several parameters that should be considered before choosing a TIM for application. These parameters include,

- Thermal conductivity within the material
- Conforming (wetting abilities)
- Electrical insulation (if needed)
- Coefficient of thermal expansion (CTE)
- Mechanical clamping
- Outgassing
- Surface roughness
- Ease of installation and reworkability
- Long term stability and reliability
- Operating temperature range

- Price

The thermal conductivity outlines how efficient a certain material is for heat transfering. The higher the thermal conductivity, the more efficient the material is at transferring heat. However, as illustrated in Section 3.1, thermal performance is not solely dependent on material thermal conductivity. As shown in Equation (31), the interface is divided into contact resistances as well as bulk resistance within a material. Bulk resistance can be decreased by increasing thermal conductivity within the material and trying to achieve the lowest possible material thickness. However, to obtain the lowest possible thermal resistance, the focus on TIM should be minimizing the thermal contact resistances as well. A material that conforms the mating surfaces well will fill the air voids efficiently, leading to decrease in thermal contact resistance. (Tong, 2011)

As explained in Chapter 3.1, surface chemistry and applied pressure have distinct impact on the thermal resistance of the thermal interface. Different thermal interface materials perform differently on this function, while some TIMs are more suitable for high quality surface-finished interfaces and other TIMs functions with rougher surfaces as well. An increased mounting pressure increases conforming of TIMs minimizing the contact resistance. Moreover, some TIMs are intended to be used with other TIMs, such as thermal greases, to fully gain the thermal properties promised in datasheets. (Sarvar, et al., 2006)

The coefficient of thermal expansion (CTE) describes the amount of relative expansion of material during temperature shifts (ppm/K). The thermal vibration of atoms increases with increased temperature. Vibration causes the separation distance to rise between neighbouring atoms. The degree of CTE expansion depends on atomic bonding structure. The stronger the bond levels between atoms, the lower the coefficient of thermal expansion. Ceramics, for example, have low CTE while metals have loose bond levels and therefore high CTE. Moreover, polymers are known to have high CTE, especially thermoplastics and elastomers. If there is a mismatch of CTE between mating surfaces, mechanical stresses will be induced which can cause premature failures of the component. The CTE of TIM and CTEs of mating surfaces should be similar enough to avoid such failures. (Tong, 2011)

TIMs can be either electrically insulated or electrically conductive. If insulation is not needed, electrically conductive TIMs can be used to improve EMI shielding performance. Metallic TIMs and metal – based compounds are electrically conductive while ceramic – based are not. (Tong, 2011) Outgassing is a phenomenon where volatile gasses are released when materials are exposed to elevated temperatures in low atmospheric pressures. Since polymers outgas to some extent, they should be avoided in aerospace applications. (Sarvar, et al., 2006) Furthermore, TIMs should be easy to apply during installation and, if needed, replaced during maintenance (Tong, 2011). Reliability of TIMs is discussed in more detail in Chapter 4.

3.3 Different types of TIMs

The reduction in total thermal contact resistance can be achieved with several different thermally conductive materials. The materials can be categorized mainly into metallic, organic and graphite based TIMs. Research has also been done on some advanced TIMs. Metallic TIMs are further divided into different solders and low-melting alloys (LMA). Organic TIMs can be categorized into thermal greases and gels, phase change materials (PCM) and thermally conductive elastomers. The graphite sheets are an example of graphite-based materials. Carbon-nanotubes and the use of nano-fibres as fillers are an example of advanced TIMs. (Tong, 2011)

When comparing different TIMs, it is important to keep in mind that TIMs performance varies during its lifetime. Prasher et al. (2006) remind that some TIMs might have excellent thermal performance in the beginning of their lifetime but they degrade during operation and the end life thermal performance is unacceptable. On the other hand, some TIMs are noticed to increase their thermal performance during their lifetime. Although, the previous being the case, TIMs are often compared by thermal resistance and thermal conductivity which TIMs yield at the beginning of the use life. The thermal characterization of different TIMs can be done by a laser flash method, a calorimetric method and by thermal analysis through electronic assemblies. (Ousten & Khatir, 2011)

3.3.1 Metallic TIMs

Metallic TIMs are often made of solder alloys to form a solid metal sheet or preform. The material used can be for example indium. Indium possesses high thermal conductivity (80 W/mK) which is far more than with conventional polymeric TIM (< 5 W/mK). Metallic TIMs can also exhibit favorable solder or wetting behaviour upon reflow which reduces the thermal resistance of mating surfaces. Reflow is a process in which components are attached to each other by heating solder and substrate which causes the solder to melt and wet the surfaces by surface tension. To form a reliable interconnection, most of the metallic TIMs are required to be subjected to reflow. One of the major disadvantages related to metallic TIMs is the relatively high CTE mismatches between TIM and other components. (Lewis, et al., 2007) While metallic TIMs form permanent interconnections between components it is clear that the disassembly of the product is difficult if needed. Furthermore, metallic TIMs can be divided into reflow solders, nonreflow solders, Low Melting Alloys (LMA), hybrid metallic solder materials and gold-gold interconnections (Tong, 2011).

3.3.2 Thermal greases and compounds

Thermal greases are usually made of silicone or hydrocarbon oils with thermally conductive ceramic or metallic fillers to form a paste. Fillers increases the thermal capacity of pastes and provide the body to minimize flow out of the interface. Thermal grease is applied to one of the mating surfaces and when pressed against other surface, the grease fills voids and gaps between the interface thus removing poorly conducting air. Two mating surfaces come into contact at their high points. Due to the paste-like consistency of thermal greases, any excess grease will flow out from the interface, allowing the BLT to be as thin as possible. With thermal greases, the thermal interface must be maintained with spring clips or other mounting hardware. (deSorgo, 1996)

Greases are excellent to fill up the microscopic voids between surfaces, thus they are most widely used TIMs in microelectronics cooling (Prasher, 2006). Therefore, it is clear that the reliability of thermal greases is one of the most studied among other TIMs (Due & Robison, 2013). Furthermore, according to Due & Robison (2013) the performance of thermal greases tend to increase while in operation. This is due to the better wetting of the thermal greases when exposed to high temperatures.

Although thermal greases provide very low thermal resistance, there are several drawbacks which is why the use of other materials may be preferable. In literature it is generally accepted that thermal greases suffer from grease pump-out and grease dry-out during power cycling, resulting in increased thermal resistance (Due & Robison, 2013). Failure mechanisms are strongly dependent on the temperature and the temperature cycle number of application (Sarvar, et al., 2006). Due to its ”messy” structure there are challenges during handling in a manufacturing process. For example, applying the right amount of grease each time to each

device might prove to be challenging (Blazej, 2003). In addition, any excess grease will flow past the edges of the power semiconductor and might cause contamination to other components (Sarvar, et al., 2006). Furthermore, thermal greases do not provide electrical insulation between the heat sink and the power semiconductor.

Thermally conductive compounds are improvement of thermal greases. Initially, compounds flow as freely as thermal greases. Therefore, compounds eliminate the air voids efficiently and resulting thermal resistance is very low, similar to thermal grease. After installation, thermal compounds cure with heat to a rubber film and develop secondary properties such as adhesion. Compounds with adhesive properties do not necessarily require mechanical fastening. Because of the cured rubber form, thermal compounds do not suffer from migration or dry joint problems associated with thermal greases. Furthermore, any excess materials are easily removed after curing. In addition, compounds are better to fill large air voids where grease would leak from the joint due to its migratory nature. (deSorgo, 1996)

Along with thermal greases and thermal compounds, a third paste-like thermal material exists. Thermal conductive gels are almost identical to thermal greases. Difference is that gel is cured to form cross-linked polymer chains which provide lateral stability to minimize the problem associated with liquid TIMs. Thermal gels have a slightly lower thermal conductivity than thermal greases. (Tong, 2011) Futhermore, according to Prasher (2006), gel is nothing but a cured grease and does not suffer from pump-out.

3.3.3 Thermally conductive elastomer materials

Thermally conductive elastomers are elastomeric materials which contain thermally conductive fillers. Depending on used fillers, elastomers can be categorized into insulated TIM and non-insulated TIM. Insulated TIMs are usually filled with thermally conductive ceramic fillers while non-insulated TIMs are loaded with high thermal conductivity metallic or graphite fillers. The thermal conductivity of elastomer is much less compared to the heat sink thus the use of elastomers limits the overall ability of heat dissipation. (Tong, 2011)

The typical form of thermally conductive elastomer is a silicone pad (also referred as gap pads or gap fillers) filled with ceramic particles which is reinforced with woven glassfibre or dielectric film to achieve electrical insulation. Typical ceramic fillers are BN and alumina. In addition to silicone, urethane can be used as base material. (Tong, 2011) Elastomer pads are available in thickness from about 0.1 – 5 mm and hardness from 5 to 85 Shore A. Since elastomer films can provide electrical insulation, they are typically used with discrete power devices where electrical insulation is required. (deSorgo, 1996)

Elastomer films do not flow freely like thermal greases which makes the manufacturing process easier. In addition, elastomers are often manufactured to respond to the actual component size, which helps the manufacturing process further (Blazej, 2003). Elastomers will, however, deform if sufficient compressive load is applied to conform surface irregularities. Furthermore, pads require relatively high clamping pressures to obtain sufficient thermal resistance. At low pressures, elastomer can not fill air voids between the surfaces well enough. According to deSorgo (1996), mounting pressure between 2000 kPa-3500 kPa is required. A permanent mechanical clamping is also required to maintain the sufficient thermal resistance. Finally, because of moderate thermal performance, elastomer films are often used in applications with modest thermal requirements (Blazej, 2003).

Thermally conductive adhesive tapes were invented to eliminate the need for mechanical clamping. Tapes are double-sided pressure sensitive adhesive films filled with ceramic powder and are often supported with aluminum foil or a polyimide film for the strength and

ease of handling. (deSorgo, 1996) Polyimide films also provide electrical insulation. As base material epoxy and silicone based formulations are used (Blazej, 2003). The main purpose of these adhesives is to eliminate the need for mechanical clamping, which have an effect on the size and weight of the application. Adhesive tapes require some initial mating pressure to conform irregularities between surfaces. After the joint is formed, mechanical clamping can be removed. Like with elastomer pads, Adhesive tapes can not fill large air voids between non flat surfaces but unlike with liquid adhesives no cure time is required. Required pressure for initial installation varies between 70 kPa and 350 kPa for a few seconds duration. The bond, which is formed, can be considered permanent and the heat sink is reliably attached to the power semiconductor. While thermal tapes provide the ease of installation, several drawbacks exist. Thermal resistance is only slight better compared to dry joint due to the fact that thermal tapes do not fill air gaps as well as liquids. Thermal resistance is also highly dependent on surface qualities. (deSorgo, 1996) Although, at its best a high level cooling and long term reliability can be achieved, thermal adhesives lack of reworkability which is not practical in several cases. (Blazej, 2003)

3.3.4 Phase change materials

Phase change materials combine the thermal performance of grease with the convenience of an elastomer pad. According to the name, phase change materials (PCM) change their state through temperature shifts. During the temperature shift PCMs change their state from solid to liquid which is used with TIMs because a liquid structure has higher conformability which is needed for minimizing interfacial air gaps between surfaces. Above melting temperature PCMs does not function as adhesive and effective clamping is needed. For TIM applications organic PCMs are preferred. These include paraffin waxes or silicon-based materials. The thermal performance of PCM can be enhanced by using thermally conductive fillers, such as alumina, graphite or aluminum. The fillers do not melt along with base material but can have effect on the charasteristics of PCM, including the melting temperature and heat of fusion. While organic PCMs have low thermal conductivity, the use of fillers is important. Due to the low thermal conductivity of organic PCM, the use of fillers is important.
(Blazej, 2003) (deSorgo, 1996)

PCMs should melt slightly above room temperature so that the materia is a liquid while it functions as a TIM. Compositions that transform from a solid form at room temperature to a mixture of solid and liquid phases at various operating temperatures exists. The liquid from the mixture makes intimate contact with the contact surfaces while the solid retains the integrity of the gap. At this temperature, PCM acts as thermal grease and forms a thin BLT. (deSorgo, 1996) Although, PCMs are not categorized as to be an adhesive TIMs, they still hold some adhesiveness after it is placed on application. This has effect on to the reworkability of the application in order to not break the expensive components where the PCM is attached. (Blazej, 2003)

3.3.5 Graphite sheets

Graphite sheets are manufactured from highly pure natural graphite flakes to form a flexible sheet. These sheets are naturally porous and density varies between 0.60 and 1.4 g/cm^3. For TIM applications graphite sheets have been impregnated with polymers, such as minerals or synthetic oils, to improve its thermal performance. (Tong, 2011)

Typically, graphite sheets yield thermal conductivity above 3 W/mK and have great thermal stability. Other advantages of graphite sheets are excellent resilience and flexibility which

conforms well to mating surfaces. Moreover, graphite is known of the low thermal expansion coefficient and chemical inertness. However, graphite is effective TIM if the thickness of sheet is low (0.13 mm) and density is low (1.1g/cm^3). Flexible graphite sheets also require much higher contact pressures than other TIMs (11.1 MPa).

3.3.6 Advanced TIMs

Traditionally, TIMs have been manufactured with polymeric carriers filled with highly conductive particles to improve their thermal performance. Conventional TIMs function well enough when an interaction gap can be minimized (bond line thickness 0.0254 mm or less). However, if gaps between surfaces are larger, conduction within the interface material dominates the interface thermal resistance and poor thermal performance results. To overcome this limitation new thermal interface materials have been developed which are discussed briefly below. (Tong, 2011)

Conventional polymer-based TIMs wets the mating surfaces well but to achieve improvement in thermal conductivity (1 W/mK – 8 W/mK), TIMs are highly loaded with thermally conductive particles. Typically, particles can fill out even 60 – 70 % of the whole composition. The thermal conductivity with particle loaded polymers is limited as the space between thermally conductive particles limits the efficiency of fillers used. To overcome this problem, fiber based polymer TIMs have been developed. These fibers create a continous thermal path from one surface to another thus reducing the resistance within the polymer. High conductivities can be achieved with a relatively low volume fraction of conductive fibers. Fibers are hold in place with an adhesive layer and encapsulation. Fiber based TIMs do not suffer from pump-out or drying and are easily reworkable. Typical filler material is carbon or graphite fibers. (Tong, 2011)

Along with graphite sheets, other carbon based TIMs have been developed. These include, but are not limited to, graphene filled TIMs and Carbon Nanotubes (CNT). Graphine is attractive as filler material while it has excellent thermal conductivity, great mechanical strength and small CTE. The thermal conductivities of graphenes have been measured around 3 000 W/mK – 5 000 W/mK. Furthermore graphene based TIMs have advantages of high packing density and possibilities to bond the surface. (Tong, 2011) Carbon nanotubes can be interpretended as graphene sheets rolled into cylinders which may be formed from one tube or multiple tubes. Depending on the number of tubes, carbon nanotubes are called single-walled nanotubes (SWNT) or multi-walled nanotubes (MWNT). SWNT consist of sigle sheet whereas MWNT consist of stact of graphene sheet wrapped in concentric tubes. Multiwalled CNT have been reported to have thermal conductivity of 3000 W/mK and effective thermal conductivities from 15 W/mK to 200 W/mK. CNTs can be used as fillers to enhance the thermal performance of polymeric TIMs or CNTs can be woven into mats or sheets to use as individual TIMs. However, despite the high thermal conductivity, CNTs as fillers have not been reported to be good in practise. Despite having excellent chemical and physical attributes, CNTs are not merged well into other materials. One of the reasons for this is that CNTs have poor dispersion within a matrix and poor adhesion to the host material. (Sarvar, et al., 2006)

Table 1 brings together traditional TIMs which were discussed. Typical characteristics of each TIM is reported in the first column. Advantages and disadvantages are reviewed in the second column. The last column presents the thermal resistance of each TIM in typical application where it is used.

Table 1: Comparison of traditional TIMs in power semiconductor applications. Modified from (deSorgo, 1996), (Prasher, 2006), (Sarvar, et al., 2006), (Ousten & Khatir, 2011), (Tong, 2011).

TIM	Characteristics	Advantages	Disadvantages	Thermal performance (Kcm^2/W)
Metallic TIMs	Made of solder alloys to form a solid metal sheet or preform	• High thermal conductivity	• High CTE-mismatch between other components • Disassembly	
Thermal grease	Typically silicone oil with thermally conductive fillers to form a paste	• High bulk thermal conductivity • Greases fill excellent microscopic voids leading to mimimal thermal resitance • TIM delamination is not a concern	• Thermal cycling can result in pump-out and dry-out • Manufacturing issues due to ”messy” structure • Excess grease can flow past power semiconductor edges and contaminate other components • Handling in manufacturing process • Thickness difficult to control	0.2-1
Elastomer film	Polymer based films filled with conductive particles and can be reinforced with woven glassfibre or dielectric film	• Not messy and easy to handle • No pump-out or migration • Resist humidity and other harsh environment • Dielectric properties • Can be easily cut to size of mounting surfaces • Eliminates problem of applying exact the amount of grase with each application	• Thermal conductivity lower than grease • Delamination might be a problem • Higher cost than grease • Does not fill microscopic voids as efficient as greases • Permanent clamping needed • Curing migh be required	1-3
PCM	Polyolefin, epoxy, low molecular weight polyesters, acrylics, tycially with BN, or Al_2O_3 fillers. When heated turns to liquid, fills voids and returns to solid.	• Conforms to surface irregularities before curing	• Lower thermal conductivity than grease. • Mechanical clamping needed • Fillers does not melt with base material • Holds adhesiveness after placed on application	0.3-0.7
Graphite sheets	Graphite flakes processed into sheet by the combination of a chemical, thermal and mechanical treatment.	• Thermal stability • High conformability • Low CTE	• Requires relatively high pressures • Manufacturing difficulties	NA

4 Reliability analysis

The reliability of electric devices is attaining greater attention among electrical device manufacturers. In recent times, the size of electronic devices has been decreased while, at the same time, the performance requirements have been increased. Electronic devices, especially on the consumer side, must have faster operation, smaller size and lighter structure. In addition, the same customers are expecting cheaper and more reliable electronic devices. These considerations directly affect the component level of electronic products which have to operate more efficiently and more reliably. Efficient thermal management is required to ensure high reliability of products and power densities of power semiconductor devices.

Up to this point of the study, power semiconductor devices, TIMs and their connection have been reviewed. One goal of this thesis is to study the long term reliability of thermal interface materials. Therefore, this Chapter introduces reliability and life testing concepts. In Section 4.1, the fundamentals of reliability are discussed. Section 4.2 and Section 4.3 focuses on reliability issues and life testing of power electronics and thermal interface materials.

4.1 Fundamentals of reliability

Reliability is described by Chung et al. (2016) as: ”Reliability is the probability that an item will perform a required function without failure under the stated conditions for a stated period of time”. Therefore, there is a close relationship between reliability and probability. This section describes the key terms and definitions related to reliability calculations. The section focuses on giving an idea of what is the reliability of a product and how reliability of a product can be described.

4.1.1 Failure distributions

Failure distributions are widely used in probability calculations and in reliability analyses. Failure distribution shows the histogram of failure occurrence during a product’s lifetime (Chung, et al., 2016). Failure distributions are mathematically defined by probability density functions (PDF). The probabilities to failure can be calculated from probability density function $f(x)$ with the define integral according to Equation (34).

$$P_{failure} = \int_0^x f(x) = F(x) \tag{34}$$

where $F(x)$ is cumulative density function. Cumulative density function is the probability of a failure occurring before or after a certain time. Reliability $R(x)$ of a product is therefore a complement of $P_{failure}$ and can be written as:

$$R(x) = 1 - P_{failure} = 1 - \int_0^x f(x) = 1 - F(x) \tag{35}$$

The failure rate function (also known as hazard rate function) is described by Chung et al. (2016) as the conditional probability of failure in the interval, $x - (x + \Delta)$. The failure rate

describes how often faults occur, for example, one failure per week. Failure rate can be calculated as: (Chung, et al., 2016)

$$h(x) = \frac{f(x)}{R(x)} \tag{36}$$

- Weibull distribution

There are several failure distributions used in life data analysis and one of the most common is the Weibull distribution. The Weibull distribution is named after its invertor Waloddi Weibull and it is used due to its versatility and relative simplicity (Reliasoft, 2016). Three parameter Weibull distribution expressed by its propability density function is written as (Chung, et al., 2016):

$$f(x) = \frac{\beta}{\eta^{\beta}} x^{\beta-1} \exp\left(-\left(\frac{x-\gamma}{\eta}\right)^{\beta}\right) \tag{37}$$

where β is the shape parameter (also known as the Weibull slope), η is the scale parameter and γ is the location parameter also called the failure-free period. The Weibull distribution has a different shape depending on parameters. In many practical applications, the location parameter is not used and the value can be set zero. In this case, the Weibull distribution becomes a two parameter distribution. (Reliasoft, 2016)

From Equations (35) and (36) the propability function and hazard function for Weibull distribution can be derived:

$$R(x) = \exp\left(-\left(\frac{x-\gamma}{\eta}\right)^{\beta}\right) \tag{38}$$

$$h(x) = \frac{\beta}{\eta^{\beta}} x^{\beta-1} \tag{39}$$

The importance of Weibull distribution is further explained by Chung et al. (2016): Weibull distribution is useful in the reliability analysis because it can be used to model various life time behaviours. The shape and characteristics of the Weibull distribution are dependent on Weibull parameters β and η. If β = 1, for example, the Weibull distribution becomes exponential distribution with a constant hazard rate. When $\beta < 1$ the failure rate decreases and when $\beta > 1$ failure rate increases over time. In such case, the Weibull distribution has a shape of a bathtub curve. The bathtub curve is futher discussed in the next Section.

4.1.2 Bathtub curve

The bathtub curve is widely used in reliability analysis of electronic components and systems although there is disagreement on its applicability. The name “bathtub curve” comes from the fundamental reliability theory that the hazard rate of an electronic component has the shape of a bathtub. The curve comprises three intervals as follows: (Klutke, et al., 2003)

1. Early life interval
2. Midlife interval
3. Wearout interval

At the interval one, the failure rate is high due to quality control issues. Faults may occur from design flaws or installation errors. The failure rate decreases rapidly. At interval two, the failure rate is constant and faults occur from random events such as device malfunctions or human related errors. This interval is called the "useful" life of system or device. The hazard rate begins to increase as the device reaches its designed lifetime. Faults occur from wearout mechanisms or degradation symptoms. Eventually, every device reaches interval three. The bathtub curve is shown in Figure 20.

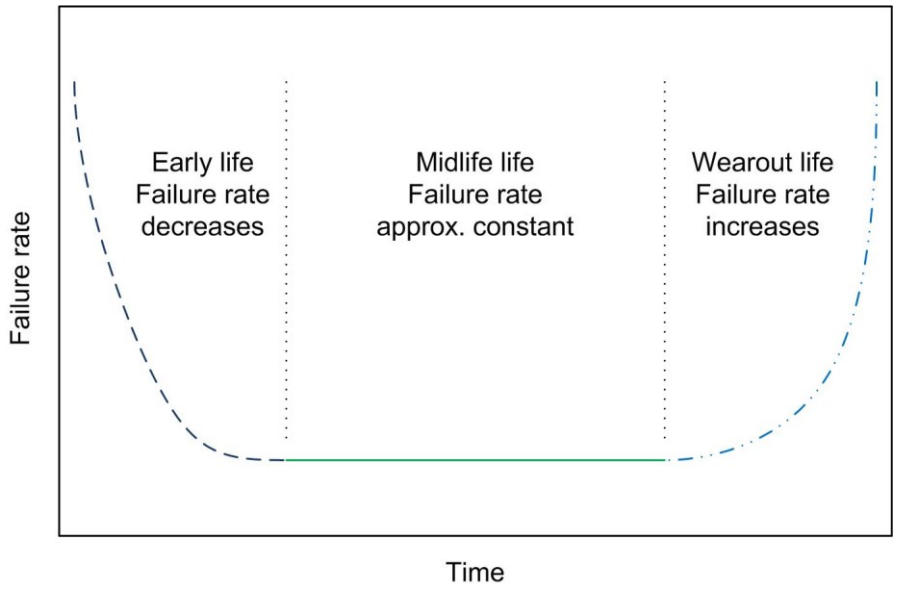

Figure 20: Bathtub curve.

4.1.3 Life time and percentile life

The life time of a product can be determined as follows: "Life time is the time to which an item reaches its failure criteria" (Chung, et al., 2016). Failure criterion is fulfilled when the item does not function the way it is supposed or the item becomes hazardous.

Lifetime is not always the best way to describe the reliability of the product. Reliability engineers are usually more interested in percentile life. Percentile life is the time when a certain number of items are decomposed with a certain probability. For example, B10 lifetime is the time when 10 % of the items are decomposed with the probability of 0.9. (Chung, et al., 2016)

4.1.4 MTTF and MTBF

Mean-time-to-failure (MTTF) and Mean-time-between-failure (MTBF) are commonly used terms in reliability engineering. MTTF denotes the expected time for failure for a non-

repairable system while MTBF describes the time between two failures for a repairable system. When the hazard rate is constant, MTTF and MTBF can be calculated as follows: (Chung, et al., 2016)

$$MTTF/MTBF = \frac{1}{h(x)} \tag{40}$$

In statistics, MTTF and MTBF are expected values of the failure distribution functions. The disadvantages of these terms are further explained by Chung et al. (2016): The failure rate changes over the lifetime of a component, thus it is not constant for most of the durable components. Furthermore, MTTF and MTBF correspond to the time when 63 % of the items have failed and the reliability is 0.37. MTTF and MTBF provides very limited information for reliability design and cannot be used efficiently for comparing the reliability of different components.

4.2 Reliability and life testing

Reliability and life time testing is a very fast growing field in the consumer and industrial electronics. Reliability and life time testing provide manufacturers knowledge of whether their products, components or systems perform the required functions in predetermined environments for the desired time. Moreover, reliability and life time tests expose the failure mechanisms and the weakest parts of products and can be used to improve reliability before the faults occur at customer conditions.

Actual reliability testing can be done in several ways. For example, the test can be done in normal operating conditions and continued until the first fault occurs. Testing can be ongoing reliability testing (ORT) which means that products are selected randomly from a production line and ensured that the quality is still the same as it was at the beginning of product manufacturing. One reliability test method is called accelerated life time testing (ALT) which is important for the purposes of this study. ALT is discussed more in Section 4.3.

Thermal interface materials play an essential part when maintaining the desired operation point of a electronic component. Therefore TIM has considerable effect on the whole reliability of an electronic product or a component. Due to similar operating conditions and stresses, that are experienced during the operation of power semiconductor devices, the reliability testing of TIM is fairly related to the reliability testing of power semiconductors. Due & Robison (2013) divides the reliability testing of TIM into two categories: specially designed tests for TIM and generic microelectronic component tests that often relate to accepted standards. Furthermore, Due & Robison (2013) outlines that the reliability of TIM can be described by how well the thermal contact resistance is maintained from the original value during operation. The changes in contact resistance have effect on the junction temperature of the electronic component. This increase in junction temperature can lead to malfunctions or even to a complete failure of the power semiconductor device.

The long-term reliability of TIM depends on the package to which it is installed, the environment it is exposed to and the cyclic nature of its operation. Exactly the same TIM may be used in two completely different devices and in one case fail prematurely and in the other actually improve the performance. There is not very clear understanding with regard to the fundamental mechanism causing TIM failure as there are very few publications of on physics of failure of TIM degradation. (Due & Robison, 2013)

As indicated above, the reliability testing of TIM follows the reliability testing of power semiconductor devices. Even if the methods are similar, the interpretation of results may differ. The reliability of TIM is often a ”gray area” while the responsibility of electronic package reliability ends with its manufacturer. After electronic package, the reliability of the whole system is left to a customer’s responsibility. Due & Robison (2013) discusses the complications related to the reliability testing of TIMs: TIM reliability testing is not mature when compared with other reliability issues in power electronic packaging. There are no uniform test protocols and there is rather a collection of publications where different researchers have tested different TIMs with different tests levels and durations. With this said, it is clear that one can not easily find straightforward testing protocols for TIM and the interpretentions of results rely on the individual capacities of a researcher. Estimating the performance degradation of TIMs in field conditions is a big challenge.

Although there is a demand for more uniform testing guidelines for TIM testing, some basic principles still hold place. Section 4.3 covers the basics of temperature based accelerated tests and describes some tools to further evaluate the life time performance of TIM based on former tests. For the outcome of this study it is not reasonable to examine all types of reliability tests.

4.2.1 Determination of test sample size

Before a reliability test can be started, a test sample size N, must be determined. The sample size can be determined in numerous ways and the driving factor can be as simple as for example money which is allocated for a reliability test (Kececioglu, 1994). However, if a relatively small sample size is chosen, the results could be wrongly interpreted. One method for choosing sample size is called estimation. The object is to find N such that the true but unknown parameter is contained in a specific confidence interval with probability $(1-\alpha)$ (Kececioglu, 1994).

4.3 Accelerated reliability and life time tests

One form of reliability testing is accelerated life time testing. The main idea of accelerated tests is to expose devices, components or systems to stresses that are more severe than normal or use stress levels, in order to shorten time to failure. With accelerated testing, the failure mechanisms and reliability parameters, such as MTTF and MTBF, the failure rate and average life can be determined and estimated without testing high amount of samples and in a reasonable time (Sony, 2000). For many products the life time can be so long that testing under operating conditions is not time-wise and economically practical. In conclusion, ALT is a method of quickly finding information about a product’s life performance.

In accelerated testing for power semiconductor devices, higher stress levels can be achieved by using, for example, higher temperatures, pressures, vibration, voltages, cycling rates or combinations of each. It is important to notice that failure mechanisms that are used in accelerated tests should be the same as those observed under use stress conditions. (Kececioglu, 1994)

According to various sources, acceleration by the temperature is the most commonly used stress condition in power electronics reliability testing. (Chung, et al., 2016), (Jedec, 2004), (Sony, 2000) Evidence has shown that even 55% of failures in power electronic devices are due to high temperatures and temperature cycling. Furthermore, reliability testing of power electronics can be divided into environmental testing and endurance testing. Environmental testing includes temperature cycling, thermal shock, vibration and autoclave. Endurance

testing includes power cycling, temperature storaging and humidity related tests. Power electronic reliability tests are often described in international standards such as JEDEC and MIL-STD-883. (Chung, et al., 2016)

According to Due & Robison (2013) it can be seen that temperature related reliability tests are considered in three most common test categories in TIM testing. In addition, reliability testing of TIM can be divided into temperature and humidity tests, temperature and power cycling and high temperature storage/bake/soak tests.

The acceleration factor (AF) denotes how consuming the acceleration of an accelerated test has been. AF represents the ratio of the life in the customer's operating stress environment to the life in the reliability test. For example, if the expected lifetime of a product is 10 years and the product fails after 0.1 years the acceleration factor of the test is 10y/0.1y = 100 times. Different acceleration factors exist for different stresses. The AF can be written as:

$$AF = \frac{L_{use}}{L_{test}} \tag{41}$$

where L_{use} is the expected lifetime of a product and L_{test} is the time after product fails in the accelerated test.

4.3.1 Power cycling

In power cycling, the acceleration factor is temperature difference across the package die and the heat sink. The temperature difference is generated by turning the power semiconductor device on and off for a desired time. In TIM testing the temperature difference is usually generated by a power electronic component as it simulates the real operating conditions. The thermal cycling effect could also be interpreted by another mechanisms for example by heating a simple resistor above TIM and a heat sink. However, this method has a few uncertainty factors as the thermomechanical stresses might be different.

Usually during power cycling test the ambient temperature is kept constant and temperature differences result only from power losses. In power electronics testing the purpose of power cycling is to generate significantly accelerated stress conditions in power electronics module leading to early wear-out mechanisms and degradation symptoms. (Chung, et al., 2016), (Wolfgang, 2015)

The temperatures, time constants and dissipated power is specific to each power cycling test. Some advice is given in literature indicating that the high temperatures in PC are typically 80 – 110 degrees. (Due & Robison, 2013) Nonetheless, the test usually has the following procedure. The junction temperature of power module is heated to its maximum value T_{max}. After T_{max} is reached, heating is switched off and the junction temperature cools to desired value T_{min}. One power cycle consist of active heating and cooling. After T_{min} is reached the active heating is turned on again and the cycle is repeated. The temperature changes in junction temperature can be written as:

$$\Delta T_j = T_{max} - T_{min} \tag{42}$$

The medium temperature for the power cycling test is defined as:

$$T_m = T_{min} + \frac{T_{max} - T_{min}}{2} \quad (43)$$

The typical outcome of a power cycling test is an increase in the junction temperature of a power semiconductor device. Formation of cracks in solder attachment between the devices and power substrates increases the thermal resistance of the power module junction and the junction temperature rises (Chung, et al., 2016). The rise in junction temperature can also be induced by the weakening in TIM layer which is examined in this study.

As discussed before, the temperature swing in a power semiconductor module induces different failure mechanisms. These failure mechanisms are caused by CTE differences leading to high thermomechanical stresses in power modules affecting the TIM layer. A widely found failure mechanism for thermal greases during power cycling tests are pump-out and dry-out due to the CTE mismatch of die and heat sink (Due & Robison, 2013), (Gowda, et al., 2005). Failure mechanisms in power semiconductor devices are briefly described in (Sarkany, et al., 2014): The two most common failure mechanisms in power semiconductors are a die attach and bond wire degradation. Bond wire degradation can be further divided into complete detach of the bond wire and formation of cracks and fissures in bond wire structure.

A challenge in power cycling is the measurement of junction temperature. Because of the transient nature of the junction temperature, the method for junction measurement must be fast enough. (Chung, et al., 2016)

4.3.2 Temperature cycling

Compared with power cycling, the temperature cycling for TIM is a far more studied subject (Due & Robison, 2013). It is similar in a way that the acceleration factor is generated by temperature difference across the test subject but in this case the ambient temperature is cycled. This being the case, there are no temperature gradients between the package die, TIM and the heat sink because all the components are subjected to the same temperature. It is typical in temperature cycling that the extremes of temperatures are considerable larger in comparison with PC and the time constants are longer.

Temperature differences are typically obtained in environmental chambers in which the test objects are located. Temperature cycle is repeated until the desired number of cycles is achieved. Again the test parameters vary between different tests but some principles are discussed in literature for example by Chung et al. (2016): The test object must be located in a way that air can flow without interruption near the object. Extremes of the temperature cycle are usually from -40 degrees to 125 degrees although extremes from -50 degrees to 150 degrees have also been used by Gowda et al. (2005). Chung et al. (2016) continues by denoting that dwell time at extreme temperatures must be greater than 10 minutes and the EUT must reach the extreme temperature in 15 minutes. It is also mentioned that the transfer time from hot to cold must not exceed 1 minute. It has to be noted that the previous guidelines are considered for power electronics reliability testing. As noted by Due & Robison (2013) there is lack of standardized test protocols for TIM which leads to inconsistent outcomes and uncertainty of analysis of the results.

In power electronic modules, the failure mechanisms are considered different when comparing the outcomes from temperature cycling and power cycling. According to Reddy et al. (2015) temperature cycling usually causes solder cracks while power cycling results in bond wire degradation. For TIMs the failure mechanisms depend on the TIM material. The

pump-out of particular thermal greases is also noticed in the temperature cycling. According to Due & Robison (2013), some TIM is said to improve their performance over time in temperature cycling despite the pump-out mechanisms. The same phenomenon is noticed in particular thermal greases, adhesives, pads and putties. This reduction in the thermal resistance is due to the wetting of the contact surfaces in high temperatures or due to the reduction in the bond line thickness. Ousten et al. (2011) noticed no significant changes in R_{th} with elastomer films and graphite films during the temperature cycling. Only PCM deteriorated and R_{th} was increased by 30 %.

4.3.3 Degradation models

As was mentioned, the purpose of the accelerated reliability tests is to generate stress conditions which lead to early wear-out mechanisms or degradation symptoms. Design engineers are obsessed to know the performance of TIM at the end of its life time at operating conditions. Another case from the actual accelerated testing is to benefit from the measured results. Due & Robison (2013) denote that accelerated tests are performed to obtain results in a manageable timeframe and the operating environment is far from normal. This results in uncertainty of prediction of the end of life performance of TIMs. Having said that, one important aspect of accelerated testing is to develop degradation models based on accelerated data, which predict the change in thermal resistance over time at use conditions. According to Due & Robison (2013) this is typically done by generating two R_{th} curves versus time and developing an empirical relationship which ostensibly extrapolates to use condition. With this information degradation models can be used to predict the thermal resistance of TIM and determine if it will stay below the defined threshold during its entire design lifetime.

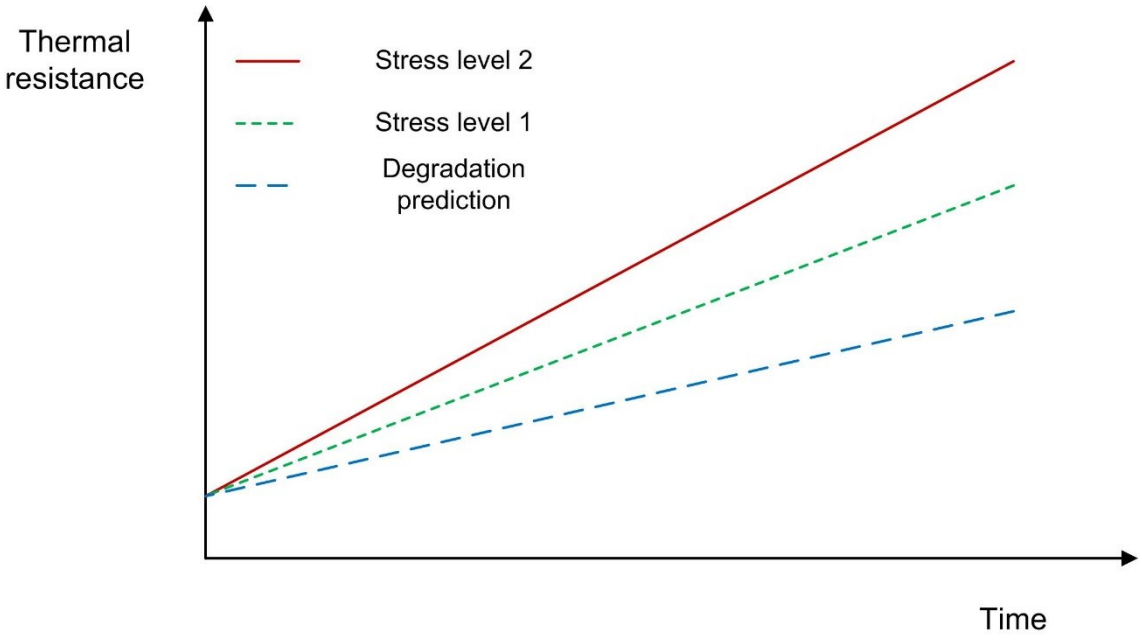

Figure 21: Example curves for the degradation prediction of TIM performance.

In addition, several degradation models exists in open literature. For TIMs those are typically divided into linear in time, non-linear in time and asymptotic or saturation in time. (Goel, et al., 2008)

Linear in time

Linear in time model assumes that R_{th} changes linearly over time. The most common linear degradation model is called Arrhenius model. Arrhenius model is a well-known acceleration model for power semiconductor devices and microelectronics components when the acceleration factor is temperature. It is based on the so called activation energy term E_a which varies between different materials. Common Arrhenius relation is given in Equation (44).

$$K = Ae^{\frac{E_a}{kT}} \tag{44}$$

where, K is estimated life, k is Boltzmann's constant, T is temperature and E_a is activation energy. For thermal interface materias Arrhenius relation can be expressed as:

$$R_{th}(T,t) = R_{th}(T,0) + \beta \mathrm{e}^{-\frac{E_a}{kT}} \tag{45}$$

where $R_{th}(T,t)$ is the degraded thermal resistance at time t and $R_{th}(,0)$ is the thermal resistance at the beginning. The coefficients β and E_a are determined through fitting of the test data. Another linear degradation model is called power law equation. It can be used when thermo-mechanical stresses, such as power cycling, is used,

$$R_{th}(T,t) = R_{th}(T,0) + \beta S^n t \tag{46}$$

where S is thermo-mechanical stress condition, such as change in temperature. Again the coefficients β and n can be determined through fitting of the test data.

Nonlinear in time

The degradation of TIMs are not always linear. In such case, a common practise is to use modified Arrhenius or power law equations. Equation (47) shows an example of modified non-linear degradation model.

$$\ln\big(\theta(T,t)\big) = \theta(T,0) + \beta e^{-\frac{E_a}{kT}} t \tag{47}$$

Asymptotic or saturation in time

The most complex degradation model is a case when R_{th} saturates over time. R_{th} will decrease until no further degradation takes place. A model for such case can be written as follows:

$$\ln\big(\theta(T,t)\big) = \theta(T,0) + \beta e^{-\frac{E_a}{kT}} t \cdot \ln(t+1) \tag{48}$$

After a model for degradation is established the next step is to extrapolate the degradation trend at the use conditions.

5 Measurements

Two main objectives of this thesis was to develop an accelerated life time test system and to do life time tests and thermal performance comparison tests for preselected thermal interface materials. This Chapter presents the developed test system along with the measurement results and uncertainty analysis of relevant measurements. Section 5.1 discusses the method for which the test system was based on. Section 5.2 discusses the actual test system in more detail. Section 5.3 discusses test results from power cycling test and Section 5.4 test results from thermal performance comparison tests. Section 5.5 reviews uncertainties related to measurements and uncertainties related to actual results. Finally, conclusions of measurements are made and future of the study is discussed.

5.1 Test method

One goal of this thesis was to design and implement an accelerated life test system for different thermal interface materials used in discrete power transistor applications. Accelerated test for power semiconductor devices were discussed in Section 4.3. As noted earlier, weakening in TIM layer increases the thermal resistance between a heat sink and a power transistor. This weakening can also affect the dielectric breakdown strength of TIMs. For the acceleration of failure mechanisms, a power cycling test system was chosen to be designed. In power cycling, temperature gradients exist between a power transistor, a TIM and a heat sink. This is not the case with the temperature cycling, where all the components are subjected to the same temperature. Thus, power cycling closely replicates the actual cyclic stress in applications where power transistors are used as explained in Section 4.3.1.

A control circuit for power transistors, a control logic and a mechanical test frame were designed by author. Discrete power transistors are controlled on and off at the top of TIMs to cause aging within materials. As for a discrete power transistor, an N-Channel MOSFET was chosen with TO-247 case. The MOSFET is operated in saturation, as voltage-controlled current source, hence dissipation of heat occurs. This power dissipation is related to a voltage drop over, and to a current flow through the transistor. The aging is monitored by measuring the temperature on both sides of TIMs. Since, the power dissipation is kept constant through the whole test, the thermal resistance can be calculated according to Equation (12).

Since, discrete power transistors are used, thermocouples can not be drilled easily to the case of the component. Hence, a copper plate is placed below each transistor to ease the temperature measurements. Thermocouples were drilled to a copper plate and to a heat sink.

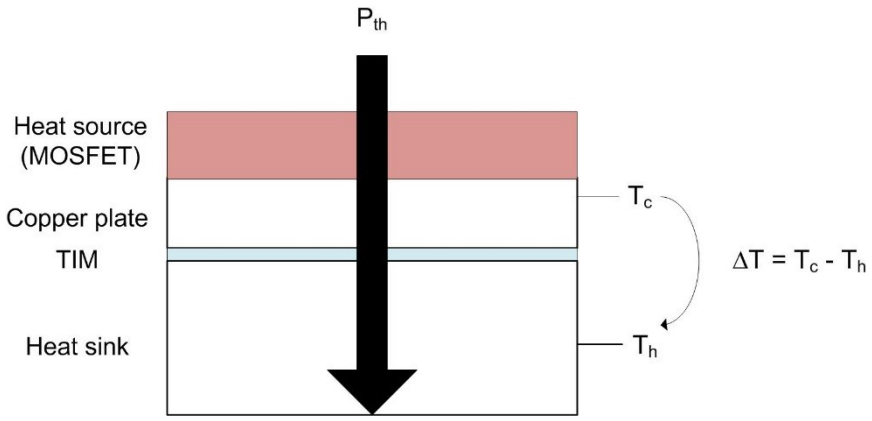

Figure 22: A copper bar (CU) is placed below the MOSFET and thermocouples are drilled in it and in the heat sink. The aging of TIMs is monitored by measuring ΔT.

For statistically significant results, there must be several measurements from the same measurement point as stated in Section 4.2.1. However, in this study, the most essential point was the comparability of measurements. Moreover, expenses were a driving factor when designing the test system. The number of power transistors and thereby number of TIMs in the test frame was determined to be 20. After the control circuit was designed, a printed circuit board (PCB) and a mechanical test frame were designed. The circuit board was designed with a Eagle CAD software. Schematic of the PCB can be found on Appendix A. The mechanical test frame was designed with Vertex G4 software. The block diagram of the whole testing system can be seen in Figure 23. Some of these elements are further discussed in the next Section.

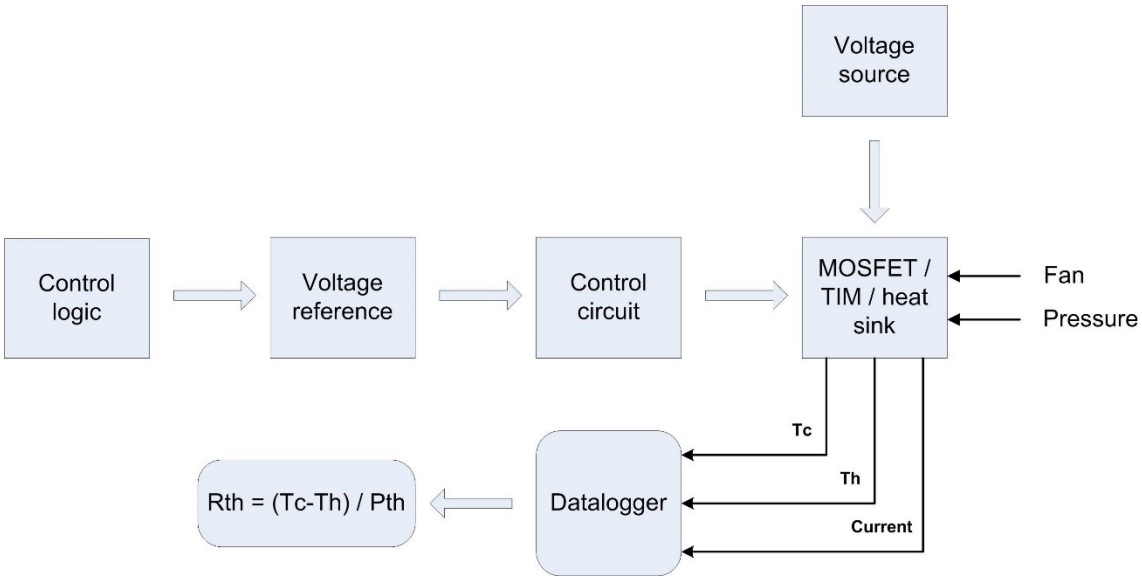

Figure 23: The schematic of the test protocol.

5.2 Test device

The control circuit of one MOSFET (Q_1) can be seen in Figure 24. With resistors R_1, R_2 and R_5 the current flow through a MOSFET can be adjusted, thus the power dissipation of one MOSFET can be varied. In addition, resistor R_5 is used for the current measurement of each control circuit. This is done with one ohm shunt resistor over which the voltage is measured. In addition, since the operation of the control circuit is dependent on the current measurement, R_5 must be a high precision resistor.

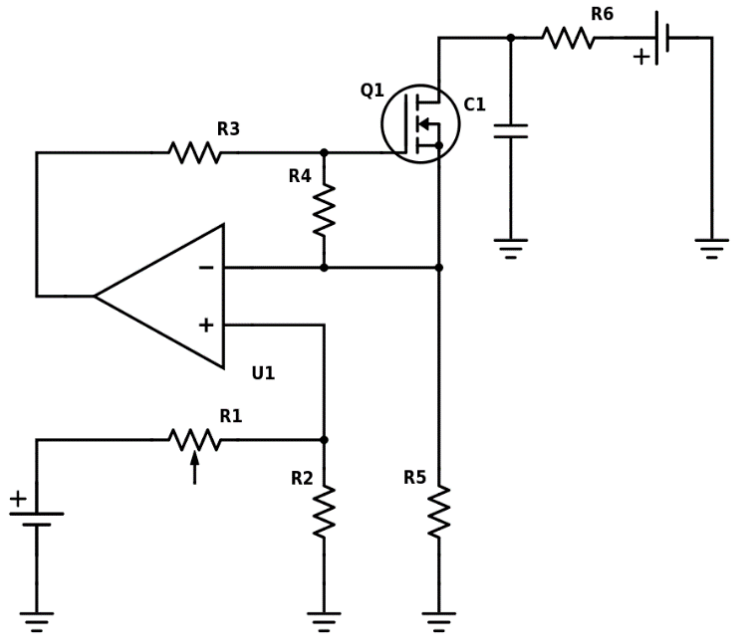

Figure 24: Control circuit of one MOSFET. R_1 = 2.55 kΩ, R_2 = 200 Ω, R_3 = 20 Ω, R_4 = 1kΩ, R_5 = 1 Ω, R_6 = 10 Ω and C_1 = 4.7 µF.

In order to obtain comparable results, the current flow through different MOSFETs must be exactly the same during the tests. In practice, this is achieved with a trimmer resistor which is placed in place of R_1. With the trimmer resistor, the current can be adjusted to be the same despite the inaccuracies of other components in the control circuit.

The operational amplifier (U_1) adjusts its output voltage such as the voltage difference between non-inverting (+) and inverting (-) input is close to zero. The operational amplifier is used to keep the power dissipation of MOSFETs constant through the whole test. Variations, for example, in the DC voltage level could affect the power dissipation of power transistors and affect the results of the tests. R_3 is a gate resistor. Since power transistors are not used as switches, the dimensioning of the gate resistor affects mainly the gain of the operation amplifier. C_1 and R_6 form a RC-filter. Without a RC filter, the DC voltage begins to oscillate due to the common DC voltage source with all control circuits. This phenomenon was found experimentally by measuring the DC voltage with an oscilloscope. The RC circuit was dimensioned with LT Spice program. Since, the power dissipation of one MOSFET is linearly dependent on Drain-Source voltage, R_6 must be a high-precision resistor. This ensures the same voltage drop over each control circuit.

The operation of the control circuit was simulated with LT Spice program. The dimensioning of different components was also done with LT Spice program. Operation and the design were verified with a prototype.

After the control circuit was designed and simulated, a PCB was created by the Eagle CAD software. Overall two PCBs were manufactured with each holding ten separate control circuits. The need for the RC filter was discovered after manufacturing PCBs and therefore RC circuits were implemented at the side of the PCBs. Furthermore, every control circuit is protected with fuses.

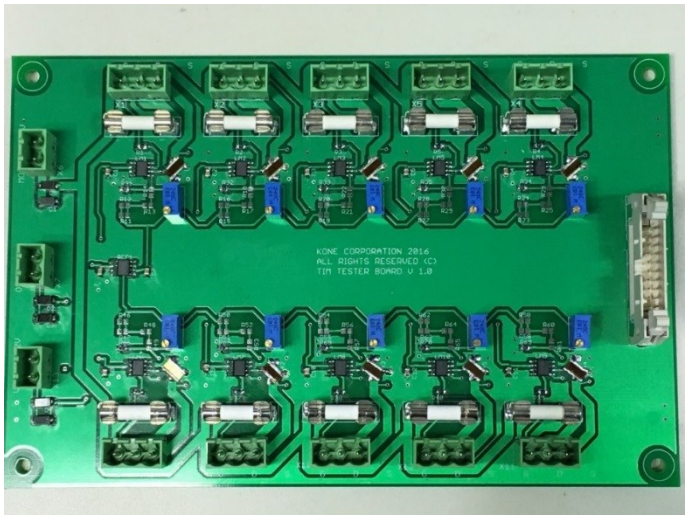

Figure 25: One PCB holding 10 control circuits. RC circuit was added afterwards and was built at the side of the PCB.

The main goal in the mechanical test frame design was to design a mechanical clamping element which maintains a constant pressure over the MOSFET during the whole test and the applied contact pressure is known or can be calculated. This is important since, as explained in Section 3.1 and shown in Equation (32), pressure variations have an effect on the heat transfer over the interface. If it is desired that thermal resistance changes only because of weakening in a TIM layer, the heat dissipation and the pressure must be constant through the whole test. This was resolved by designing a mechanical clamping unit which is based on a lever arm and gravity. By inserting a weight at the end of the lever arm with right dimensions, the pressing force is multiplied with factor ten at the top of the MOSFET. Hence, with a two kilogram weight, an approximately 200 N force is applied over MOSFET. As long as the air pressure remains constant, the pressure over a single MOSFET is constant and known.

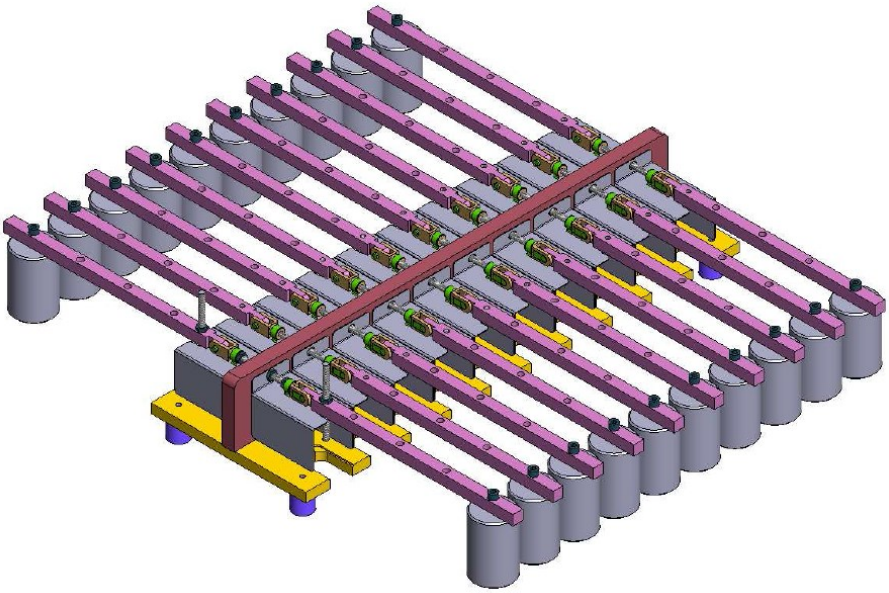

Figure 26: The mechanical test frame.

The mechanical test frame holds 20 heat sinks, copper bars and lever arms between which power transistors and TIMs are inserted. In addition, separate fans are used to cool the test spot more efficiently. Each test spots are separated from each other and the replace air is taken from above of each test spot. PCBs and the control logic are placed in boxes near the test frame. Figure 27 shows the whole test setup along with the measuring devices.

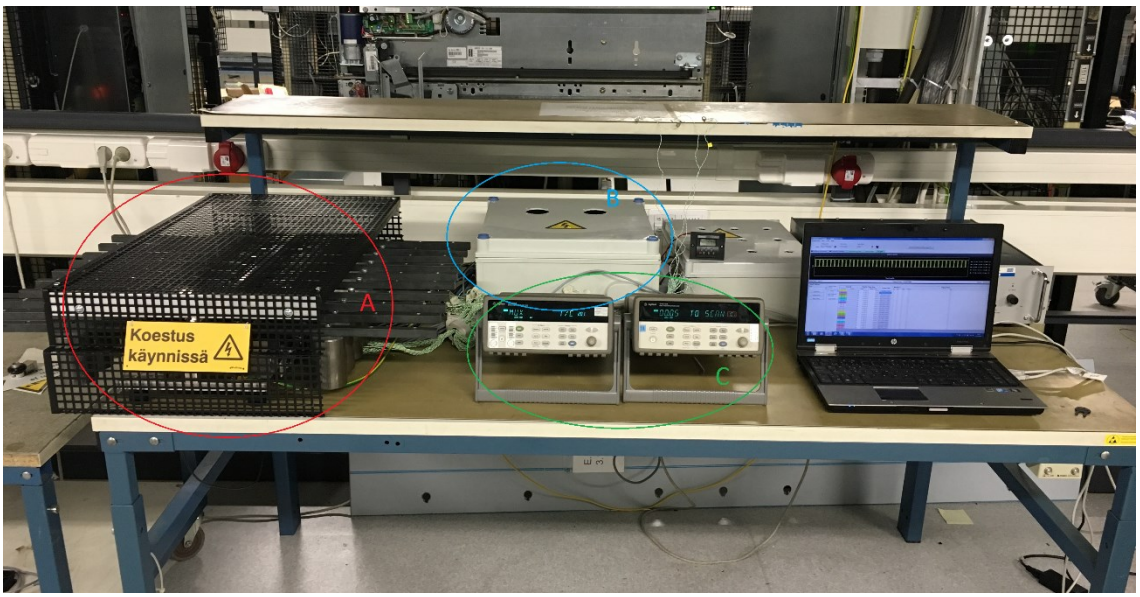

Figure 27: Test setup. A) The mechanical test frame with a contact protection. B) PCBs in a protection BOX. C) Measuring devices.

The created test setup can be used in two ways to obtain information on different TIMs:

- Test type 1: Comparison of thermal performance of TIMs.
- Test type 2: Power cycling of TIMs.

The temperature profile for each test can be seen below. In addition, the force applied to TIMs can be varied between 0 – 200 N in both tests. The power dissipation of MOSFETs is kept constant in both test profiles. However, the power dissipation can be adjusted to a desired value as explained before. In the power cycling test, the power dissipation along with t_{on} and t_{off} affect the maximum and minimum temperature of the test.

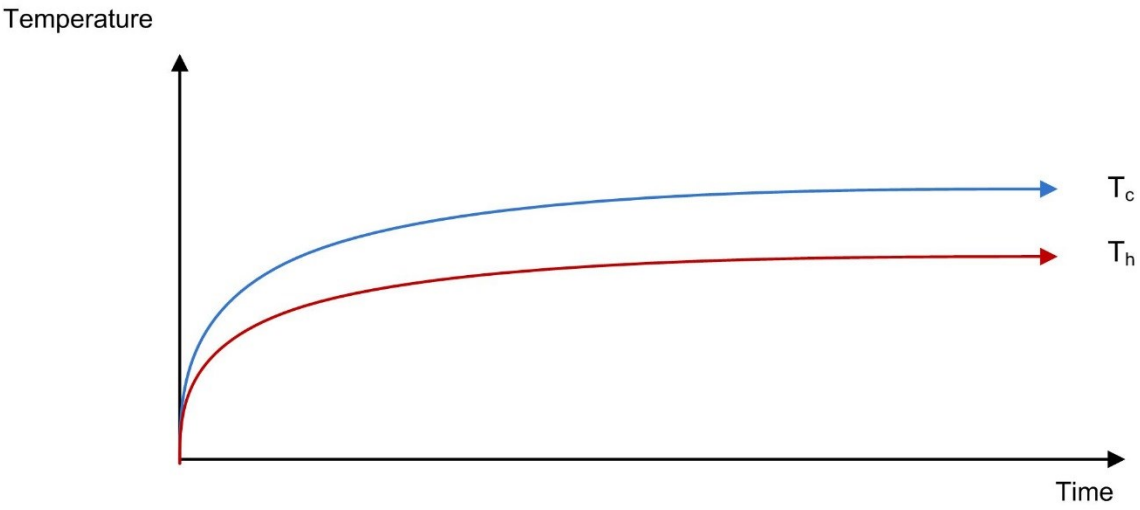

Figure 28: Test type 1. A temperature profile for the thermal performance comparison. T_c is the temperature of copper plate and T_h is the temperature of heat sink.

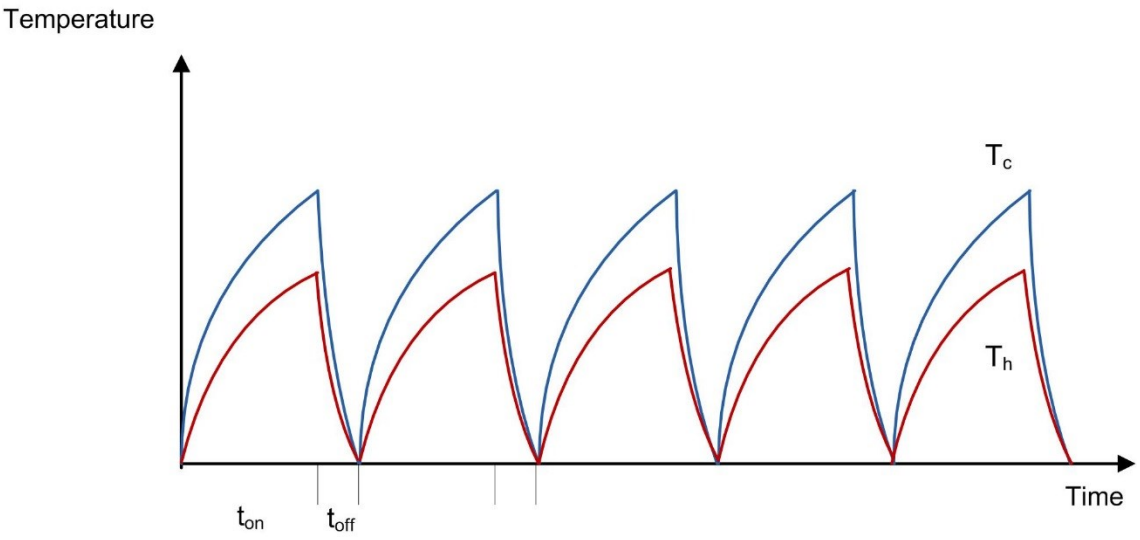

Figure 29: Test type 2. A temperature profile for the power cycling test. T_c is the temperature of copper plate and T_h is the temperature of heat sink.

Since the power dissipation and the pressure can be kept constant and those parameters are known, the test system can be used to analyze how a surface roughness affects the heat

transfer. In addition, since the pressure can be varied and it can be applied to different locations in a transistor, different mounting methods can also be studied.

A few limitations exist while using the test system. These limitations occur mainly from the component sizing and can be altered in the future if necessary. However, with current dimensioning, these limitations apply. Parameters in Table 2 comprise one test spot. The capacitor used for the RC circuit limits the maximum voltage. Since, capacitors withstand 400 V, this value can not be exceeded. However, if necessary, capacitors can be changed if higher voltages are required. Furthermore, the RC circuit determines maximum value for the current flow as well. The resistor R_6 withstands power dissipation P_{pd} = 0.6 W thus I_{max} can be calculated from $I_{max}^2 = P_{pd} / R$.

The maximum power dissipation in a single MOSFETs is 160 W although with the previous voltage and current limitations the maximum power dissipation in the test system can not exceed 98 W. Moreover, the junction temperature of one MOSFET can not exceed 150 ºC. Since, the junction temperature is not directly measured, a safety limit must be kept in the copper plate temperature measurement.

The lever arm in the mechanical test frame has four different points for the gravity weights. For these tests, two kilograms weights were manufactured. With the current sizing, this limits the pressure, which can be applied, to four different values. Values are presented in Table 2.

Finally, the dimensions of the power transistor limit the size of the test samples. Since, the power cycling mainly causes failure mechanisms due to the differences in CTE, the results of this study can not be directly converted to relate failures in, for example, IGBT modules. When the case size increases, the CTE differences increases and can cause more prominent failures.

Table 2: Test system limitations.

$\boldsymbol{U_{max}}$	400 V
$\boldsymbol{I_{max}}$	245 mA
$\boldsymbol{P_{max}}$	160 W
$\boldsymbol{T_{cumax}}$	~135 ºC
Sample size	15.75 × 20.15 (mm)
Pressure	18 / 33 / 48 / 63 (N/cm^2)

5.3 Power cycling measurements

Before the measurements were started all heat sinks and copper bars were treated with a very fine abrasive paper (grit > 1000) to achieve smooth and even surfaces. As already explained in Section 3.1 surface roughness affect the thermal resistance thus it is important to do the tests with similar heat sink surfaces. The surface roughness of heat sinks was measured and results can be found in Appendix B. The pressure used in the test, is given by the TIM manufacturer. t_{on} and t_{off} was determined experimentally to obtain the desired maximum and minimum temperatures. The maximum temperatuture of the test was determined to be 125 °C. Test parameters, used in the power cycling test, are presented in Table 3.

Table 3: Test parameters in the power cycling test.

Pressure	30.3 N/cm^2
t_{on}	300s
t_{off}	60s
T_{max}	100ºC / 125ºC
T_{min}	50ºC
Power dissipation	~30.8 W

Since, two different materials are tested, the peak temperature T_{max} is not identical. Furthermore, two preselected thermal interface materials were selected for this measurement. These materials are used in applications discussed in Section 2.2. TIMs are an elastomer film and a PCM. Characteristics of both materials are shown in Table 4.

Table 4: TIM properties.

	Elastomer film	PCM
Thermal conductivity	1.7 W/mK	1.8 W/mK
Thermal resistance	73 (mm^2·K/W)	0.32 (K/W)
Dielectric breakdown voltage	26 kV/mm	6 kV/mm
Bond line thickness	30 µm	22.5 µm

Since the power cycling test was designed to continue over 8000 cycles, the temperatures were measured only from the last 30s of the t_{on} cycle. This will ease the processing of the measurement data. Furthermore, currents and voltages were measured from each test spot with an external measurement device to verify the operation point of each power semiconductor device. Measured currents and voltages can be found in Appendix E.

5.3.1 Measurement data

Thermal interface materials were exposed to approximately 8100 power cycles with a constant pressure of 30.3 N/cm^2. To detect changes in thermal resistances, the temperature different was measured at the peak of each cycle. The average temperature difference from ten test places is presented in Figure 30. The thermal resistance is calculated according to Equation (12) and is presented in Figure 31. From here on, when analyzing the results of this study, the concept thermal performance refers to the thermal resistance as well as to the temperature difference.

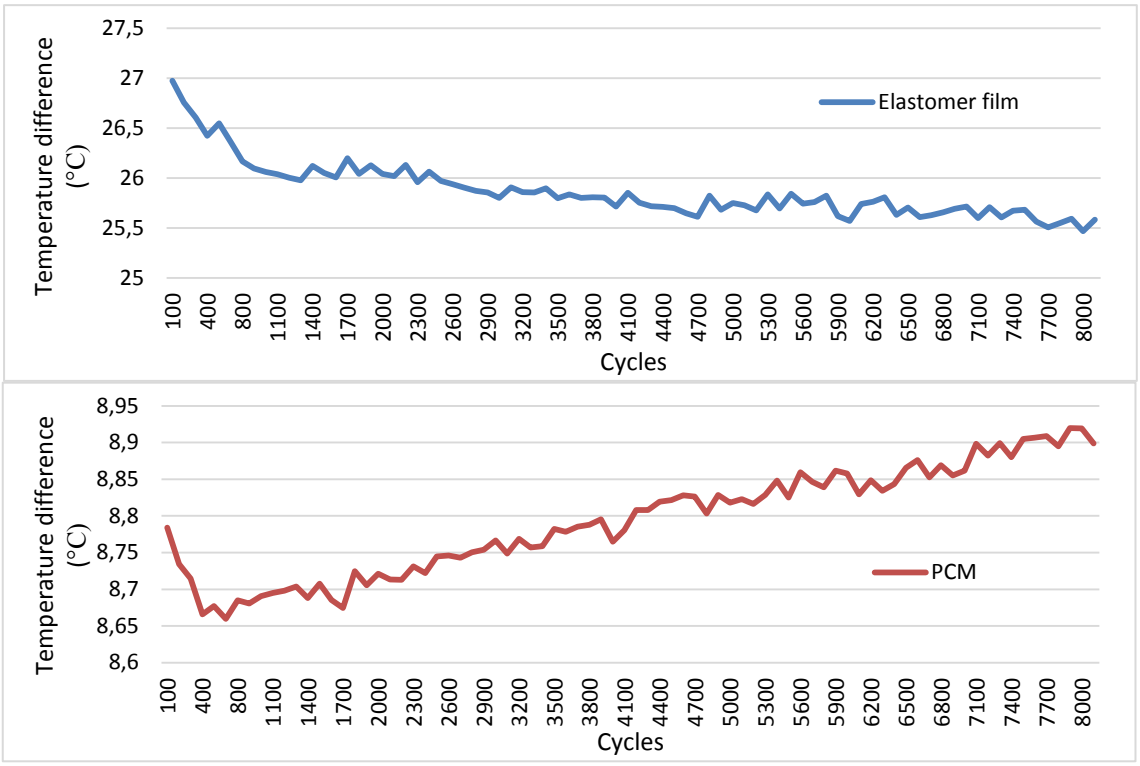

Figure 30: The change in the temperature difference during the power cycling test. On the upper graph is the elastomer film and on the lower graph is the PCM.

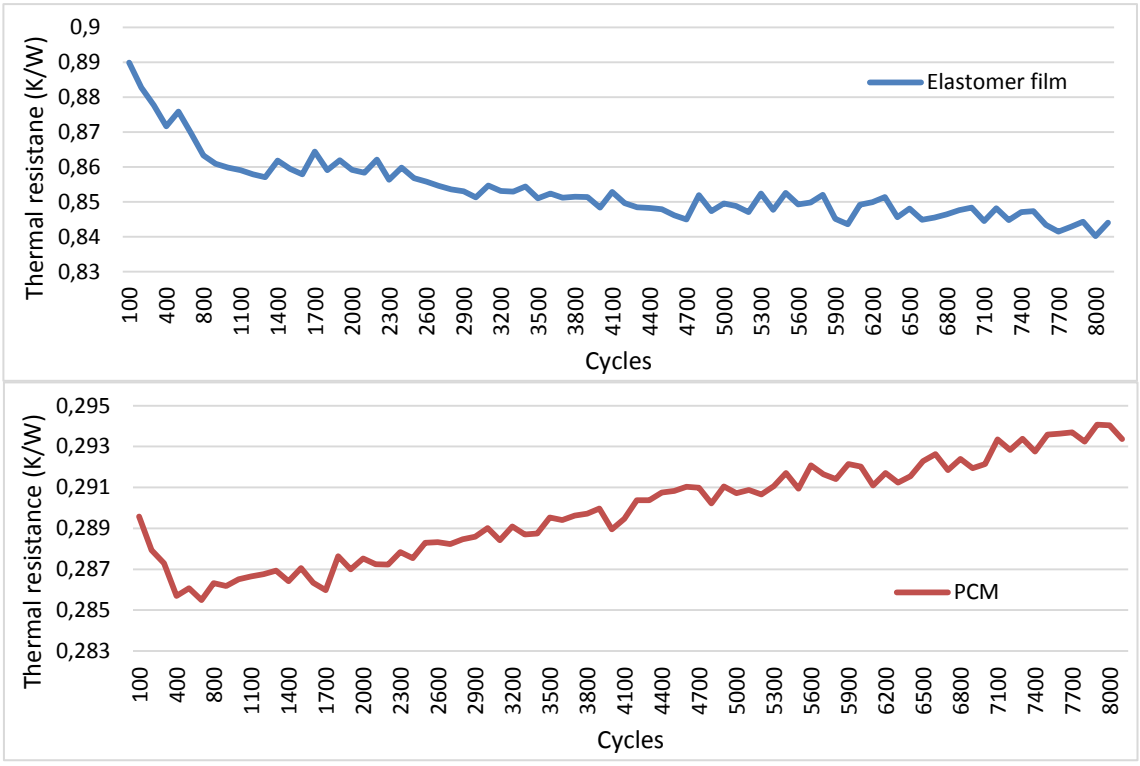

Figure 31: The change in the thermal resistance during the power cycling test. On the upper graph is the elastomer film and on the lower graph is the PCM.

Based on the test data, the temperature difference with the elastomer film decreased with approximately 1.39 degrees during 8100 cycles and with the PCM, the temperature difference

increased by 0.11 degrees during 8100 cycles. Furthermore, the thermal resistance with the elastomer film decreased by 0.046 K/W and the thermal resistance with the PCM increased by 0.0038 K/W from the initial value. As a percentage, the decrease with elastomer film is 5 % and increase with PCM is 1.3 %. Hence, the thermal performance of the elastomer film actually improved and the thermal performance of the PCM decreased. The improvement in performance could occur from the fact that the elastomer film binds and settles itself more efficiently to the air gaps between surfaces due to the thermal stress and movement. At the beginning of the test, (cycles < 1000) the improvement was more rapid and continued to improve throughout the whole test. Such as the elastomer film, the performance with the PCM improved at the beginning of the test. (cycles < 800). The improvement could occur again from better conforming between surfaces which is caused by thermal movement. However, it should be noted that the PCM cures itself in the interface after it is installed. Hence, at the beginning of the test, the PCM is already better conformed. The tape can not increase its performance as long as the elastomer film and the optimum thermal performance is obtained relatively early. Futhermore, it should be noted that the thermal performance of PCM did not saturate at all and immediately began to weaken after the best thermal performance (zero point) was obtained. Nonetheless, the change in the thermal performance was not significant after the zero point (~0.07 K/W during 7300 cycles). Futhermore, the elastomer film continued to improve its performance throughout the whole test and the point of the best thermal performance has not been achieved yet.

5.3.2 Regression analysis

To analyze the life time behaviour of TIMs further, a regression curve was adapted to the measurement data. This was done with a Minitab software. Figure 32 and Figure 33 presents the regression analysis for temperature differences and Figure 34 and Figure 35 for thermal resistances.

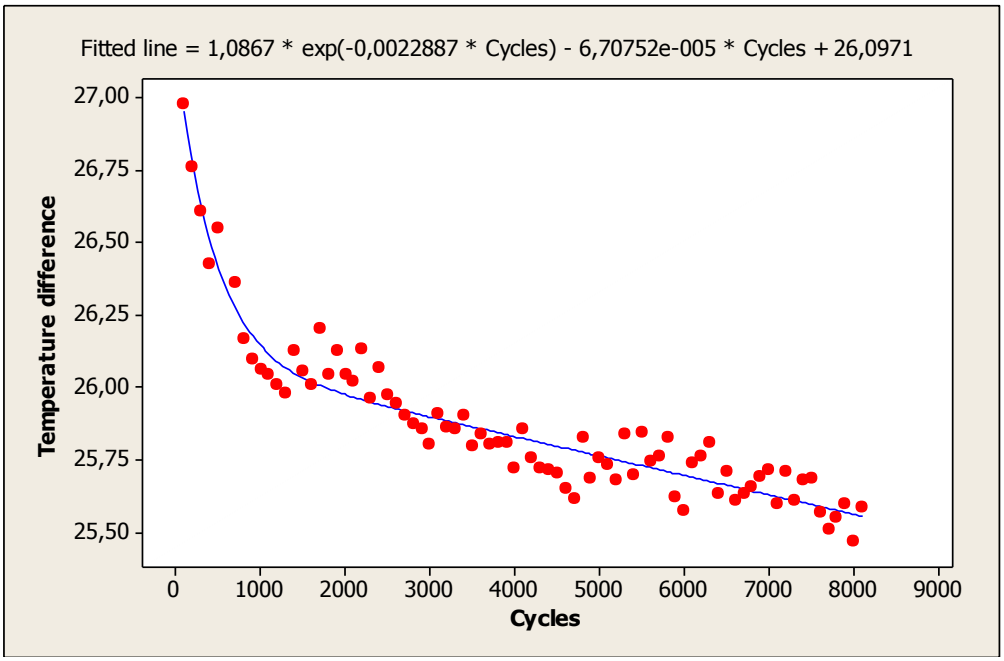

Figure 32: Fitted line plot for the temperature difference of the elastomer film.

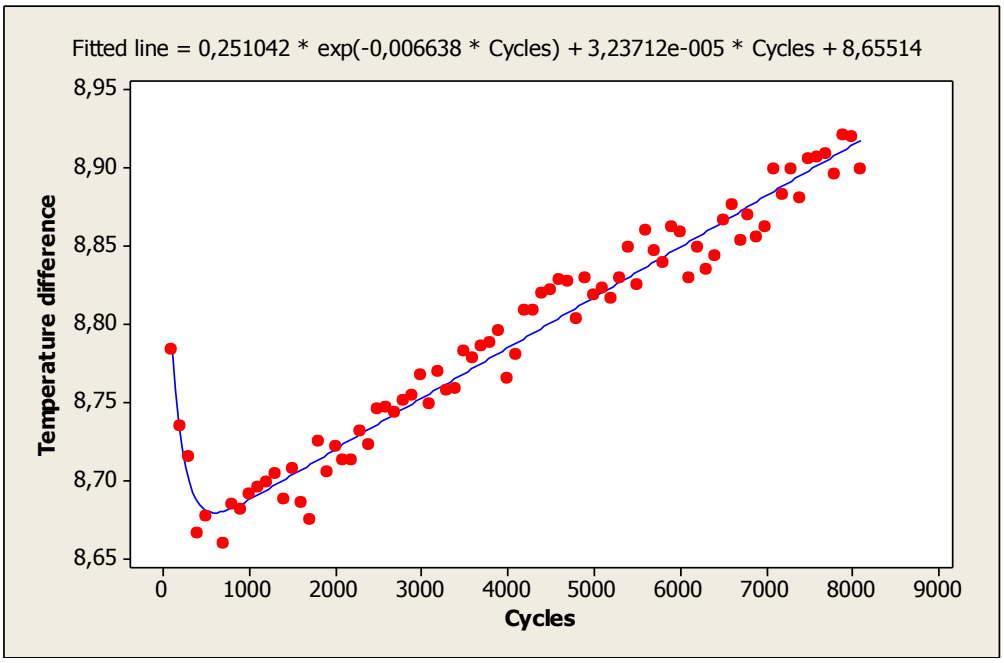

Figure 33: Fitted line plot for the temperature difference of the PCM.

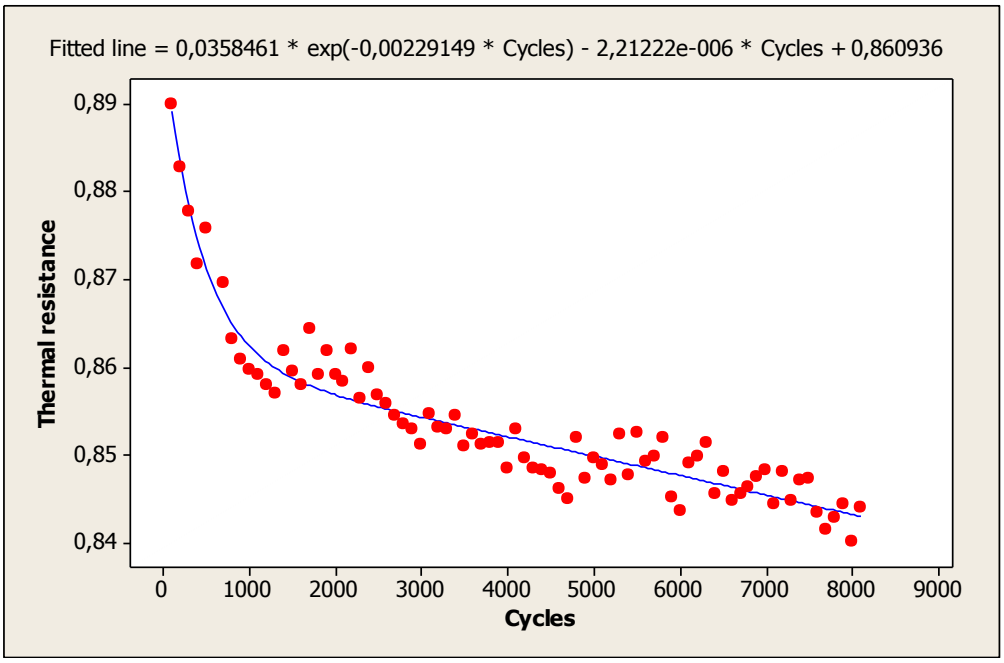

Figure 34: Fitted line plot for the thermal resistance of the elastomer film.

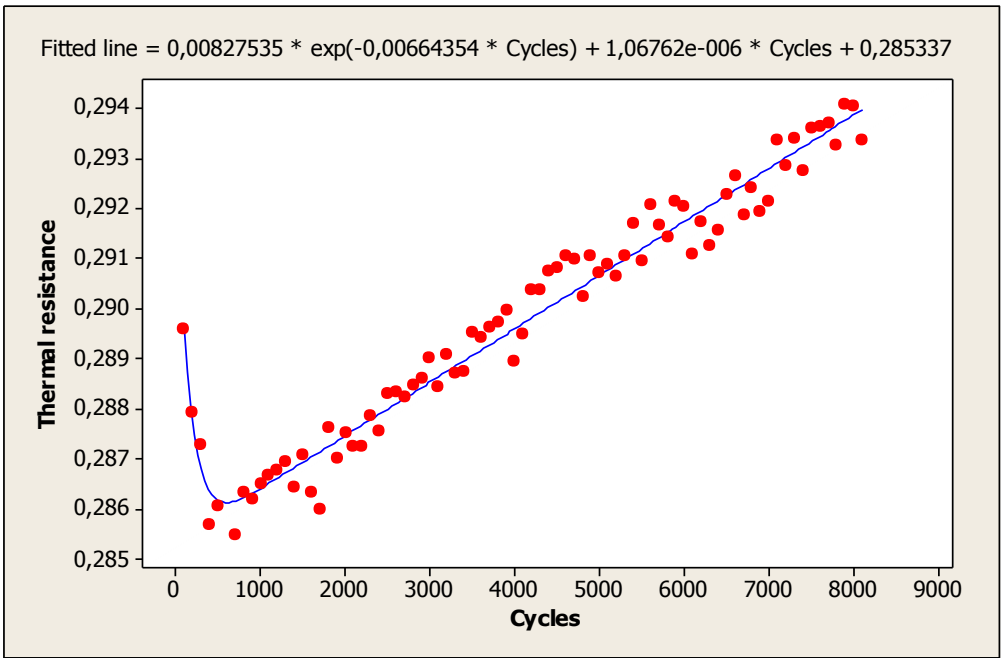

Figure 35: Fitted line plot for the thermal resistance of the PCM.

Based on the regression analysis the degradation models for both TIMs can be established:

$$R_{th}(T,n) = A * e^{B*n} - C \cdot n + D \tag{49}$$

where n is cycle number and coefficients A, B, C and D can be determined from the measurement data. The degradation trend is a combination of nonlinear degradation model and a linear degradation model with an offset D. Different degradation models were presented in Section 4.3.3. With a degradation model the life time behaviour of a TIM can be predicted. The estimated change for the temperature difference and for the thermal resistance according to degradation models is presented in Figure 36 and in Figure 37.

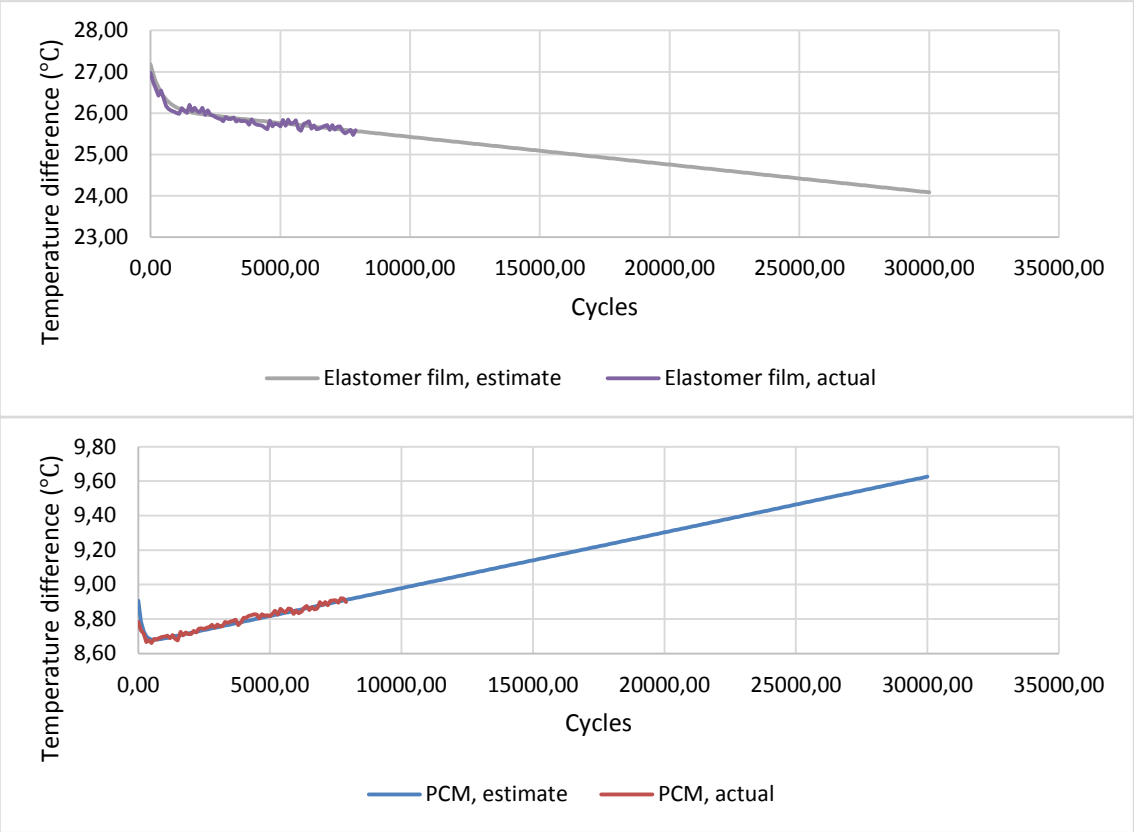

Figure 36: The life time prediction for the temperature difference. On the upper graph is the prediction for the elastomer film and on the lower graph is the prediction for the PCM.

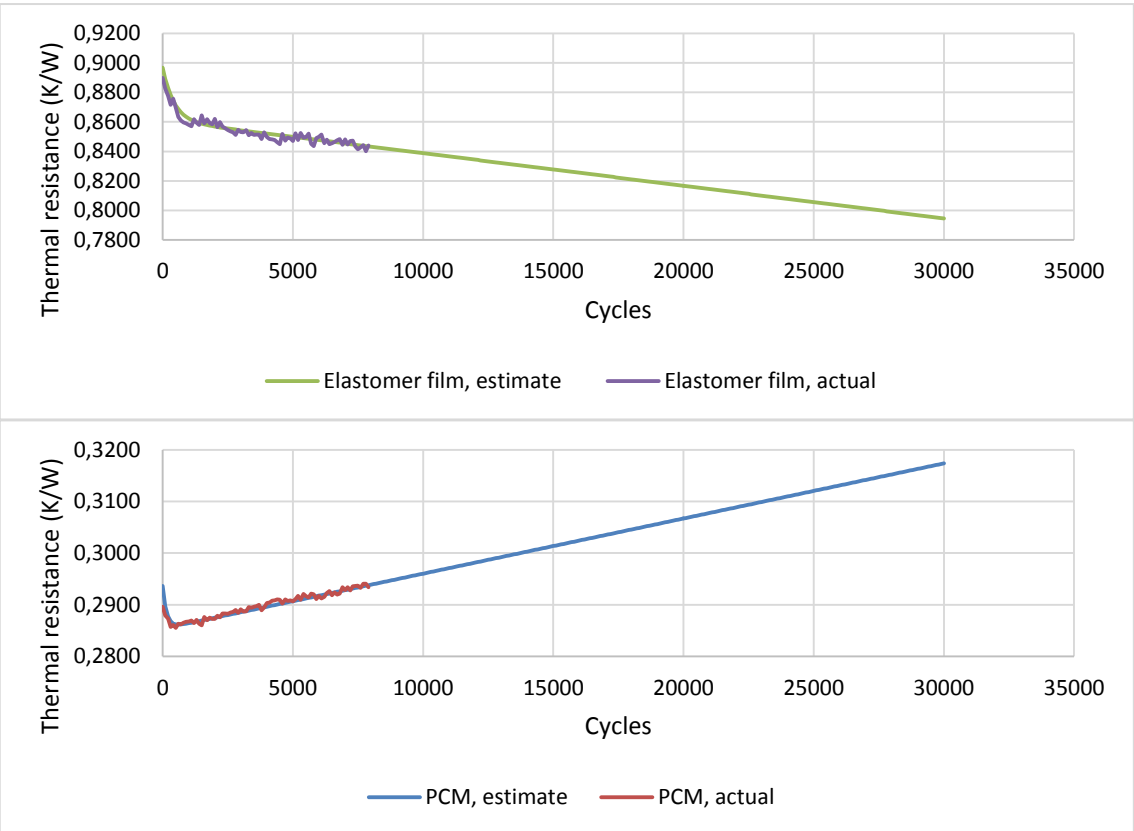

Figure 37: The life time prediction for the thermal resistance. On the upper graph is prediction for the elastomer film and on the lower graph is prediction for the PCM.

Since, the actual measurement data consist only from 8100 cycles it is not wise to analyze the life time behaviour further. To obtain more reliable results the number of cycles should have been greater. However, the regression analysis fit the measurement data well. There are not yet signs of saturation of thermal performance with either TIMs. Nonetheless, with elastomer film, the saturation can be expected to occur soon since the thermal performance can not improve indefinitely. Therefore, one should be careful when making conclusion from the regression analysis related to the elastomer film. As well as with the elastomer film, the performance of PCM could saturate. The behaviour of PCM is, however, not generally known and the possible saturation is hard to predict. However, with the current test data the estimate for the thermal performance of TIMs is analyzed as it is presented above. The rate of change in the thermal resistance with the elastomer film is estimated to be 0.011 K/W over 5000 cycles and with the PCM 0.005 K/W over 5000 cycles. Hence, the degradation of PCM is not significant. Based on the literature review (Section 4.3), there are no clear understanding which causes the degradation of TIMs. A closer look at the data reveals another very important performance characteristic. The best thermal performance is not obtained necessarily at the beginning of life time. This underlines the fact that a material showing the best performance at the beginning of the life time might not be the most ideal TIM for the application. The best thermal performance with the elastomer film is not yet achieved. However, to obtain the same thermal performance with the PCM, the elastomer film should withstand enormous numbers of power cycles. This could lead to other problems, for example, decrease in the dielectric breakdown voltage.

To analyze the actual life time of one material at the operating conditions, a second degradation test is required as explained in Section 4.3.3. However, within the time limits of this study it was not possible to achieve. Even so, the degradation model at operating condition can be expected to follow the same degradation trend with different thermal model coefficients. Hence, the second degradation test at operating conditions does not need to take such a long time. The obtained degradation models can be used to predict life times and to analyze the degradation trends of TIMs.

5.4 Performance comparison measurements

The performance comparison test was done with the same thermal interface materials, presented in Section 5.3, Table 4. The purpose of this test was to compare the initial thermal resistances of fresh samples and to analyze the effect of interface pressure to thermal resistance. In total of four different interface pressures were used. The tests were continued until temperatures stabilized. Power dissipation was chosen to be 10 W. Once again the voltages and currents were measured with an external measurement device and results can be found on Appendix E. The test parameters are summarized in Table 5.

Table 5: Test parameters in performance comparison test.

Pressure	18 / 33 / 48 / 63 N/cm^2
t_{on}	1 hr
t_{off}	-
T_{max}	60 °C
T_{min}	-
Power dissipation	~10 W

5.4.1 Measurement data

The temperature difference with different interface pressures is presented on the left hand graph in Figure 38. Thermal resistances are once again calculated according to Equation (12) and are presented on the right hand graph in Figure 38.

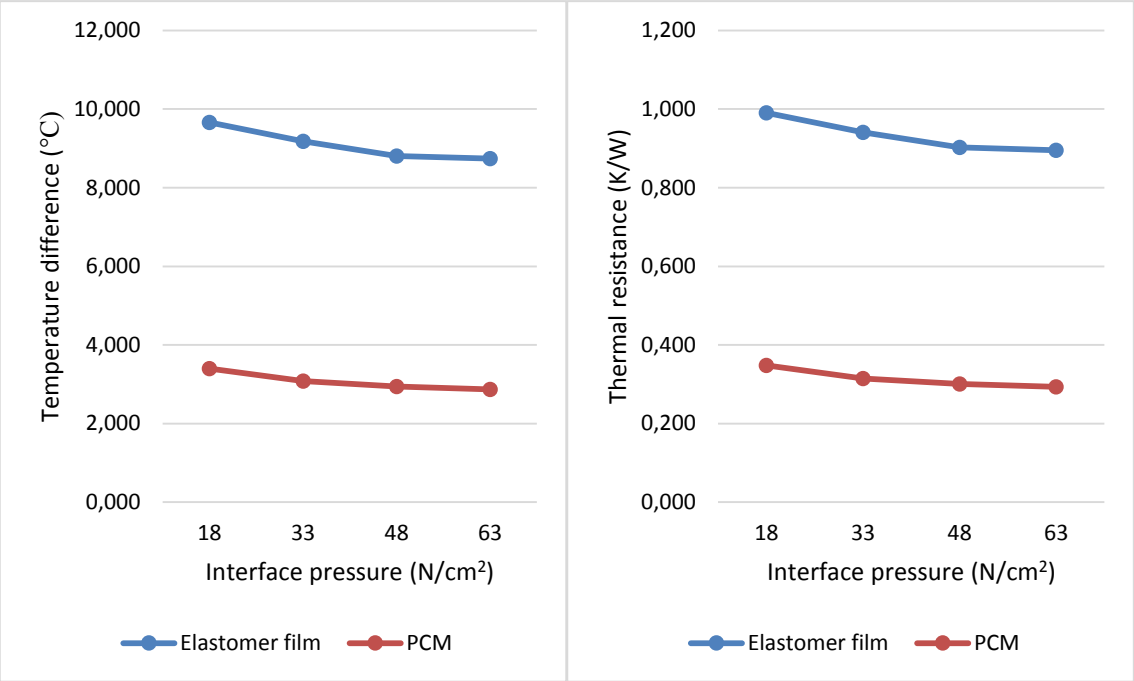

Figure 38: The temperature difference and the thermal resistance with different interface pressures. On the left hand graph is the temperature difference and on the right hand graph is the thermal resistance.

Based on the measurement data, elastomer film has approximately three times higher thermal resistance than PCM. This is a significant result since both materials are used in somewhat similar applications. However, according to manufacturers, the dielectric breakdown voltage is four times higher with elastomer film. Futhermore, the thermal resistance decreases while the pressure increases as it was presented in Section 3.1 Equation (33). The change in thermal resistance with increased pressure is higher with elastomer film (0.095 K/W) than with PCM (0.054 K/W). However, expressed as a percentage from the initial value, the change in thermal resistance is higher with PCM (16 %) than with elastomer film (10 %). Futhermore, the elastomer film manufacturer, provides information on how pressure affects the thermal resistance. Change in thermal resistance is approximately 1 K/W with pressure variation from 20 to 60 N/cm^2. This corresponds to our results remarkably well (0.095 K/W with pressure variation from 18 to 63 N/cm^2).

5.5 Uncertainty analysis

This Section covers the uncertainty analysis of measurement results. Section 5.5.1 discusses general uncertainty concepts. Section 5.5.2 explains uncertainty in the temperature measurements and Section uncertainty in the voltage measurements. Section 5.5.4 discusses overall uncertainties related to the calculated thermal resistances.

5.5.1 Theoretical approach for determining uncertainty of measurements

An error is always present in measurements. Due to this fact, a measurement results without any knowledge about the accuracy of the measurement is rarely useful. If only one measurement is made, the error in measurement is analyzed on the basis of the accuracy of the measuring device. However, if it is possible, multiple measurements from the same measurement point must be done. Hence, the measurement result is the arithmetic mean $\bar{x}$ of independently measured quantativies x_i and can be calculated according to Equation (50).

$$\bar{x} = \frac{1}{n}\sum_{j=1}^{n} x_i \tag{50}$$

However, a measured value Y may depend on several input quantities $x_1, x_2, x_3, \dots x_N$ according to Equation (51). (JCGM, 2008)

$$Y = f(x_1, x_2, x_3 \dots x_N) \tag{51}$$

This relation can often be expressed by a mathematical equation. However, it might be difficult to write all quantities into the same equation. In such case, a function f can be determined experimentally or by a simulation or by combination of both. The input quantitatives $(x_1, x_2, x_3 \dots x_N)$ can be categorized into two main categories. The first category contains quantitatives which can be determined from the current measurement. These include single observations, repeat observations and experience – based values. The second category consists of data which is brought from external sources, for example, from measurement standards and handbooks. (JCGM, 2008)

The standard uncertainty $u(x)$ of measurement can be determined by two different methods. These methods are called type A uncertainty and type B uncertainty. Type A uncertainty can be determined by statistical methods. Type B uncertainty, however, is evaluated by scientific judgement based on all the available information on the possible variability of x_i. Type A uncertainty, for example, can be determined by repeating measurements n times. A measurement result is average of n measurements and the standard uncertainty is the average standard deviation of group n. Type B uncertainty does not improve by repeating measurements and, for example, can be determined from a calibration certificate of a measurement device. (JCGM, 2008)

A systematic error is an error which occurs from the test equipment or the test method. A systematic error, for example, occurs from lack of calibration or incorrect zero point setting. A systematic error can be eliminated from measured values if the origin of error is identified. The random error is always present in measurements and cannot be removed for good. However, random error can be estimated and reduced by repeating measurements n times.

If the number of measured quantitatives is more than ten, a statistically reliable experimental variance σ^2 can be calculated according to Equation (52). The type A standard uncertainty is determined as the experimental standard deviation of the mean $u(\bar{x})$ and can be calculated according to Equation (53). (JCGM, 2008)

$$\sigma^2 = \frac{1}{n-1}\sum_{j=1}^{n}\left(x_j - \bar{x}\right)^2 \tag{52}$$

$$u(\bar{x}) = \frac{1}{\sqrt{n}}\sigma \tag{53}$$

When calculating the uncertainties of measurements one should be careful between using standard deviation σ and standard deviation of the mean $u(\bar{x})$. Standard deviation indicates where the next data point falls with 68 % probability and standard deviation of mean indicates where the next sample average point falls with 68 % probability. Therefore, if results are reported as average of measurements, the standard deviation of mean should be used insted of standard deviation. Coverage factors apply with both parameters. This means that if data distribution is approximately normal then about 68 percent of the data values are within $\bar{x} \pm u(x)$ Furthemore, about 95 percent are within $\bar{x} \pm 2u(x)$ and 99.7 percent are within $\bar{x} \pm 3u(x)$. Moreover, with 99.9 % coverage factor, measurements falls between $\bar{x} \pm 3.29\, u(x)$. This level of confidence will be used from now on in this study. Futhermore, it should be noted that measurement results must be normally distributed in order to employ previous uncertainty concepts. It is commonly known that measurements are normally distributed. However, to be absolute sure this will be studied and presented in the next Section.

For the type B uncertainty, a different approach is given. Device manufacturers provide upper (a_+) and lower (a_-) limits for uncertainty in measurement. Hence, a rectangular probability density function is assumed when determining uncertainty. The estimate for a rectangular probability function x_i can be calculated according to Equation (54) and type B standard uncertainty $u(x)$ according to Equation (55). (JCGM, 2008)

$$x_i = \frac{1}{2}(a_+ + a_-) \tag{54}$$

$$u(x) = \sqrt{\frac{1}{12}(a_+ - a_-)^2} \tag{55}$$

If the absolute value of upper and lower limits are the same, the standard uncertainty can be presented as follows:

$$u(x) = \frac{a}{\sqrt{3}} \tag{56}$$

Standard uncertainty related function f is obtained according to Equation (57).

$$u_c^2(y) = \sum_{i=1}^{n}\left(\frac{df}{dx_i}\right)^2 u^2(x_i) \tag{57}$$

Sometimes it might be easier to use relative standard uncertainty which can be calculated according to Equation (58).

$$\frac{u_c^2(y)}{f} = \sum_{i=1}^{n} \left(\frac{df}{dx_i}\right)^2 \cdot \frac{1}{f}\, u^2(x_i) \tag{58}$$

Occasionally, we are interested to know how sensitive the function f is for changes in its parameters. This can be calculated by using the total differential method. The maximum error of f can be calculated according to Equation (59). It should be noted that Equation (59) gives the maximum error of function f since, equation assumes that all errors affect the same direction.

$$|\Delta f| \leq \left|\frac{\partial f}{\partial x}\Delta x\right| + \left|\frac{\partial f}{\partial y}\Delta y\right| + \left|\frac{\partial f}{\partial z}\Delta z\right| + \ldots \tag{59}$$

where $\Delta x, \Delta y, \Delta z$ are the absolute measurement errors. The relative sensitivy, which is often more interesting, can be calculated according to Equation (60).

$$\frac{|\Delta f|}{f} \leq \left|\frac{\partial f}{\partial x}\Delta x \cdot \frac{1}{f}\right| + \left|\frac{\partial f}{\partial y}\Delta y \cdot \frac{1}{f}\right| + \left|\frac{\partial f}{\partial z}\Delta z \cdot \frac{1}{f}\right| + \ldots \tag{60}$$

5.5.2 Uncertainty in temperature measurements

To reverse the systematic error in the temperature measurements, the temperature sensors were calibrated before starting tests. All thermocouples were placed in an environmental chamber. A total of five different reference temperatures were used to determine the error in temperature measurements. Reference temperatures were 80, 90, 100, 110 and 120 celsius degree. Reference points were chosen near the supposed maximum temperatures of measurements. At each test point, the test was continued until the temperatures were stabilized. The ambient temperature in the environmental chamber was verified with a calibrated K thermocouple and a calibrated Fluke thermometer. In addition, the indication of the Fluke thermometer was compared with the temperature sensors of the environmental chamber. These temperatures displayed the same values with 0.1 degree accuracy. By determining temperature measurement error experimentally, the error in the measurement device and thermocouple is removed. This method produces precise results. The uncertainty after calibration, related to temperature measurements, is the uncertainty related to the calibration device summed to the standard deviation of mean of measurements at the measurement temperature. Temperature calibration results and the standard deviations can be found on Appendix C. Furthermore, each thermocouple sensor displayed the reference value with the highest error of 2.28 °C. For each thermocouple sensor, a line equation was drawn to obtain systematic error in each temperature measurement. The line equation was used as a correction factor when calculating results in this thesis. In Figure 39, x-axis is the actual temperature and y-axis is the temperature indication of the temperature sensor. The correct temperature can be obtained from the correction curve.

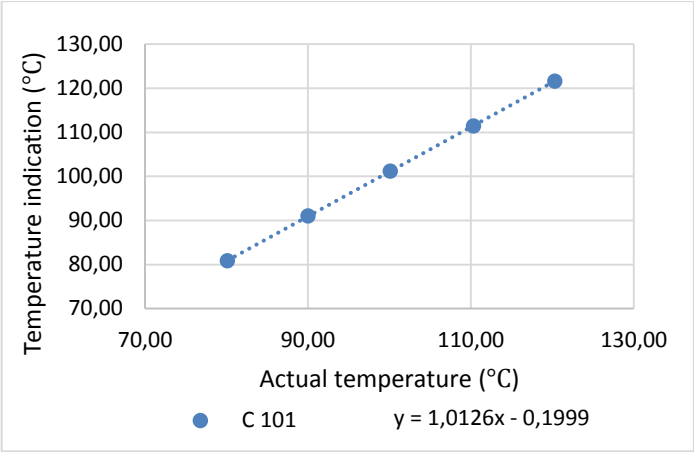

Figure 39: For each temperature channel, a line equation was drawn to obtain the systematic error in temperature measurements. The line equation functioned as a correction factor when calculating the results of this study.

As mentioned the uncertainty left in the temperature measurements is the uncertainty in the calibration device summed to the type A standard uncertainty at the test temperature. Above -100 celsius the accuracy of Fluke thermometer, which was used as a calibration device, is given as: ± (0.05 % of reading + 0.3) ºC with a resolution of 0.1 ºC. Hence, in the worst case scenario, the indication of a single thermocouple is 127 degrees. This will result in uncertainty of ± 0.3635 degrees. Since the resolution of the thermometer is 0.1 ºC the error in calibration could be as bad as ± 0.4 ºC. The type B standard uncertainty for the calibration device is calculated according to Equation (56) and is 0.23 ºC. Moreover, type A uncertainties for each thermocouple sensor were calculated at the test temperature and are presented in Appendix C. Futhermore, 99.9 % confidence levels are calculated and are presented in the same Appendix. The highest uncertainty with 99.9 % confidence level is 0.159 °C. This summed to the calibration error will result in maximum overall error in temperature measurements of ± 0.559 °C. This result will be used in Section 5.5.4.

As discussed, it is in common knowledge that measurement results are normally distributed. Nonetheless, a probability plot of temperature measurement channels was done to ensure this.

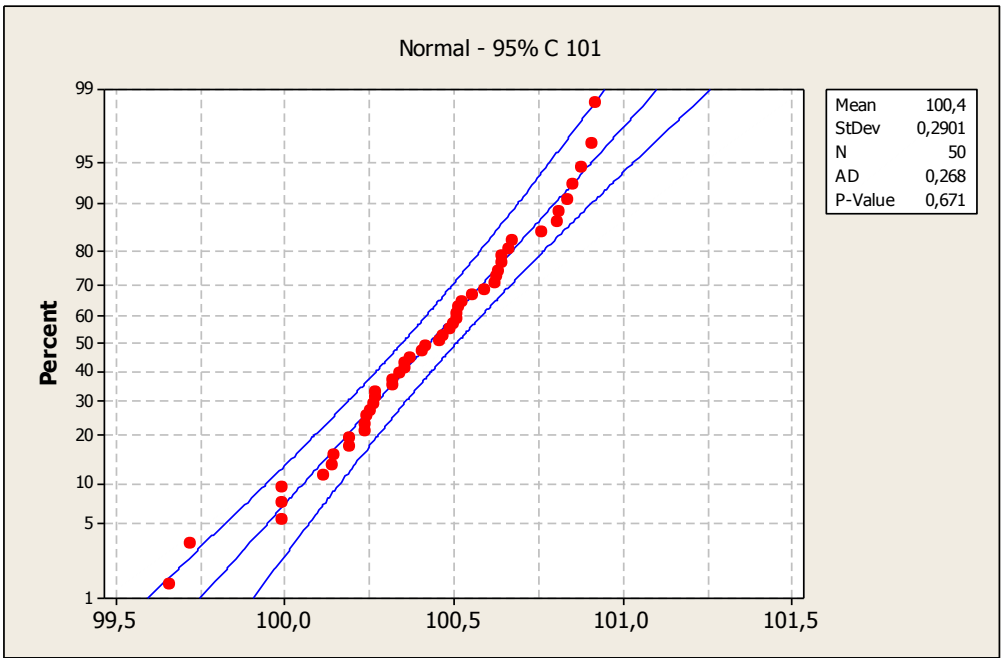

Figure 40: Probability plot of temperature measurement of channel 101. The red dots are temperature measurements from the same test point. Measurements are normally distributed. Sample size is 50.

Since measurement points are almost completely inside the blue lines, it can be stated that measurements are normally distributed. Therefore, the results of this study are qualified.

5.5.3 Uncertainty in voltage measurements

In total of two different voltage measurements were done: A voltage measurement over the shunt resistor and a DC voltage measurement. The voltage over the shunt resistor was measured with Agilent datalogger and the DC voltage with a Fluke multimeter. Uncertainty in voltage measurements is estimated according to type B uncertainty. From Agilent datalogger specifications the error in voltage measurements is given as: ± (0.0002 % of reading + 0.0001 % of range) V. This results in the absolute error of ± 0.3 mV and type B standard uncertainty of 0.173 mV.

The accuracy of Fluke multimeter is given as: ± (0.05 % from reading + 1) V with resolution of 0.1 V. In the worst case, the DC voltage was 168.5 V hence, the absolute error in DC source voltage measurement is ± 1.1 V and the type B standard uncertainty is 0.635 V.

5.5.4 Uncertainty in overall results

Uncertaity components are summarized in Table 6.

Table 6: Uncertainties in measurements.

Uncertainty component	The type of analysis	68 % coverage factor	99.9 % coverage factor
Thermocouples	Type A	Presented for each temperature channel in Appendix C	Presented for each temperature channel in Appendix C
Calibration accuracy	Type B	0.23 °C	0.76 °C
Shunt resistor voltage measurement	Type B	0.17 mV	0.57 mV
DC-voltage measurement	Type B	0.63 V	2.09 V

Standard uncertainties indicates how accurate is a single measurement or a average of measurements. However, the sensitivy of calculated results to changes in it's parameters is often more interesting. The thermal resistance is calculated according to Equation (61).

$$R_{th} = f = \frac{R_{shunt}}{U_{dc}U_{shunt}} (T_1 - T_2) \tag{61}$$

where R_{shunt} is the resistance of shunt resistor and U_{shunt} is the voltage over shunt resistor. The partial derivates are calculated below. From Equations (62) – (66) it can be seen how much change in one parameter could cause error in the calculated thermal resistance. These errors are calculated with a worst case scenario with 99.9 % confidence level presented for voltage measurements in Table 6 and for temperature measurements in Appendix C.

$$\frac{\partial f}{\partial T_1} \Delta T_1 \cdot \frac{1}{f} = \frac{\Delta T_1}{T_1 - T_2} = 6.5\ \% \tag{62}$$

$$\frac{\partial f}{\partial T_2} \Delta T_2 \cdot \frac{1}{f} = \frac{\Delta T_2}{T_1 - T_2} = 6.5\ \% \tag{63}$$

$$\frac{\partial f}{\partial U_{dc}} \Delta U_{dc} \cdot \frac{1}{f} = \frac{\Delta U_{dc}}{U_{dc}} = 1.2\ \% \tag{64}$$

$$\frac{\partial f}{\partial U_{shunt}} \Delta U_{shunt} \cdot \frac{1}{f} = \frac{\Delta U_{shunt}}{U_{shunt}} = 0.3\ \% \tag{65}$$

$$\frac{\partial f}{\partial R_{shunt}} \Delta R_{shunt} \cdot \frac{1}{f} = \frac{\Delta R_{shunt}}{R_{shunt}} = 0.1\ \% \tag{66}$$

where ΔT_1, ΔT_2, ΔU_{dc}, ΔU_{shunt}, ΔR_{shunt} are absolute errors of parameters in Equation (61). Hence, in the worst case, the calculated results could be wrongly interpretended with 14.6

percent. Although it is not shown, the worst case scenario with noncalibrated thermocouples was also calculated. With the noncalibrated thermocouples the results could be misinterpreted by 53 percent. Without calibrating the thermocouples the results of this work could not be used to make any reasonable statement of the thermal performance of TIMs.

Along with the uncertainty in measurements, some uncertainty exists due to the non-similarities in each test spot in the test frame. For example, the weights of the heat sinks, copper bars and weights used for pressure are not identical. Weights were measured and are presented in Appendix D. These variations could affect results since the heating time is dependent on the mass of heat sinks and copper bars. If time constants are different, the T_{max} of each test spots could vary due to these inaccuracies in the test frame. In addition, environmental conditions such as ambient temperature and air pressure could affect the overall results. Hence, ambient temperature was measured simultaneously with R_{th} measurements. The air pressure was assumed to have remained the same. Furthermore, inaccuracies in the air cooling could affect the overall results. The velocity of air cooling was not measured but before starting the test it was verified that each place in the test frame cooled to the same temperature.

5.6 Conclusion and future directions

References used in this study come from very large research field. The study untilized basic literature from power semiconductor devices, accelerated reliability testing and thermal interface materials. Furthermore, the latest research results from TIM and power semiconductor device testing were studied. Conclusions made in this study were verified from several references which can be considered reliable. The test system for TIM aging is based on method which corresponds to the best to the actual use conditions. This does not mean that other aging methods could not be used to cause reliable aging affects in thermal interface materials. Within the time limits of this study, other aging methods were not feasible to implement.

With the power cycling test, an empirical model for the degradation of TIMs was established. This model can be used to analyze the life time behaviour of certain TIMs. However, to analyze the actual life time, a second degradation test would have been required. Within the time limits of this thesis, this was not possible to ahieve but will be done in the future. Even so, the life time analysis is highly dependent on application where TIMs are used thus the accurate determination of general life time of a single TIM is not possible. To establish a threshold to increase in thermal resistance, thermal interface material used should be closely linked to the application. Nonetheless, developed empirical model can be used to support the design of electric drives. The degradation models in operating conditions can be expected to follow the degradation model with different coefficients. Furthermore, the comparison of the thermal performance and degradation trends is possible via the test system. The test system enables a fast testing of fresh TIM samples since unfamiliar TIMs are not required to be inserted into applications where they are used.

Based on the thermal performance comparison tests, the PCM has three times lower thermal resistance than elastomer film. Indicative results have been already noticed in the literature review (Section 3.3). However, according to manufacturers the dielectric breakdown voltage is over four times higher with the elastomer film. Since, used in similar applications and based solely on the thermal performance analysis, the PCM should be used instead of elastomer film in both applications. However, if the elastomer film provides adequate thermal charasteristics and higher dielectric breakdown voltage is required the use can be rationalized

since other benefits, for example, the ease of installation and lower price could be more important as was discussed in Section 3.2. The effect of the interface pressure was also studied in this thesis. Based on the literature review (Section 3.1) and measurement data, the thermal resistance can be reduced by increasing the interface pressure with both materials. Moreover, with the elastomer film, the reduction in the thermal resistance was almost equal to reduction which the elastomer film manufacturer has given.

To minimize uncertainties in measurement results, several actions were taken. Components selected for each control circuit were chosen to be as accurate as possible. The interface pressure is obtained by gravity and if the air pressure is kept constant, it will remain the same during the whole test. Furthemore, the surface roughness of heat sinks was measured. Moreover, the monitoring of aging was solely dependent on the temperature measurement over the interface. The calibration of temperature sensors was necessary. Afterwards, it was found that without the calibration the results of this study could have been useless. Finally, the power dissipation was measured from every test place to ensure the same power dissipation of power transistors. Although as much as possible was taken into account some uncertainty still remained in the calculated results. The accuracy of one average measurement with 99.9 % confidence interval was truly accurate (the highest uncertainty of ± 0.159 °C). However, due to the inaccuracy of the temperature calibration device some uncertainty still exists in the temperature measurements. To further improve accuracy, a more accurate calibration device should be used. However, this uncertainty can not be removed for good from the results.

An important parameter related to TIMs in discrete power transistor applications is the dielectric breakdown voltage. Since the bottom of a discrete power transistor has the same electrical potential than U_{DS} a TIM must be electrically insulated. A sufficient dielectric breakdown voltage must be maintained during the operating life. Hence, the performance of thermal interface materials is not solely dependent on thermal properties. However, the dielectric breakdown voltage was not measured in this study. It would have required more complicated test setup since the heat sinks of the test setup were not insulated from the mechanical test frame. Futhermore, if taken away from the test frame, and measured in an external dielectric breakdown voltage test system, the degradation in dielectric breakdown voltage could be misinterpreted. The test system will be modified in the future to support the dielectric breakdown voltage measurements. Futhermore, if the dielectric breakdown voltage is desired to be measured, the pollution degree of heat sinks and copper plates should also be measured. Since, being tested at its best several months in the test frame, dirt and dust could go between heat sink and thermal interface material, which could further weaken the dielectric breakdown strength.

Finally, during the start up of the test system, disruption in the U_{GS} was found. Since, power transistors are wired to the PBC and not attached directly, the disruption could occur from electromagnetic interferences in the test laboratory. A suggestion for the future test system, is to change the wires for insulated wires to prevent disruption from external sources.

6 Summary

Power semiconductor devices create heat during operation. This heat must be transferred from the device as efficient as possible to ensure safe operation and higher power densities of components. The dissipation of heat is first transferred to a thermal solution which is further cooled by air or liquid. One of the critical components in the path of heat flow is the thermal interface material which exists between a power semiconductor device and a heat sink. The thermal interface material represents the highest thermal resistance thus weakening in the TIM layer can cause damage to the component or to the whole application. This has led to the constant search for better TIMs and for methods for estimating the performance of TIMs during the life time of a product. Estimating the degradation trends in operating conditions is a big challenge. The purpose of this thesis was threefold: Analyze the reliability and life time of preselected thermal interface materials used in discrete power transistors. Second, to compare different interface pressures used in attachment of power semiconductor devices. Third, the heat transfer mechanisms from power semiconductor device to heat sink were intented to be studied.

The study started by introducing basic power semiconductor devices which are used in power conversion devices, after which a few important applications were introduced. In addition, Chapter 2 discussed losses in power semiconductor devices, thermal models for the power semiconductor devices and fundamentals of the heat transfer. Chapter 3 responded to the third research question since heat transfer between two solids was examined. In addition, important characteristics of TIMs were introduced. Two models for analyzing heat transfer were presented: one for ideal TIM and one for nonideal TIM. It was found that heat transfer between solids is governed by multiple factors, for example, by surface roughness, applied pressure, the softness of materials and thickness and thermal conductivity of TIMs. In addition, total of 5 different TIMs were compared for this thesis in literature review. Materials were thermal grease, elastomer film, PCM, metallic TIMs and graphite sheets. Based on the comparison by literature review, the thermal grease has the lowest thermal resistance. However, it suffers from thermal grease pump out and dry out effect and cannot be used in discrete power transistor applications, since electrical insulation is required. Metallic TIMs and graphite sheets yield high thermal conductivity but lack from reworkability and electrical insulation abilities. In addition, graphite sheets require high contact pressures which can not be often obtained in discrete power transistor applications since spring clips are used for mounting. Elastomer films are usually chosen for discrete power transistor applications. Elastomer films yield moderate thermal conductivity and a relatively high contact pressure is required for operation. However, elastomer film comes with an electrical insulation and the installation is relatively easy.

After third research question was answered, Chapter 4 explained reliability and life testing concepts. Based on the analysis, it was found that most of the failures in power semiconductor devices are induced by temperature related failure mechanisms. Furthermore, power cycling was found to be a reliable acceleration method, since it replicates the actual use conditions well. It was found that analysis of accelerated TIM degradation data might prove to be difficult since testing lacks of uniform test guides and analysis of test data have been relied in an individual researcher's capabilities. However, the analysis of accelerated test data is often done by plotting two thermal resistance curves versus time and predicting the degradation trend in operating conditions. Furthemore, several degradation models can be found in the literature for TIMs: linear in time, nonlinear in time and asymptotic in time.

The main purpose of this thesis was to analyze the reliability and the life time of a few selected thermal interface materials used in two applications. For this purpose, an accelerated life test

system was designed. The system replicates power cycling, since it corresponds the best to the actual use conditions and the failure mechanisms are caused by CTE differences between layers. A mechanical test frame, two printed circuit boards and control logic was designed by the author. The test system can be used to test in total of 20 samples of different TIMs. Pressure, power losses and maximum and minimum temperatures can be varied depending upon the need. In addition, the developed test system can be used to the compare thermal performance of TIMs with different pressures and different stresses.

For the power cycling test and for the pressure comparison test, an elastomer film and a PCM with 10 samples of each were chosen to be tested. In power cycling test TIMs experienced in total of 8100 cycles. The aging was monitored by measuring the temperature difference over TIMs. During aging tests, the thermal resistance of elastomer film decreased by 5 % and the thermal resistance of PCM increased by 1.3 %. A regression analysis was done to determine the life time behaviour of TIMs further. Based on the measurement data, an empirical degradation model for both TIMs was established. The degradation model can be used to analyze the life time behaviour of both TIMs. The performance of elastomer film improved throughout the whole test. The performance of PCM increased at the beginning but started to decompose relatively early. The improvement in both cases could occur from the abrasion of the material caused by temperature strains on the interface. However, since the performance of certain TIMs might improve, the material which yields the highest thermal conductivity at the beginning of the test might not be the best solution when considering long time reliability and thermal performance. The use life performance analysis would have required second degradation test which was not possible to achieve within the time limits of this thesis. However, power cycling results can be used to estimate life time performance and to analyze the degradation trends of materials.

Based on the pressure comparison tests and aging tests PCM has three times lower thermal resistance hence the PCM should be used instead if greater thermal performance is required. Futhermore, based on the literature review and measurement data, the interface pressure has effect on the thermal resistance of the interface. 45 N/cm^2 increase in the interface pressure decreased the thermal resistance with elastomer film by 10 % and with PCM by 16 %. The decrease with the elastomer film is almost the same as it is stated in the manufacturers datasheet. The corresponding curve was not found for the PCM.

Finally, the uncertainties of measurement results were discussed. To overcome the uncertainty in temperature measurements, the thermocouples were calibrated before starting the tests. After calibration, uncertainty components related to temperature measurements consist of uncertainty in the calibration device and the standard deviation of the mean. Uncertainty related to voltage measurements was determined with type B standard uncertainty. Moreover, the effect of single measurement to the calculated thermal resistances was studied. It was found that without the calibration, the results of this study could have been wrongly interpreted. However, with calibrated thermocouples, the measurement results are truly reliable.

In order to fully benefit from the degradation models, a second degradation test should have been done as stated several times in this thesis. With a second degradation test, the life time in operating condition could be predicted since TIMs can be expected to follow the developed degradation models. Furthemore, a threshold for change in thermal resistance should be determined. This threshold, however, is application specific and will be different depending on several factors. Manufacturers do not provide boundaries simply for thermal resistances hence the life time of a TIM without any connections to applications is not possible in general to analyze. Another important aspect related to TIMs is the dielectric breakdown voltage. The thermal resistance threshold could be adapted to the case when the dielectric breakdown voltage is not high enough. However, the current test system does not support the dielectric

breakdown voltage measurement and should be modified in the future to support these measurements.

References

Accreditation, E. c.-o. f., 1999. *Expression of the Uncertainty of Measurement in Calibration.* s.l.:s.n.

Bejan, A. & Kraus, A., 2003. *Heat Transfer Handbook.* 1 ed. Hoboken, New Jersey: John Wiley & Sons, p. 1496.

Berringer, K., Marvin, J. & Perruchoud, P., 1995. Semiconductor Power losses in AC inverters. *IEEE Conference Publications,* Volume 1, pp. 882 - 888.

Blazej, D., 2003. Thermal Interface Materials. *Electronics cooling magazine,* Issue November 2003, pp. 14-20.

Chung, H., Wang, H. & Blaabjerg, F. P. M., 2016. *Reliability of Power Electronic Converter Systems.* London: The Institution of Engineering and Technology.

Chung, L., Biller, C. & Chung, H., 2002. Electronic Applications of Flexible Graphite. *Journal of Electronic Materials,* Volume 31, pp. 535-544.

deSorgo, M., 1996. *Electronics Cooling.* [Online]
Available at: http://www.electronics-cooling.com/1996/09/thermal-interface-materials-2/
[Accessed 19 8 2016].

Due, J. & Robison, A., 2013. Reliability of thermal interface materials: A review. *Applied Thermal Engineering,* 50(1), pp. 455-463.

Goel, N., Bhattacharya, A., Cervates, J. & Mongia, R., 2008. Technical Review of Characterization Methods for Thermal Interface Materials (TIM). *IEEE Conference Publications,* pp. 1461 - 1471.

Gowda, A. et al., 2005. Reliability Testing of Silicone-based Thermal Greases. *IEEE Conference Publications,* pp. 64-71.

Grujicic, M., Zhao, C. & Dusel, E., 2005. The effect of thermal contact resistance on heat management in the electronic packaging. *Applied Surface Science,* 246(1-3), pp. 290-302.

JCGM, 2008. *Evaluation of measurement data - Guide to the expression of uncertainty in measurement,* s.l.: Joint Committee for Guides in Metrology.

Jedec, 2004. *JESD22-A105C. Power and temperature cycling..* s.l.:Jedec solid state technology association.

Kececioglu, D., 1994. *Reliability & Life Testing Handbook.* 2nd ed. Englewood Cliffs, New Jersey: PTR Prentice Hall, p. 960.

Klutke, G., Kiessler, P. & Wortman, M., 2003. A Critical Look at the Bathtub Curve. *IEEE Journals & Magazines,* 52(1), pp. 125 - 129.

Kyyrä, J., 2013. *Suuntaajatekniikka,* Espoo: Sähkötekniikan laitos.

Lewis, B. et al., 2007. *Thermal interface material and solder preforms.* [Online]
Available at: https://www.google.com/patents/US7187083
[Accessed 23 8 2016].

Liu, Y., 2012. *Power electronic packaging : design, assembly process, reliability and modeling.* E-book ed. New York: Springer, p. 612.

Mohan, N., Undeland, T., Robbins & W.P, 2003. *Power electronics, converters, applications, and design.* 3rd ed. Hoboken: John Wiley & Sons, Inc.. , p. 824.

Narumanchi, S., Mihalic, M., Kelly, K. & Eesley, G., 2008. Thermal interface materials for power electronics applications. *IEEE Conference Publications,* pp. 395 - 404.

Niiranen, J., 2007. *Tehoelektroniikan komponentit.* Espoo: Otatieto, p. 234.

Ousten, J. & Khatir, Z., 2011. Study of thermal interfaces aging for power electronics applications. *IEEE Conference Publications,* pp. 1 - 10.

Prasher, R., 2006. Thermal Interface Materials: Historical Perspective, Status, and Future Directions. *Proceedings of the IEEE,* 94(8), pp. 1571-1586.

Prasher, R. S., 2001. Surface Chemisty and Charasteristics based Model for the Thermal Contact Resistance of Fluidic INterstitial Thermal Interface Materials. *Journal of Heat Transfer,* Osa/vuosikerta 123, pp. 969-975.

Reddy, Tolbert & Ozpineci, 2015. Power Cycle Testing of Power Switches: A Literature Survey. *IEEE Journals & Magazines,* 30(5), pp. 2465-2373.

Reliasoft, 2016. *Reliability Hot Wire.* [Online]
Available at: http://www.weibull.com/hotwire/issue14/relbasics14.htm
[Accessed 8 30 2016].

Rohsenow, W., Hartnett, J. & Cho, Y., 1998. *Handbook of heat transfer.* 3rd ed. New York: McGraw-Hill Companies.

R, P. & S, R., 2001. Surface Chemistry and Charasteristics Based Model for the Thermal Contact Resistance of Fluid Interstital Thermal Interface Materials. *Journal of heat Transfer,* 123(5), pp. 969-975.

Sarkany, Z., Vass-Varnai, A. & Rencz, M., 2014. Analysis of Concurrent Failure Mechanisms in IGBT Structures During Active Power Cycling Tests. *IEEE Conference Publications,* pp. 650 - 654.

Sarvar, F., Whalley, D. & Conway, P., 2006. Thermal Interface Materials - A Review of the State of the Art. *IEEE Conference Publications,* Volume 2, pp. 1292-1302.

Sony, 2000. *Semiconductor quality and reliability handbook.* [Online]
Available at: http://www.j-journey.com/j-blog/wp-content/uploads/2012/05/Sony_Reliability_Chapter-4.pdf
[Accessed 30 8 2016].

Tong, X., 2011. *Advanced Materials for Thermal Management of Electronic Packaging.* 1st ed. New York: Springer, p. 616.

ToolBox, T. E., n.d. *The Engineering ToolBox.* [Online]
Available at: http://www.engineeringtoolbox.com/thermal-conductivity-d_429.html
[Accessed 19 7 2016].

Viswanath, R., Wakharkar, V., Watwe, A. & Lebonheur, V., 2002. Thermal Performance Challenges from Silicon to Systems. *Intel Technol. J,* Volume 4, pp. 1-16.

Wolfgang, 2015. *Accelerated testing of Power Modules.* Espoo/Helsinki, s.n.

Volke, A. & Hornkamp, M., 2012. *IGBT Modules.* 2nd ed. Munich: Infineon Technologies AG, p. 534.

Yovanovich, M., Culham, J. & Teerstra, P., 1997. *Calculating interface resistance.* [Online]
Available at: https://www.electronics-cooling.com/1997/05/calculating-interface-resistance/
[Accessed 27 8 2016].

Appendix A Schematic of test board

This Appendix presents the schematic of one test board. In total of two printed circuit boards were manufactured. PCBs were designed with a Eagle CAD software.

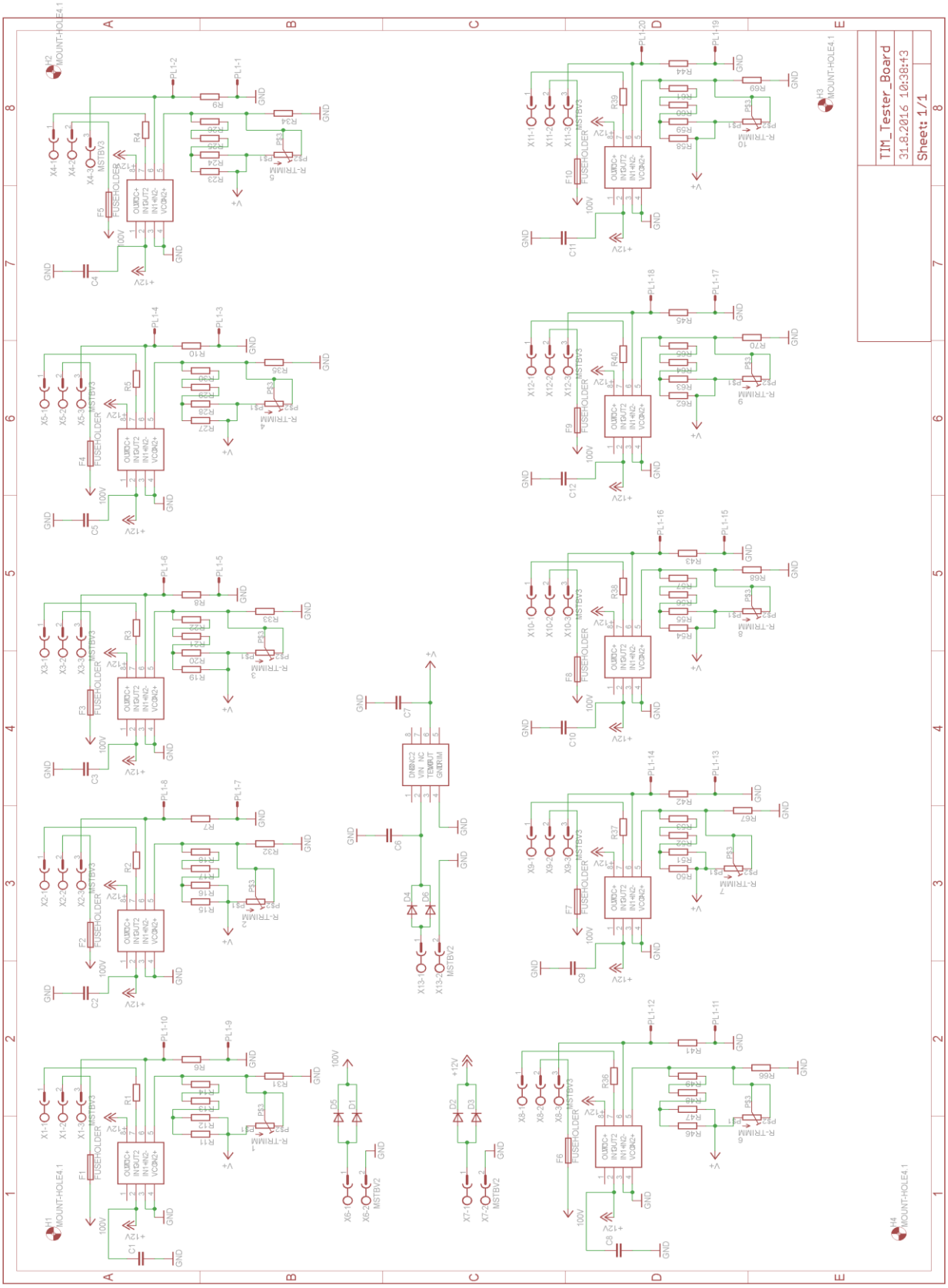

Appendix B Surface roughness measurements

This appendix presents the surface roughness measurements.

Table B.1: Surface roughness measurement results. Surface roughness of the heat sinks was measured in both parallel and transverse directions in relation to the cooling fins. Surface roughness R_a value was measured three times in both directions.

Parallel measurements [R_a]				**Transverse measurements [R_a]**				
Heat sink	**1**	**2**	**3**	**Average**	**1**	**2**	**3**	**Average**
1	0.316	0.148	0.159	**0.208**	0.278	0.266	0.296	**0.280**
2	0.445	0.270	0.106	**0.148**	0.148	0.227	0.169	**0.181**
3	0.235	0.294	0.325	**0.285**	0.310	0.300	0.413	**0.341**
4	0.214	0.224	0.252	**0.230**	0.176	0.188	0.253	**0.206**
5	0.366	0.333	0.210	**0.303**	0.467	0.316	0.460	**0.414**
6	0.109	0.049	0.079	**0.079**	0.078	0.077	0.083	**0.079**
7	0.103	0.112	0.118	**0.111**	0.080	0.080	0.091	**0.084**
8	0.127	0.121	0.117	**0.122**	0.135	0.129	0.100	**0.121**
9	0.102	0.110	0.110	**0.107**	0.073	0.090	0.090	**0.084**
10	0.105	0.086	0.091	**0.094**	0.095	0.079	0.086	**0.087**
11	0.243	0.257	0.222	**0.241**	0.203	0.213	0.193	**0.203**
12	0.268	0.282	0.285	**0.278**	0.303	0.273	0.273	**0.283**
13	0.168	0.182	0.238	**0.196**	0.267	0.247	0.373	**0.296**
14	0.191	0.234	0.221	**0.215**	0.346	0.223	0.259	**0.276**
15	0.290	0.315	0.276	**0.294**	0.333	0.310	0.377	**0.340**
16	0.578	0.590	0.740	**0.636**	0.629	0.714	0.850	**0.731**
17	0.350	0.324	0.315	**0.330**	0.376	0.737	0.392	**0.380**
18	0.176	0.191	0.219	**0.195**	0.293	0.293	0.245	**0.277**
19	0.320	0.246	0.377	**0.314**	0.324	0.403	0.339	**0.355**
20	0.182	0.233	0.198	**0.204**	0.231	0.276	0.391	**0.299**

Appendix C Calibration results of temperature sensors

In this Appendix is the calibration results of each temperature measurement channel. In addition, standard uncertainties calculated according to type A standard uncertainty and 99.9 % confidence level are presented.

Table C.1: Calibration results of each temperature measurement.

Channel	**T_{ref}=80,1 °C**	**T_{ref}=90,0 ºC**	**T_{ref}=100,1 ºC**	**T_{ref}=110,3 ºC**	**T_{ref}=120,3 ºC**
101	80.81	91.05	101.21	111.41	121.62
102	80.76	90.97	101.15	111.33	121.51
103	80.77	90.97	101.15	111.31	121.50
104	80.88	91.07	101.30	111.48	121.68
105	80.87	91.05	101.28	111.45	121.64
106	80.92	91.08	101.35	111.51	121.70
107	80.83	90.97	101.23	111.37	121.54
108	80.86	91.01	101.27	111.42	121.59
109	80.85	90.99	101.26	111.40	121.56
110	80.82	90.97	101.24	111.38	121.54
111	80.64	90.75	100.97	111.05	121.15
112	80.83	90.95	101.23	111.35	121.48
113	80.75	90.86	101.11	111.21	121.32
114	80.74	90.86	101.11	111.21	121.32
115	80.67	90.79	101.01	111.09	121.18
116	80.61	90.76	100.96	111.05	121.15
117	80.53	90.68	100.86	110.96	121.05
118	80.46	90.64	100.77	110.85	120.92
119	80.52	90.73	100.82	110.88	120.92
120	80.36	90.61	100.68	110.77	120.84
201	77.82	87.99	98.05	108.20	118.24
202	78.05	88.20	98.31	108.46	118.51
203	78.01	88.14	98.24	108.36	118.40
204	78.29	88.44	98.58	108.72	118.80
205	78.42	88.55	98.74	108.87	118.96
206	78.55	88.67	98.87	108.99	119.08
207	78.48	88.61	98.81	108.94	119.04
208	78.66	88.80	99.03	109.16	119.27
209	78.62	88.72	98.95	109.07	119.16
210	78.68	88.80	99.04	109.16	119.27
211	78.68	88.79	99.03	109.15	119.26
212	78.74	88.83	99.07	109.14	119.22
213	78.77	88.87	99.12	109.22	119.32
214	78.73	88.83	99.06	109.15	119.25
215	78.82	88.94	99.17	109.26	119.36
216	78.74	88.90	99.14	109.25	119.39
217	78.67	88.83	99.05	109.16	119.30
218	78.62	88.79	98.96	109.04	119.14
219	78.61	88.80	98.96	109.06	119.17
220	78.75	89.00	99.16	109.29	119.44

Table C.2: Standard uncertainties of thermocouples. In addition, 99.9 % confidence interval is presented. Values are calculated for power cycling test and for performance comparison test.

Channel	σ, power cycling	σ, performance comparison	Type A uncertainty, power cycling	Type A uncertainty, performance comparison	99.9 % Confidence interval, power cycling	99.9 % Confidence interval, performance comparison
101	0.290	0.254	0.041	0.036	0.135	0.118
102	0.282	0.268	0.040	0.038	0.131	0.125
103	0.254	0.235	0.036	0.033	0.118	0.109
104	0.249	0.241	0.035	0.034	0.116	0.112
105	0.240	0.259	0.034	0.037	0.112	0.120
106	0.240	0.268	0.034	0.038	0.112	0.125
107	0.253	0.264	0.036	0.037	0.117	0.123
108	0.248	0.274	0.035	0.039	0.115	0.127
109	0.267	0.267	0.038	0.038	0.124	0.124
110	0.258	0.280	0.037	0.040	0.120	0.130
111	0.283	0.281	0.040	0.040	0.132	0.131
112	0.274	0.286	0.039	0.040	0.127	0.133
113	0.245	0.262	0.035	0.037	0.114	0.122
114	0.237	0.282	0.033	0.040	0.110	0.131
115	0.278	0.278	0.039	0.039	0.129	0.130
116	0.270	0.289	0.038	0.041	0.125	0.134
117	0.272	0.252	0.038	0.036	0.126	0.117
118	0.267	0.271	0.038	0.038	0.124	0.126
119	0.280	0.232	0.040	0.033	0.130	0.108
120	0.275	0.235	0.039	0.033	0.128	0.109
201	0.326	0.308	0.046	0.044	0.152	0.143
202	0.331	0.313	0.047	0.044	0.154	0.145
203	0.171	0.334	0.024	0.047	0.080	0.156
204	0.165	0.330	0.023	0.047	0.077	0.153
205	0.193	0.318	0.027	0.045	0.090	0.148
206	0.192	0.313	0.027	0.044	0.089	0.146
207	0.211	0.304	0.030	0.043	0.098	0.141
208	0.207	0.307	0.029	0.043	0.096	0.143
209	0.284	0.307	0.040	0.043	0.132	0.143
210	0.278	0.300	0.039	0.042	0.129	0.140
211	0.319	0.297	0.045	0.042	0.148	0.138
212	0.319	0.301	0.045	0.043	0.149	0.140
213	0.343	0.239	0.048	0.034	0.159	0.111
214	0.332	0.245	0.047	0.035	0.154	0.114
215	0.321	0.235	0.045	0.033	0.149	0.109
216	0.314	0.238	0.044	0.034	0.146	0.111
217	0.281	0.245	0.040	0.035	0.131	0.114
218	0.269	0.247	0.038	0.035	0.125	0.115
219	0.286	0.282	0.040	0.040	0.133	0.131
220	0.267	0.279	0.038	0.039	0.124	0.130

Appendix D Weigths of heat sinks, copper bars and gravity weights

This appendix presents the measured weights of heat sinks, copper plates and gravity weights used in the tests.

Table D.1: Weights of heat sinks, copper bars and gravity weights.

Test place	Heat Sink (g)	Cu (g)	Weight (g)
1	62.68	8.24	1992.29
2	62.66	8.33	1993.63
3	63.18	8.38	1993.45
4	63.24	8.39	1993.95
5	63.17	8.35	1993.66
6	63.17	8.37	1993.43
7	63.33	8.22	1994.46
8	63.25	8.5	1992.79
9	63.25	8.32	1992.98
10	63.21	8.51	1992.45
11	63.04	8.04	1994.34
12	63.13	8.29	1993.66
13	62.48	8.34	1993.92
14	63.25	8.24	1993.4
15	63.04	8.19	1992.96
16	63.13	8.11	1993.28
17	63.29	8.07	1994.07
18	62.34	8.29	1993.7
19	63.29	8.41	1993.67
20	63.03	8.24	1994.02

Appendix E Power dissipation in measurements

In this appendix is the currents and voltages measured from power cycling test and performance comparison test. Currents and voltages were measured in order to obtain similar and comparable results.

Table E.1: Power dissipation in power cycling test.

Test place	Voltage (V)	Current (A)	Power dissipation (W)
1	168.5	0.179	30.2
2	168.5	0.180	30.4
3	168.5	0.180	30.4
4	168.4	0.180	30.3
5	168.4	0.180	30.3
6	168.4	0.180	30.3
7	168.4	0.180	30.4
8	168.4	0.180	30.3
9	168.5	0.180	30.4
10	168.3	0.180	30.3
11	168.3	0.181	30.4
12	168.3	0.180	30.3
13	168.3	0.180	30.2
14	168.2	0.180	30.3
15	168.2	0.180	30.2
16	168.2	0.181	30.5
17	168.2	0.181	30.4
18	168.2	0.180	30.2
19	168.1	0.180	30.3
20	168.3	0.180	30.2

Table E.2: Power dissipation in performance comparison test.

Test place	Voltage (V)	Current (A)	Power dissipation (W)
1	54.4	0.179	9.8
2	54.5	0.180	9.8
3	54.5	0.180	9.8
4	54.4	0.180	9.8
5	54.2	0.180	9.8
6	54.4	0.180	9.8
7	54.4	0.180	9.8
8	54.4	0.180	9.8
9	54.4	0.180	9.8
10	54.2	0.180	9.8
11	54.2	0.181	9.8
12	54.2	0.180	9.8
13	54.3	0.180	9.7
14	54.2	0.180	9.8
15	54.2	0.180	9.7
16	54.1	0.181	9.8
17	54.2	0.180	9.8
18	54.1	0.179	9.7
19	54.0	0.180	9.7
20	54.2	0.179	9.7